OXIDATION OF NUCLEAR- AND MATRIX-GRADE GRAPHITE FOR VHTR AIR INGRESS ACCIDENT SCENARIOS

A Dissertation

presented to

the Faculty of the Graduate School

at the University of Missouri-Columbia

In Partial Fulfillment

Of the Requirements for the Degree

Doctor of Philosophy

---

by

YOONJO J. LEE

Dr. Tushar K. Ghosh, Dissertation Supervisor
Dr. Sudarshan K. Loyalka, Dissertation Supervisor

DECEMBER 2016

The undersigned, appointed by the Dean of the Graduate School, have examined the dissertation entitled

Oxidation of Nuclear and Matrix-Grade Graphite for VHTR Air Ingress Accident Scenarios

presented by Yoonjo J. Lee

a candidate for the degree of Doctor of Philosophy

and hereby certify that, in their opinion it is worthy of acceptance.

_____

Dr. Tushar K. Ghosh

_____

Dr. Sudarshan K. Loyalka

_____

Dr. Mark A. Prelas

_____

Dr. Robert V. Tompson

_____

Dr. Paul C. H. Chan

DEDICATION

This work is dedicated to my parents, the faculty, my partner Josh and everyone else who believed in me. Extra thanks to Josh who was always in the background of my dreams. He stuck with me through law school and now this. We simply did not want to be starving artists anymore. A life full of adventures will surely need financial backing.

ACKNOWLEDGEMENTS

I would like to first and foremost acknowledge my advisors Dr. Tushar Ghosh and Dr. Sudarshan Loyalka, who encouraged me and supported me throughout the degree whether it was with the smallest issue or the most exigent problems. I could always count on my advisors to be there for me, and they believed in me. I appreciated the opportunity they gave me to pursue this advanced degree and the day I finish it will clearly be the proudest moment of my life. I am so grateful for the opportunities to do the research, talk, travel and publish papers on numerous occasions.

Special thanks go to all the faculty members on my PhD committee who took time out of their busy schedules to meet with me and help me through the end. The staff, Latricia Vaughn and James Bennett, were tireless in their efforts to help me all these years, and I am forever indebted to them.

I would also like to specifically thank my fellow students, Matt Simones and Kyle Walton, on their resourcefulness and teamwork during and after school hours to help me with the laboratory equipment.

Finally, I would like to recognize the financial support that made my research and graduate school completion possible. During the course of my research and graduate education, I received a Graduate Assistantship in an Area of National Need (GAANN) fellowship from the U.S. Department of Education and also a Nuclear Regulatory Commission (NRC) fellowship.

TABLE OF CONTENTS

LIST OF TABLES

Table

Page

LIST OF ILLUSTRATIONS

Figure

Page

ABSTRACT

One of the most severe accidents anticipated for the Very High Temperature Reactor (VHTR) is an air ingress accident caused by a pipe break, where the reactor vessel and core become fully immersed in air as the core temperature rises potentially reaching 1873 K. Graphite oxidation is predicted to be severe under these conditions. Gasification of graphite impacts its geometry and reduces thermal and mechanical properties, thus affecting the safe performance and shortening the service-life of components constructed of graphite. We have studied the oxidation rate of several nuclear-grade and matrix-grade graphites including NBG-18 and IG-110 as well as GKrS, respectively. Oxidation data was collected thermogravimetrically for air ingress accident scenarios from 873 to 1873 K using a Thermax700® thermogravimetric analyzer. A semi-empirical Arrhenius rate equation was developed for the kinetic regime for each graphite grade. The activation energy for the matrix-grade graphite was within the limited historically reported values while the activation energy of nuclear-grade graphite was determined to be well within literature values. The surfaces of oxidized graphite samples were further characterized by SEM, EDS, FTIR and XPS.

CHAPTER 1

INTRODUCTION

1.1 Introduction

The Generation IV Very High Temperature Reactor (VHTR) is an advanced graphite-moderated High Temperature Gas Cooled Reactor (HTGR) that is being developed with a potential core outlet temperature up to 1273 K or higher, compared to an outlet temperature of 1123 K that is typical for historic HTGRs. Modular HTGRs with a prismatic or pebble-bed reactor core are candidates for the Next Generation Nuclear Plants (NGNP). The higher operating temperature of VHTRs poses new material challenges. New grades of reactor graphite as well as superalloy metals for heat exchanging components and pressure vessels have been developed to meet the higher performance requirements of VHTR.

Nuclear-grade graphite is an excellent core moderator, reflector and fuel element matrix material for HTGRs because of its favorable neutronic properties, low cost, high thermal conductivity, wide commercial availability and because it is easily machined. In fact, the main concern with nuclear-grade graphite other than irradiation damage is that it is readily oxidized in air at temperatures greater than 723 K. Historic nuclear-grade graphite, such as H-451, PGX and V483T are no longer commercially available to study. Moreover, new measurements on modern nuclear-grade graphite are lacking and their microstructural properties have not been fully characterized. Specifically, candidate nuclear-grade graphite for NGNP are NBG-18, IG-110, NBG-10 and PCEA,

but the NBG-18 (German) and the IG-110 (Japanese) graphite grades have been chosen specifically for use in the high irradiation dose regions of VHTR thus further motivating this study. Currently, there is a need for new experimental measurements and models to predict the applicability of modern graphite for use in VHTR.

HTGRs contain two major types of reactor graphite, nuclear-grade and matrix-grade. While the prismatic or block reactor core and reflector components may be mostly comprised of nuclear-grade graphite, a pebble-bed reactor core is largely comprised of matrix-grade graphite, commonly referred to as A3 graphite. Historically, the matrix-grade graphite was developed by the Germans to overcoat fuel particles to make fuel compacts, so it is graphite that was intended to be fabricated with the nuclear fuel. By definition, matrix-grade graphite is not nuclear-grade graphite, which is stringently defined and standardized in ASTM D7219-05 in terms of purity standards [1]. In fact, there is no standardization for matrix-grade graphite other than the historic German A3 recipe that provides some guidance to modern manufacturers. On a microstructural level, matrix-grade graphite is partially-graphitized graphite whereas nuclear-graphite is fully-graphitized graphite. This difference in graphitization is due to the fabrication temperature of the fuel compact which must occur below 2273 K, whereas highly graphitized nuclear-grade graphites are fabricated at temperatures exceeding 2773 K since graphitization of carbon atoms occurs between 2773 and 3073 K. However, for the matrix-grade graphite, if fabrication temperatures were greater than 2273 K, uranium diffusion out of the fuel kernel becomes a concern.

Other than the historic A3 recipe for fabricating matrix-grade graphite, such as A3-3 and A3-27, little is known about oxidation of matrix graphite in air or its longevity

during normal operation. Surely, modern matrix-grade graphite is still being developed but it is not yet widely available for study, modern or historic. Furthermore, if one were to obtain the material, it is likely to be wholly uncharacterized. GKrS is a candidate matrix-grade graphite that was developed by Oak Ridge National Laboratory (ORNL) since the early 2000s. The group largely adopted the German A3 recipe to manufacture GKrS and as far as the current stock of available matrix-grade graphite goes, it was the only reasonably obtainable grade for this study and it was in short supply. It is worth noting that China has one or more grades of graphitic matrix material that it is currently developing too but that is not easily available. This research provided one of the very first opportunities to characterize modern matrix-grade graphite. Since each grade of nuclear and matrix graphite vary greatly in fabrication, composition and performance there is a need to measure the oxidation rates individually and develop predictive models that are specific to the type. The microstructural changes to graphite before and after oxidation damage are of great interest for VHTR.

1.2 Purpose and scope of the proposed research

The purpose of this research is to obtain experimental data on the oxidation rate of nuclear-grade graphite NBG-18 and IG-110 as well as matrix-grade graphite GKrS in air ingress accident conditions for VHTR and to obtain the rate expression. The air oxidation of nuclear graphite can occur in essentially two scenarios: (1) the slow and gradual oxidation of nuclear graphite during normal operating conditions of VHTR by oxidizing impurities inevitably circulating in the coolant gas; and (2) the severe and

rapid oxidation caused by an air ingress accident, which is one of the major accident scenarios anticipated for VHTR. The second scenario is the focus of this study. After the reactor core has already suffered a depressurization accident and there has been long-term loss of forced convectional cooling, an air ingress accident due to a pipe break can cause the reactor core and vessel to become fully immersed in air while the temperature of the core rises, potentially reaching 1873 K. The air oxidation of graphite impacts its geometry and microstructure as well as reduce thermal, mechanical and neutronic properties. During an air ingress accident, the oxidation rate of nuclear and matrix-grade graphite is predicted to be very high.

The oxidation rates of three different graphite grades NBG-18, IG-110 and GKrS will be studied in VHTR air ingress accident conditions. The research to be completed for each grade is essentially two-fold: (1) oxidation measurements and (2) microstructural characterization before and after oxidation treatment. Oxidation measurements will be obtained thermogravimetrically. Thermax700 from FischerScientific®, a thermogravimetric analyzer (TGA), will be used to measure the isothermal rates of oxidative mass loss at a chosen temperature. Graphite samples will be subjected to isothermal oxidation runs for temperatures between 873 K and 1873 K for different oxygen concentrations—5, 10, 15 and 21 mole percent. Then, a predictive Arrhenius-type oxidation model will be developed only for the kinetic regime of graphite oxidation, between 873 and 1023 K. First, we will define what VHTR air accident conditions are since temperature regimes and transitions between those regimes vary greatly from study to study. It is noted that in the kinetic regime the differences in chemical composition of graphite and the effects of microstructure are

most apparent and practical to study. Oxidation is also said to be penetrative through the bulk in the kinetic regime. Then, we will determine the temperature regimes from the data, specifically from Arrhenius plots. The process of designing the experimental conditions and regime determination are detailed in our first publication [1].

Beyond the kinetic temperature regime, graphite oxidation is controlled by a mix of chemical control and pore diffusion at intermediate temperatures or at highest temperatures by the rate of mass transfer through the bulk gas phase mixture on the surface of graphite. The semi-empirical Arrhenius equation from the kinetic theory of gases is often used to describe thermally-induced processes, such as graphite oxidation, due to its strong experimental accuracy in those kinds of temperature-based measurements. Then the oxidation rates may be determined from TGA weight loss data. Other kinetic parameters, such as the activation energy, frequency factor and order of reaction, can be determined experimentally as well.

The surface of nuclear graphite has been observed to behave in a unique manner given a specific grade. Surface chemistry and microstructural changes for nuclear- and matrix-grade graphite before and after oxidation treatment will be performed with Scanning Electron Microscopy (SEM)/Energy Dispersive X-ray Spectroscopy (EDS), X-ray Photoelectron Spectroscopy (XPS) and Fourier Transform Infrared Spectroscopy (FTIR). Overall, surface techniques will be used to confirm the presence of oxidized compounds and increased oxygen concentration on the surface of samples. Since the nuclear-grade graphite in this study was amply available, bulk machining methods will also be used on larger samples to create a density profile for oxidized samples [1]. The

matrix graphite was not available in large quantities or sizes so a density profile will not be made for those samples.

A series of three papers were published on the measurements and microstructural changes in which a predictive Arrhenius-based model was developed for the kinetic regime of graphite oxidation for NBG-18 [1], IG-110 [2] and GKrS [3], respectively. Each publication includes an overview of the prior work related to the specific grade. It is interesting to note that NBG-18 is a modern grade and at the time of the study only a few other research groups worldwide had made similar measurements. Very few papers reported any measurements in the higher temperature regimes. IG-110 is a historic grade that is still used today in the experimental pebble bed reactor (HTR-10) at Tsinghua University in China and as fuel blocks in the High Temperature Graphite-Moderated Helium-Cooled Test Reactor (HTTR) in Japan. Although it has a history of use and tests, the performance results of the IG-110 vary widely. Finally, for GKrS, this study was one of the very first studies on modern matrix-grade graphite oxidation rates.

1.3 Organization of the dissertation

The dissertation is organized as follows: Chapter 2 is the first published paper entitled, "Oxidation rate of nuclear-grade graphite NBG-18 in the kinetic regime for VHTR air ingress accident scenarios;" Chapter 3 is the second published paper entitled, "Oxidation rate of nuclear-grade graphite IG-110 in the kinetic regime for VHTR air ingress accident scenarios;" and Chapter 4 is the third published paper entitled, "Oxidation rate of graphitic matrix material in the kinetic regime for VHTR air ingress

accident scenarios." Finally, Chapter 5 describes the results and discussion of graphite oxidation of nuclear and matrix-grade graphite and recommendations for future work.

CHAPTER 2

Oxidation Rate of Nuclear-Grade Graphite NBG-18 in the Kinetic Regime for VHTR Air Ingress Accident Scenarios

Jo Jo Lee, Tushar K. Ghosh, Sudarshan K. Loyalka

Nuclear Science and Engineering Institute, Particulate Systems Research Center, University of Missouri, Columbia, Missouri 65211

Abstract

One of the most severe accident scenarios anticipated for VHTRs is an air ingress accident caused by a pipe break. Graphite oxidation could be severe under these conditions. In this work, the oxidation rate of NBG-18 nuclear-grade graphite was studied thermogravimetrically for different oxygen concentrations and with temperatures from 873 to 1873 K. A semi-empirical Arrhenius rate equation was developed for the temperature range of 873 to 1023 K. The activation energy of NBG-18 was 187 kJ/mole and the order of reaction was 1.25. The penetration depth of oxidant was about 3 to 4 mm for NBG-18 oxidized at 973 K. Increased porosity and changes in external geometry became more prominent at higher temperatures from about 1173 to 1873 K. The surface of oxidized NBG-18 was characterized by SEM, EDS, FTIR and XPS.

1. Introduction

Nuclear-grade graphite is an excellent moderator, reflector, and fuel element matrix material for High Temperature Gas Cooled Reactors (HTGRs) with circulating helium coolant. Graphite is also widely used in various nuclear applications because it is an anisotropic, chemically inert material with favorable neutronic properties as well as being highly conductive and easily machined [1]. Modular HTGRs with either a prismatic or

pebble-bed graphite fuel format are one of the candidate designs for the Next Generation of Nuclear Plants (NGNPs). The Generation IV Very High Temperature Reactor (VHTR) is a type of HTGR with a potential core outlet temperature up to 1273 K or higher compared to a typical 1123 K outlet temperature for older HTGRs. The associated increase in operating temperature from 1123 K to 1273 K is a significant factor that changes material performance requirements. Candidate materials including super alloys for heat exchanging components and new nuclear-grade graphite have been developed to try and meet these material challenges. Older nuclear-grade graphite, such as H-451, PGX and V483T graphite are no longer commercially available [2]. In addition, most of the current understanding in nuclear graphite research relies on measurements made with older grades other than candidates for NGNPs which are specifically NBG-18, IG-110, NBG-10 and PCEA. In particular, NBG-18 and IG-110 have been chosen as candidate materials for high irradiation dose regions of the VHTR [3]. Therefore, new experimental data is needed for these candidate nuclear-grade materials to fully evaluate their applicability in VHTR systems.

Although nuclear-grade graphite has excellent neutronic and chemical properties for reactor use, it oxidizes in air at temperatures above 723 K. Below this temperature the binder and filler material used in graphite manufacturing render the graphite impervious to reactants and oxidants. The concern with air oxidation is essentially two-fold: 1) the chronic oxidation during normal operation by oxidizing impurities circulating in the helium coolant and 2) severe oxidation caused by an air ingress accident. During normal operation of an HTGR, oxidizing impurities carried by the circulating helium coolant in the primary reactor system can gradually corrode reflector and fuel element components constructed of

graphite. During normal operating conditions, a chronic but very slow oxidation was observed with older grades of reactor graphite, affecting mostly the exterior surface of graphite components but with little or no loss of strength or mechanical properties [2].

The average impurity content of the helium coolant in an HTGR is shown in Table 1 for several gas reactors [4]. Impurities in the coolant during normal operations originate from initial core out-gassing and may persist due to in-leakage from heat exchanging components. Table 1 displays acceptable impurity levels under normal HTGR operating conditions and are favorable for preventing corrosion of metal components [5].

Table 1
Impurity contents in wppm of circulating helium in gas reactors during normal operation.

	H_2O	H_2	CO	CO_2	CH_4	N_2	O_2
GT-MHR	2.0	-	($CO + CO_2$ < 6.0)	-	-	-	
Peach Bottom	0.5	10	0.5	<0.5	1.0	0.5	-
Fort St. Vrain	1.0	7.0	3.0	1.0	-	-	-
AVR	0.15	9.0	45	0.25	1.0	22	-
HTTR (upper limit)	0.2	3.0	3.0	0.6	0.5	0.2	0.04
HTR-10	≤ 1.0	≤ 9.0	≤ 9.0	≤ 1.0	≤ 3.0	≤ 2.0	1.0
PBMR	<0.2	2.0-11.0	2.0-11.0	<0.2	<0.1	3.0-115	-
DRAGON	0.05-0.1	0.8-2.0	0.5-1.0	<0.02	0.15	0.15	-
THTR	<0.01	0.8	0.4	0.2	0.1	0.1	-

GT-MGR: US prismatic Gas Turbine-Modular Helium Reactor; Peach Bottom: US experimental prismatic HTGR; Fort St. Vrain: US prismatic HTGR, originally built as nuclear power plant; AVR: German experimental pebble bed reactor; HTTR: Japanese experimental prismatic High Temperature Test Reactor; HTR-10: Chinese experimental pebble-bed reactor; PBMR: South African Pebble Bed Modular Reactor, DRAGON: British experimental HTGR; THTR: German Thorium High Temperature Reactor.

However, one of the most severe accident scenarios anticipated for HTGR is an air ingress accident caused by a pipe break, where the reactor vessel and core become fully immersed in air as the temperature of the core increases, potentially reaching 1873 K. Graphite oxidation could be severe under these conditions. The gasification of graphite

impacts its geometry and reduces thermal and mechanical properties, thus affecting the safe performance and shortening the service-life of components constructed of graphite [6-8]. At accident temperatures, the oxidation rate of graphite is predicted to be very high [9, 10].

In this work, we have studied the oxidation of a current generation nuclear-grade graphite, NBG-18, manufactured by the SGL Carbon Company in Chedde, France. Graphite oxidation is generally both chemical and diffusive during an air ingress accident scenario in the temperature range of 873 to 1873 K. The specific objective of this study is to gain a better understanding of the graphite oxidation mechanism which is mainly chemically-controlled. A thermogravimetric analyzer (TGA), capable of operating up to 1973 K was used to measure the mass loss of NBG-18 graphite at various temperatures, oxygen concentrations and exposure times. Experiments were also conducted under various gas flow configurations. Isothermal mass loss rates measured with TGA were used to develop an expression for the chemically-controlled regime of graphite oxidation.

Graphite oxidation models for current nuclear grades of graphite vary widely. There is a lack of consensus on the accident conditions, experimental setup and critical parameters suitable to model a realistic accident scenario [11]. Moreover, there are diverse views on the mechanism for gasification of graphite by oxygen [11-14]. Researchers have reported that depending on the shipment batch of graphite tested, results could also vary [11, 15]. The rate of graphite oxidation could also depend on how the samples were cut or prepared [8, 15]. Petroleum-coke based nuclear graphite, such as NBG-18, is anisotropic due to its crystal structure being hexagonal with stacked basal planes of carbon atoms. Imperfect arm-chair and zigzag edge configurations could contribute to formation of surface active

free sites and oxide complexes [3]. The discrepancy in current graphite oxidation studies is also partly due to the fact that graphite oxidation reactions are fairly complex and dependant on many parameters such as reaction temperature, oxygen partial pressure, pore microstructure, formation rate of surface oxides, and potential catalytic effects due to impurities present in graphite during manufacturing [11]. While all researchers would agree that modeling graphite oxidation involves some representation of chemical, in-pore diffusion-controlled and boundary layer-controlled regimes, there is no agreement over the dominant reaction mechanisms, diffusive processes or the temperature and conditions applicable to each regime. Due to completely different pore microstructures, formulation and method of manufacture of commercially available nuclear-grade graphite, separate oxidation measurements for specific grades of nuclear-grade graphite have been necessarily made and reported by a number of researchers [1, 2, 10, 16].

2. Graphite Oxidation Kinetics Theory

Although a number of researchers have studied graphite oxidation, the controlling mechanism and reactions involved in the gasification of graphite have not been agreed upon. Graphite oxidation reactions are complex and there is a strong connection to the transport processes that are occurring. Depending on temperature, graphite oxidation proceeds in at least three different regimes. In the first regime (Regime I), uniform graphite oxidation occurs as oxygen diffuses through the bulk of the graphite specimen. The penetration depth of oxygen into the surface and subsequent diffusion into the bulk is substantial in this temperature regime. The penetration depth is on the order of several millimeters [2, 17]. Figure 1 is a schematic representation of graphite oxidation as it

progresses in three temperature regimes and also that of the oxygen concentration as it evolves across a graphite specimen.

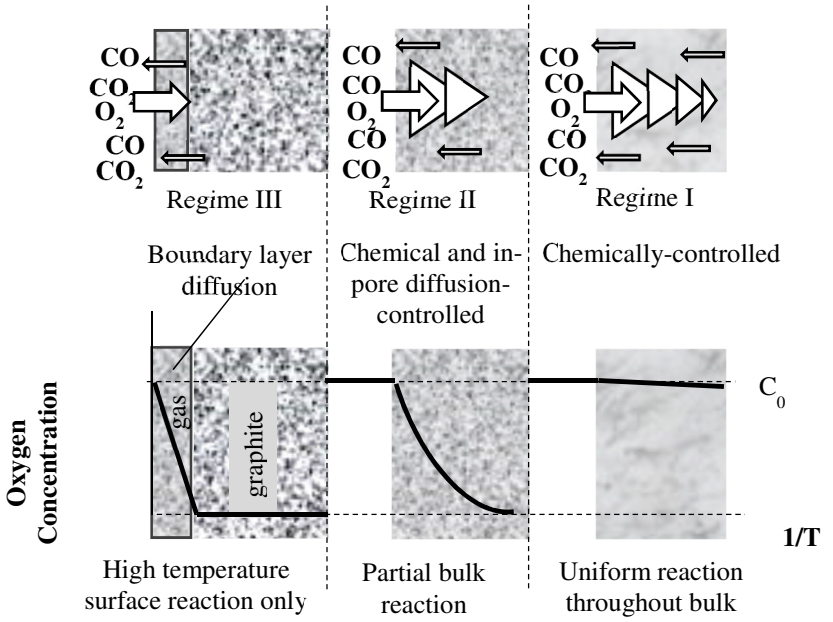

Fig. 1. Oxidation modes of porous nuclear-grade graphite from Regimes I to III.

Successive transport processes during graphite oxidation occur as follows:

(a) Diffusion of oxygen to the graphite surface and walls of open volume pores.

(b) Adsorption of oxygen atoms on the graphite surface free active sites and complexes inducing the simultaneous forming of C-O and C-H bonds and breaking of C-C bonds (dissociative chemisorption).

(c) Chemical reactions occur at the surface.

(d) Desorption of gaseous products, CO and CO_2, from the graphite surface and transport to the bulk gas mixture.

2.1 Chemical Reaction between Graphite and Oxygen

Several chemical reactions can occur during oxidation of the nuclear-grade graphite forming CO, CO_2, or both. The main product formed from the gasification of graphite, however, is carbon monoxide. The elementary reactions are as follows [18, 19]:

Graphite Oxidation:

$$C\ (graphite) + xO_2(g) \leftrightarrow\ zCO(g)$$
$$\Delta H_{rxn} = -394\ \frac{kJ}{mol} \qquad (1a)$$

$$C\ (graphite) + wO_2(g) \leftrightarrow yCO_2(g)$$
$$\Delta H_{rxn} = -111\ \frac{kJ}{mol} \qquad (1b)$$

Bouduard Reaction:

$$C\ (graphite) + CO_2\ (g) \leftrightarrow\ 2CO(g)$$
$$\Delta H_{rxn} = 172\ \frac{kJ}{mol} \qquad (2)$$

Carbon Monoxide Combustion:

$$2CO\ (g) + O_2(\mathrm{g}) \leftrightarrow 2CO_2\ (\mathrm{g})$$
$$\Delta H_{rxn} = -283\ \frac{kJ}{mol} \qquad (3)$$

Reaction (1a) is dominant and the production of CO from graphite gasification increases almost exponentially with temperature unlike the production of CO_2 from gasification of graphite that occurs at relatively low temperatures [11]. Reactions (1a), (1b) and (2) are heterogeneous reactions between gases and a solid surface, whereas Reaction (3) occurs entirely in the gas phase and is thermodynamically favorable at higher temperatures. Researchers generally agree that Reactions (1a) and (1b) occur in three regimes depending on the oxidation temperature. However, the exact stoichiometries *w, x, y* and *z* are not well-known.

In this study, the main objective is to develop a model for Regime I. In Regime I, oxygen can penetrate bulk graphite, and the oxidation rate is controlled by the chemical reaction rate of Reaction (1a) [20]. As the temperature of oxidation increases, the highest oxygen concentration is near the surface, and the concentration decreases almost exponentially with distance from the surface. At intermediate temperatures (Regime II), graphite oxidation is limited by both chemical reaction rates and in-pore diffusion. The transition from Regime I and II is very important because the mechanism of graphite oxidation can no longer be fully explained with kinetic theory. Generally, the transition temperature is affected by the density, impurity level and microstructure of graphite as well as the reaction air flow rate and flow conditions [9], [24]. The transition temperature from Regime I to II varies greatly from study to study as shown in Table 2.

Table 2
The transition temperature from Regime I to Regime II for nuclear-grade graphite oxidation in air as reported by several authors.

Author	Transition Temperature
Hinssen et al. [20]	773 to 1173 K
Fuller and Okoh [22]	723 to 973 K
Blanchard [23]	873 to 1173 K
Luo et al. [9]	873 to 1073 K
Contescu et al. [24]	923 to 1023 K

2.2 The Arrhenius Rate Equation and Order of Reaction

The Arrhenius equation is used to model various thermally-induced processes and is oftentimes used to determine different mechanisms or alternate reaction pathways [25]. Bulk oxidation of graphite in air in a chemically-controlled regime follows an Arrhenius-type rate law [18, 20]. The Arrhenius equation is given by

$$k = Ae^{(\frac{-E_a}{RT})} \quad (4a)$$

Taking the logarithms of Equation (4a) yields

$$\ln k = \ln A - \frac{E_a}{RT}$$

or

$$\log_{10} \mathrm{k} = \log_{10} \mathrm{A} - \frac{E_a}{2.303 \cdot RT} \quad (4b)$$

In Equations (4a) and (4b) above, k is the chemical reaction-velocity constant for the forward direction of Reaction (1a); A is the pre-exponential factor representing the empirical temperature dependence on the rate constant k; E_a is the activation energy, interpreted as the average change in enthalpy between products and reactants; R is the ideal gas constant; and T is the oxidation temperature [25]. According to Equation (4b), a plot of $\log k$ vs. the inverse of the absolute temperature, $^1/_T$, called an Arrhenius plot, should give a straight line with a slope of $^{-E_a}/_{2.303R}$ and a y- intercept of $\log A$.

A related parameter used to characterize different mechanisms is the order of reaction, n. From kinetic theory, the specific rate of reaction for Reaction (1a) is given by

$$r = kP_{O_2}{}^n$$

or

$$r = kC_{O_2}{}^n \quad (5)$$

where P_{O_2} is the oxygen partial pressure at the surface in Pascals or C_{O_2}—the concentration of oxygen at the surface. Reaction order, n, is obtained from the slope of the plot of $\ln P_{O_2}$

versus $\ln k$. Reaction orders can only be determined experimentally and are often fractional, not necessarily an integer.

Using the Arrhenius Equation (4a), the specific rate Equation (5) with respect to oxygen partial pressure can be written as

$$r = Ae^{\left(\frac{-E_a}{RT}\right)} \cdot {P_{O_2}}^n \quad (6)$$

If the Arrhenius plot does not yield a straight line, generally it is assumed that side reactions and different mechanisms or catalytic properties of the materials are playing significant roles in the reactions [25]. The temperature dependence of the reaction rate yields an apparent activation energy, which has been reported in the range of 145 to 270 kJ/mol for nuclear-grade graphite [8, 26]. From kinetic theory, high activation energy suggests that the reaction proceeds either in the chemical or in-pore diffusion controlled regimes.

3. Measurements

NBG-18 graphite has a bulk density of about 1.85 g/cm^3, which is less than the theoretical density of non-nuclear-grade graphite of about 2.26 g/cm^3 [1]. This difference is mostly attributed to formation of pores in graphite during the manufacturing process. NBG-18 has less than 100 wppm metal content, and is manufactured according to ASTM standard D7219-05 that sets requirements for the chemical purity of nuclear-grade graphite [27].

3.1 Specimen and Sample Preparation

A NBG-18 graphite block 304.8 mm x 152.4 mm x 152.4 mm was obtained from the manufacturer, which was machined into approximately 12.5 mm x 12.5 mm x 12.5 mm

pieces without the use of lubricant, diamond or carbide tools according to standards established in ASTM D7542-09, Section 6.1 and 6.2 [28]. This was the ideal geometry to fit the sample bucket used in the standard thermogravimetric apparatus. Each sample was washed in methanol to displace any moisture or dust from machining and then dried in a vented tube furnace for 2 hours at 423ºK according to ASTM C1179-91 [29].

3.2 Graphite Oxidation Equipment

A Thermax700 thermogravimetric analyzer (TGA) from Thermo Scientific® was used to obtain the mass change versus temperature data in real-time during NBG-18 oxidation in air. The TGA was equipped with a small volume furnace designed to prevent convection currents. Gas flow separation is necessary to prevent contamination of the reaction chamber with purge gas but also protects the balance chamber from upward flow of corrosive gases. To maintain a constant pressure above the sample and to ensure the sample is entirely surrounded by reaction air inside the furnace, reaction inlet flow rates were set to achieve gas flow separation. Graphite samples were placed in an alumina cylindrical sample bucket with a platinum bail held from an alumina extension wire. The volume of the bucket is 35 mL. The balance has a 100 g capacity with a ±1.0 µg resolution. Mixtures of dry medical-grade air in ultra-high purity research-grade helium having a total flow rate of 50 mL/min were used in the experiment. Mass flow controllers were used to control the flow rate and helium gas streams were flowed through oxygen scrubbers. The concentration of oxygen in the TGA inlet and purge was monitored with an oxygen meter. The experimental set up is shown in Fig. 2.

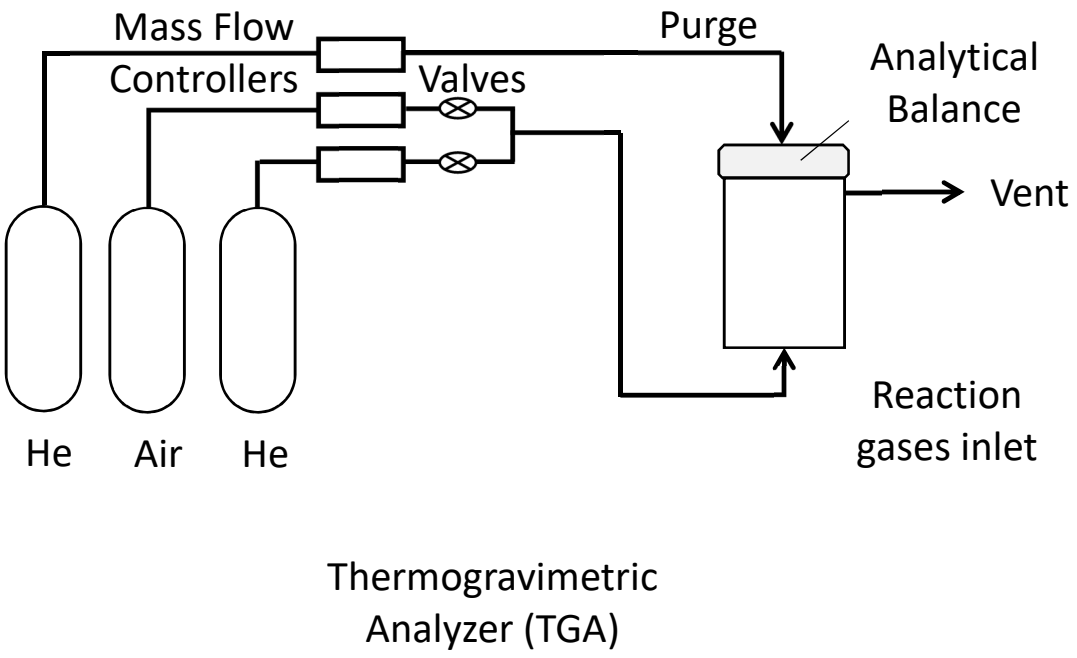

Fig. 2. A schematic of .the experimental system for studying graphite oxidation.

Graphite samples were exposed for 10 hours in four different air leak scenarios. The inlet gas stream contained 5, 10, 15 and 21 mole% O_2 concentrations. The mass loss rates were measured isothermally once the desired temperature was reached in the TGA. Mass loss data was sent from the TGA to a computer using automated data collection software.

3.3 Experimental Procedure

Graphite samples were heated at a constant rate of about 5 K/min until the desired oxidation temperature was reached, at which point samples were held at this temperature during the entire run. Also, the current experimental setup allowed changing of the TGA inlet gas stream from helium to air or a mixture containing air (i.e., O_2) and back to helium without shutting down the TGA. This feature allowed us to conduct experiments at different modes as explained below.

3.4 Modes of Experiment

Two methods were employed for collecting mass loss data with TGA.

3.4.1 Method 1, no gas switching

In the first method, which is referred to here as "no gas switching," a graphite sample was suspended in the TGA sample bucket at room temperature for 100 minutes to ensure TGA weight measurements were stabilized within ±0.01 grams before heating. Then, the heating of samples were started at a rate of 5ºK/min in the presence of the reaction gas mixtures of air in helium up to the desired temperature. The temperature was held constant during the rest of the experiment. TGA ensured that samples are always exposed to a uniform temperature zone. The isothermal oxidation temperatures were 773, 873, 923, 973, 1023, 1173, 1323, 1473 and 1873ºK and each oxidation period was about 10 hours once the desired temperature was attained. Following 10 hours of exposure, samples were cooled to room temperature at a rate of 5ºK/min in the presence of the same ultra-high purity helium.

3.4.2 Method 2, gas switching

In the second method, referred to here as "gas switching," graphite samples were heated to the target temperature in the TGA in the presence of ultra-high purity helium gas after passing it through oxygen scrubbers during ramp up to prevent any oxidation during the heating period. ASTM D7542-09, Section 12.4 and 12.5 was followed here for switching gases from an initial flow of inert gases to a flow of dry air [28]. All other parameters were kept the same as in the previous method. Once the target temperature was reached, using manual gas switching, the gas mixture containing air in helium was switched in TGA which was continued for 10 hours at the target temperature. After ten hours, the gas stream was

again switched to helium to cool the sample to room temperature. The air flow was varied in such a way that the oxygen concentration was changed from 21 mol% oxygen (100% air stream), to 15 mol%, 10 mol% and 5 mol%.

4. Results and Discussion

4.1 The Effect of Gas Switching on Mass Loss Rates

The oxidation of graphite can occur by two means. In one case, the oxygen present in the helium coolant will oxidize the graphite slowly and continuously for a long period of time. Any additional introduction of oxidants due to air ingress would cause the oxidation rate to reach a maximum before decreasing due to a large amount of graphite burnup. The transient mass loss measurements using the method of "no gas switching" are more applicable for this scenario but are not the focus of this study. On the other hand, the method of "gas switching" is more applicable to an air ingress accident scenario. In the case of a severe air ingress accident, the temperature of the graphite core increases significantly while the core becomes fully immersed in air. Figure 3 compares the effect of gas switching on the mass loss rates for NBG-18 at three different oxidation temperatures 1023, 1473 and 1873 K.

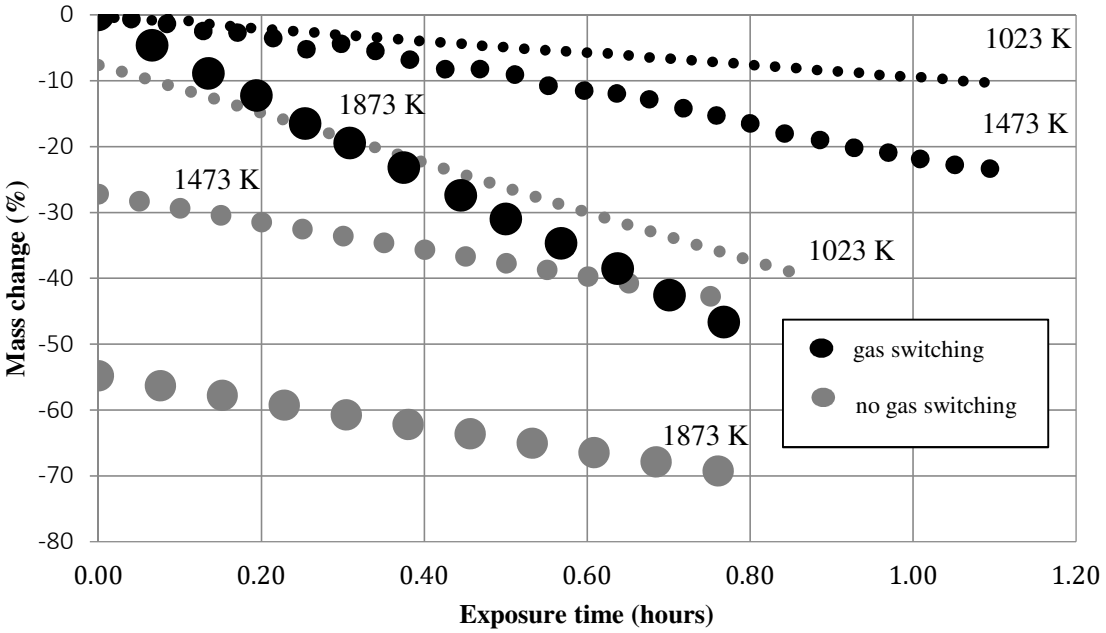

Fig. 3. TGA mass loss measurements for two modes of data collection, with "gas switching" (black) and "no gas switching" (gray).

From Fig. 3, without the use of "gas switching," the rate of mass loss actually decreased with increasing temperature. The difference in mass loss rates between gas switching and no gas switching methods suggest that different mechanisms may be involved in graphite oxidation depending on how and when graphite is exposed to oxygen. The quick oxidation of the surface at the initial heating stage may have slowed oxygen diffusion further into the graphite. Without the use of "gas switching," it is the level of burnup rather than the temperature that is a main contributing factor to the oxidation rate. Fresh additional surface would lead to increase in oxidation rates but with "no gas switching" the reaction surface reaches a maximum as oxidation increases [9, 10]. Hinnsen et al. (2008) found penetration depths decreased with increased burnup and that the reaction rate of graphite in air was not independent of specimen size [21]. Contescu et al. (2012) measured the penetration depth of oxygen into graphite at different temperatures from 873 K to 1023 K and noted that the depth of the oxidized layer decreased as oxidation temperature was increased [2]. Contescu

et al. (2012) confirmed that oxidation temperature had a more pronounced effect on the thickness of the oxidized layer of nuclear-grade graphite than the overall degree of mass loss, which is in agreement with this study [2, 30, 31]. Figure 3 suggests that when NBG-18 has lost 25 to 55% of its initial mass with no gas switching, it experiences nearly identical mass loss rates at 1473 K and 1873 K, which can be viewed as the maximum rate obtainable without the use of gas switching. Fuller and Okoh (1997) reported the maximum oxidation rate to occur at about 40% burnup [9, 22] while Su and Perlmuter (1985) reported the maximum rate to occur at about 20 to 30% burnup [9, 32]. The use of "gas switching" has ensured that the samples reach the target temperature gradually and do not lose any mass as the system is heated.

Using "gas switching" and methods outlined in ASTM D7542-09, mass loss data for NBG-18 in 100% dry-medical grade air were compared in Fig. 4 to similar recent oxidation experiments conducted at Idaho National Laboratory (2010) on NBG-18 [7, 28].

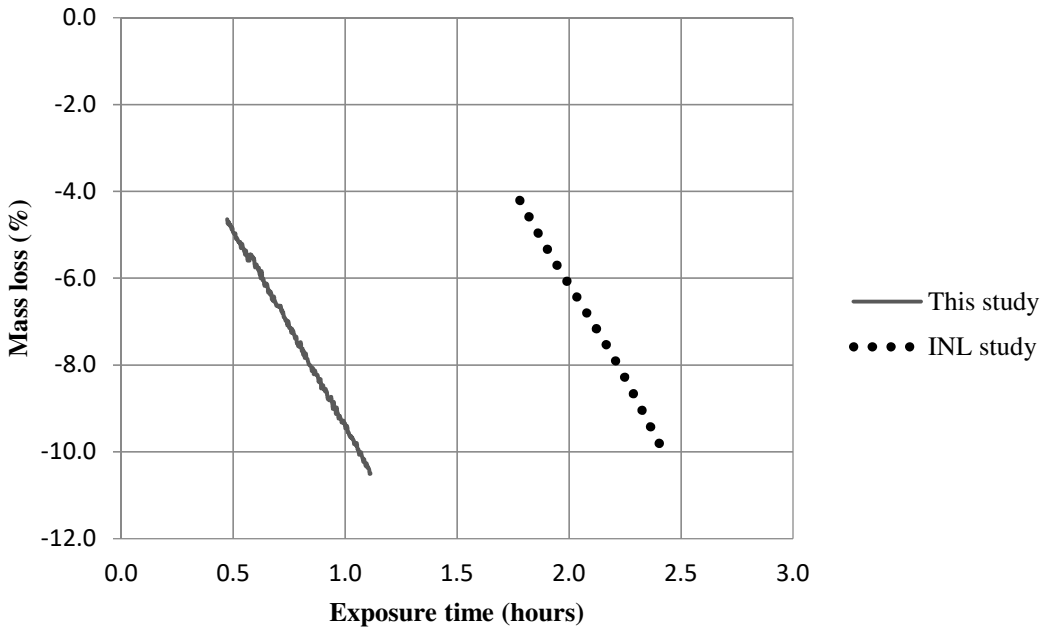

Fig. 4. The results of this study compared to INL study for NBG-18 oxidation in 100% air at 1023 K.

Interestingly, both experimental studies resulted in similar rates of mass loss based on the slopes of the curves in Fig. 4; the mass loss curve from the INL study was shifted by 45 minutes. This suggests that it took some time for the graphite sample in the INL study to reach the desired temperature even though the air was preheated. Our study and other studies have shown that the mass loss is minimal (less than 2%) below 873 K. Therefore, it appears that in the INL study, it took about 45 minutes to cross this threshold temperature when the sample begins to lose mass.

4.2 The Effect of Temperature on Oxidation Rate

Mass loss data that were obtained in the TGA "gas switching" mode using 100% dry medical-grade air at 773, 873, 923, 973, 1023, 1173, 1323, 1473 and 1873ºK are shown in

Fig. 5. Oxidation runs were performed twice to check the reliability and repeatability of the data. A very good repeatability of the data was observed.

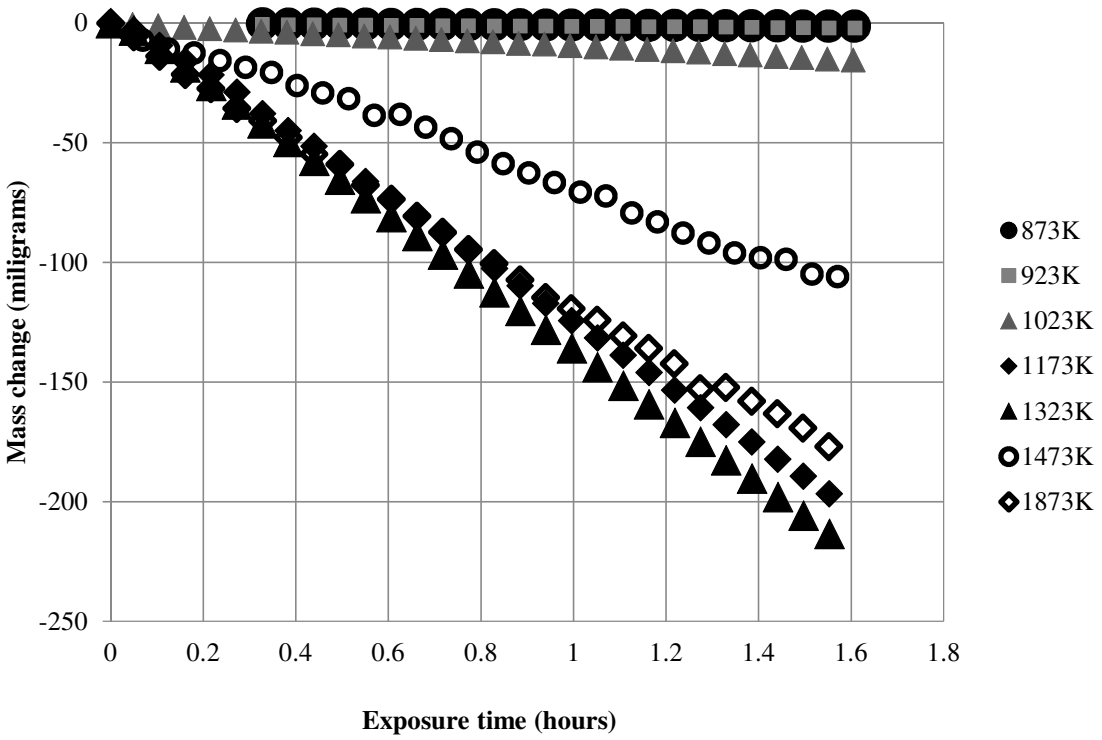

Fig. 5. NBG-18 isothermal mass loss measurements in 100% air (21 mol% O_2) for 873 to 1873 K.

At 773 K, there was no appreciable mass loss for NBG-18 nuclear graphite. At 873 K, there was about 2 to 5% average mass loss in 10 hours. Other researchers [9, 16] have noted that 20 to 30 hours of exposure were necessary to achieve this type of mass loss at temperatures lower than 873 K. According to ASTM D7542-09, the rate of mass loss is determined by a linear fit of the data obtained during 5 to 10% loss of the initial mass [28]. It is assumed that after 5 to 10% initial mass loss, a steady-state oxidation rate for nuclear-grade graphite is established [28, 29]. As the oxidation temperature was increased from 923 K to 1023 K the time to obtain 5 to 10% mass loss from oxidation was reduced to 1 to 2 hours. At oxidation temperatures between 1173 K to 1873 K, 5 to 10% mass loss was

observed within minutes. However, in this study, for higher oxidation temperatures, the mass loss rate did not reach a steady-state until at least 20 to 30% mass loss.

According to Fig. 5, the average mass loss rates increased sharply above 1023 K as the reaction between graphite and air approached a maximum at the surface and pore walls. In the temperature range of 1323 to 1473 K, there is a consistent decrease in the mass loss rates, which can be attributed to the change of oxidation mechanism from being chemically-controlled to diffusion-controlled. This phenomenon has also been observed by other researchers who attributed a decrease in mass loss rates due to excessive carbon monoxide production from the Bouduard reaction, Reaction (2a), and also to a change in total reaction surface area and sample size [9, 10]. As surface active sites become covered by product gas during oxidation, oxygen transport to the graphite surface is inhibited. The mass loss rates again decrease at 1873 K because of the change in the oxidation mechanism at this temperature. At higher temperature regimes beyond 1473 K, the oxidation rate is no longer influenced by materials characteristics but by mass transfer resistance.

Arrhenius plots were made using the slopes of the TGA mass loss data in Fig. 5 by following the procedure suggested in ASTM 7542-09. Table 3 provides the oxidation rates of NBG-18 in 100% air. It may be noted that the mass loss rate at 1473 K did not follow the increasing trend when area-normalized data was used.

Table 3
Mass loss rates, area-normalized and weight-normalized oxidation rates, average of two trials.

T	Mass Loss Rates	OR^a	OR^w
K	mgs hr^{-1}	g hr^{-1} m^{-2}	g hr^{-1} g^{-1}
773	-	-	-
873	1.261	25.070	0.002
923	1.096	21.810	0.003
973	15.023	298.416	0.048
1023	42.870	852.900	0.134
1173	114.060	2269.150	0.164
1323	140.940	2645.450	0.187
1473	77.075	1597.640	0.259
1873	174.280	3467.190	0.383

a-area normalized, w-weight normalized

Both weight- and area-normalized rates are reported in the literature, however, area-normalized rates are generally used if samples have a similar surface-to-volume ratio to each other as they do in this study. Figure 6 is a comparison of the oxidation rates of NBG-18 in 100% air between this study and that of Chi and Kim (2008), who used a 3-zone tube furnace [16]. A very good agreement between these two sets of data is observed.

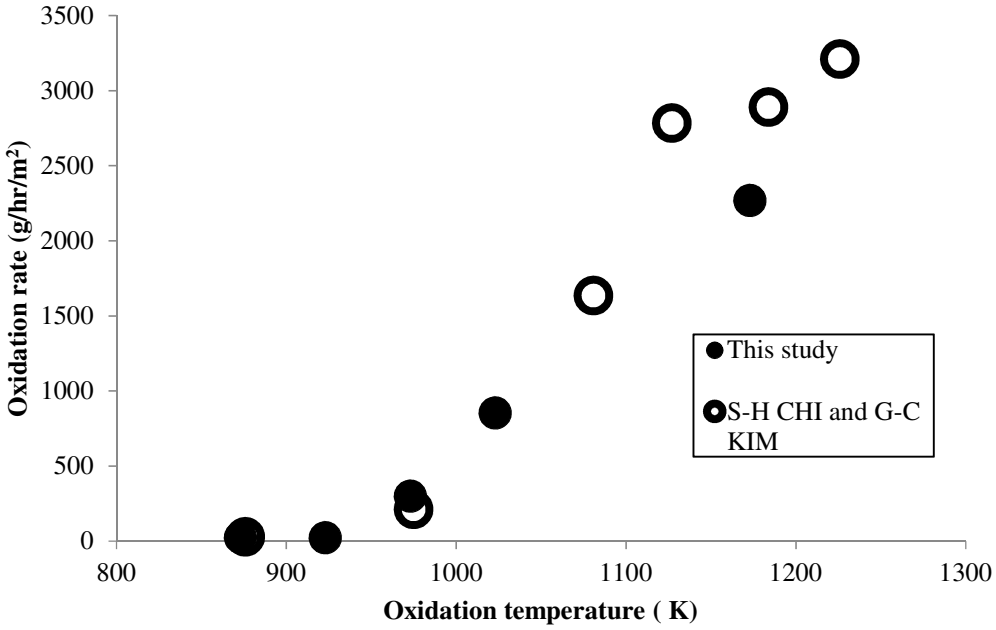

Fig. 6. Comparison of NBG-18 oxidation rates between this study and S.-H. Chi and G.-C. Kim [16].

The procedure outlined in ASTM 7542-09 was adopted to calculate the activation energies for three regimes from an Arrhenius plot. Figure 7 is the Arrhenius plot for NBG-18 oxidation regimes applicable for the mass loss rates normalized to sample surface area.

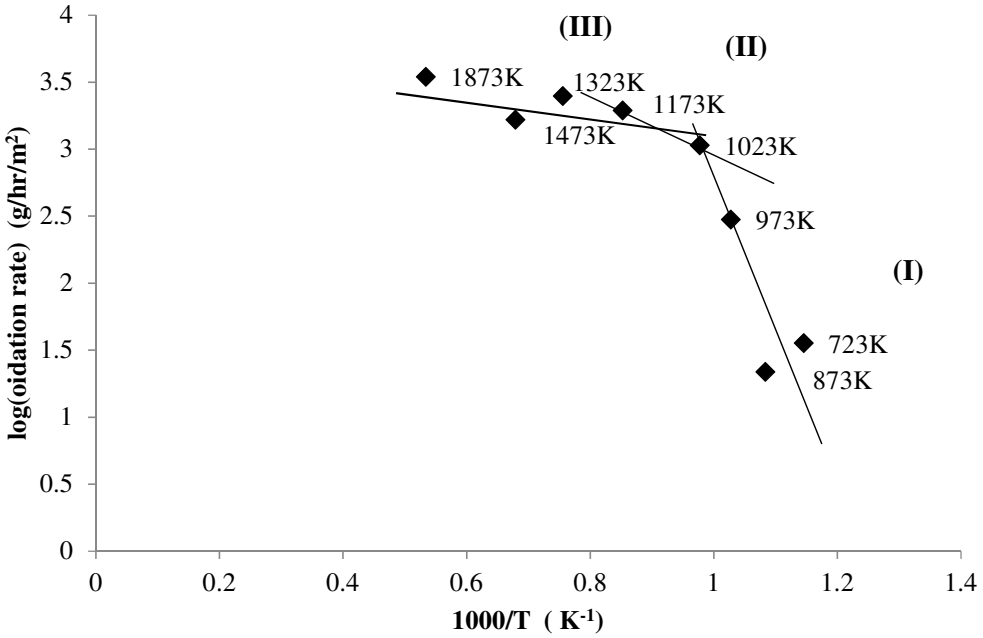

Fig. 7. Arrhenius plot of NBG-18 oxidation.

Activation energies calculated from the slopes of the best-fit lines of each regime of the Arrhenius plot are given in Table 4. The data are averaged over two runs for each regime. The activation energy for Regime I was 187 kJ/mol for NBG-18 and is well within the range of reported activation energies for NBG-18 oxidation in the literature which are compared in Table 5.

Table 4.
Summary of activation energies for NBG-18 oxidation at temperatures between 873 and 1873 K.

Regime	E_a (kJ/mole)	Temperature Range (K)
I	187.00	873 to 1023
II	32.03	1023 to 1323
III	16.29	1323 to 1873

Table 5.
Summary of activation energies for NBG-18 oxidation 100% air from previous studies and this study.

Author	Ea (kJ/mole)	Temperature Range (K)	Method
This Study	187	873 to 1023	TGA
Chi and Kim [16]	157	876 to 1081	3-zone furnace
Contescu [24]	186	873 to 1023	TGA

4.3 The Effect of Oxygen Concentration on Oxidation Rate

Figure 8 shows the effect of oxygen concentration on the mass loss rates of NBG-18 at 1023 K. The experiments were continued for 10 hours.

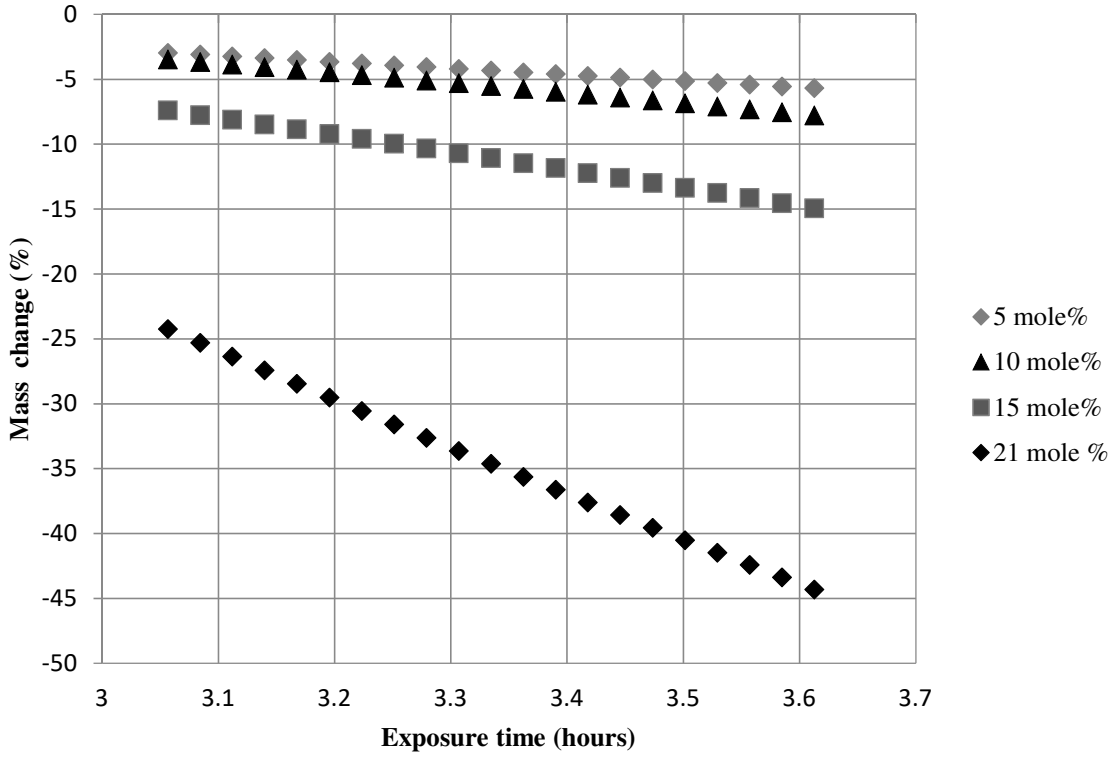

Fig. 8. TGA mass loss measurements for NBG-18 at 1023 K in various oxygen concentrations for 5, 10, 15 and 21 mole% O_2.

A steady mass loss rate was observed at all oxygen concentrations as the oxidation of graphite proceeds uniformly through the bulk of the samples at this temperature. However, for 21 mol% oxygen concentration (full leak scenario), the oxidation rate was very high compared to other oxygen concentration in the gas mixture. As the graphite is more and more exposed to an oxidative environment, it appears that in a full air ingress accident at this temperature, bulk oxidation would proceed at a steady and rapid rate.

Using the experimental mass loss data for four concentrations of oxygen at 1023 K, the order of the reaction with respect to oxygen partial pressure was determined from a linear fit of the data. Figure 9 is a plot of ln k vs. ln P_{O2} used to determine the reaction order. The reaction order of 1.25 was found. The order of reaction generally provides some indication of the effect of a reactant's concentration on the reaction rate. Reaction order does not necessarily have to be an integer value, although a number of researchers may prefer to round to an integer. The fractional order merely indicates a better fit to the data. In this case, the results indicate that the reaction order is approximately first-order of the partial pressure of oxygen on the surface of graphite. The reaction order obtained in this study is well within experimentally accepted values between 0.54 and 1.3 for dense and nuclear-grade graphites [7, 16, 18, 20].

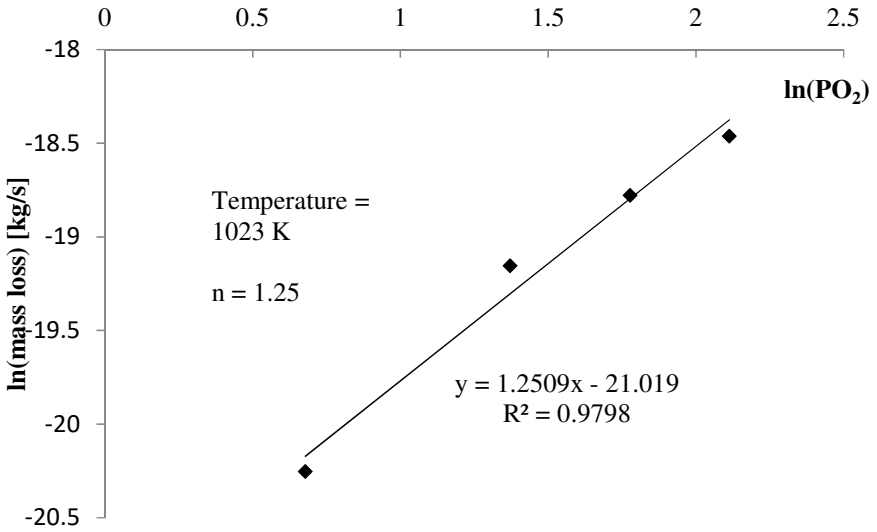

Fig. 9. Order of reaction with respect to the oxygen partial pressure for the elementary reaction between graphite and air.

4.4 The Rate Equation for the Kinetic Regime of NBG-18 Oxidation

An overall kinetic rate equation for the oxidation of NBG-18 can be written as shown in Equation (7). In Regime I between 873 and 1023 K, the slope and intercept from Fig. 7 were $-\frac{E_a}{2.303 \cdot R} = -9.768$ where $R = 8.314$ J/mol K and $\log_{10} A = 12.439$, respectively. The activation energy E_a of NBG-18 oxidation in the kinetic regime in 100% air was determined to be 187 kJ/mole and the pre-exponential factor A was 0.275×10^{13} g/hr/m^2, which is two orders of magnitude higher than that reported by Chi and Kim [16]. Using the Arrhenius Equation (4a), the reaction rate velocity for Regime I applicable from 873 to 1023 K becomes

$$k_I \left(\frac{g}{hr \cdot m^2}\right) = 0.275 \times 10^{13} \cdot e^{-\left(\frac{186.999 \frac{kJ}{mol}}{T(^\circ K)}\right)} \tag{7}$$

Using Equation (6) and the reaction order determined in Section 4.3, the specific reaction rate of Reaction (1a) with respect to partial pressure of oxygen on the surface is given by Equation (8).

$$r_I\left(\frac{g}{hr\cdot m^2}\right) = 0.275 \times 10^{13} \cdot e^{-\left(\frac{186.999\,\frac{kJ}{mol}}{T(°K)}\right)} P_{O_2}^{1.25} \quad (8)$$

4.5 Surface Characterization of Pure and Oxidized NBG-18

Changes in surface characteristics of NBG-18 due to oxidation were studied using several techniques, including scanning electron microscopy (SEM), electron dispersive spectroscopy (EDS), x-ray photoelectron spectroscopy (XPS), and Fourier Transform Infrared Spectroscopy (FTIR). Figures 10a and 10b show SEM micrographs of pure NBG-18 graphite at 52 and 10,000 times magnification. Cracks and shrinkage are visible on the pure graphite surface. At higher magnification (See Figure 10b), filler material consisting of carbonaceous sheets can be seen in more detail.

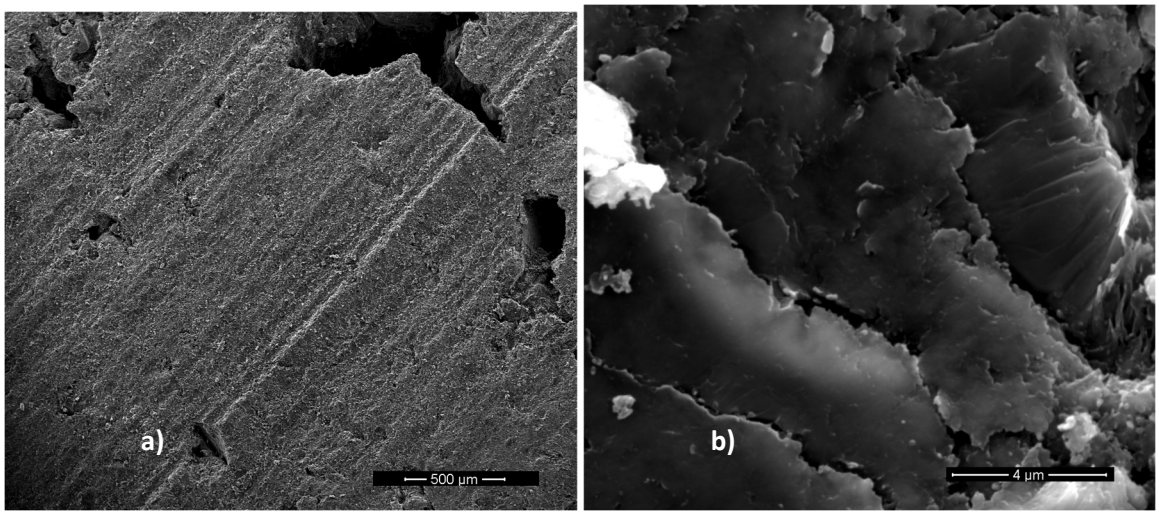

Fig. 10. SEM micrograph of the surface of pure, unoxidized NBG-18 nuclear-grade graphite, **a.)** 52X Mag. **b.)** 10000X Mag.

The microstructure of manufactured nuclear graphite consists of coke filler and binder. Figure 11 shows areas of shrinkage, pores, filler and binder materials, which surrounds the filler particles. The filler material has been identified as a particle with a

spherical geometry and a maximum diameter of about 1600 microns (medium-grain size) [3]. The spherical shape of the filler particle has been typically associated with coal-coke graphite such as NBG-18. The nature of the coke determines how the filler and pore microstructure form. Shrinkage is often found around the filler particle as basal planes of carbonaceous material are established during calcinations [3].

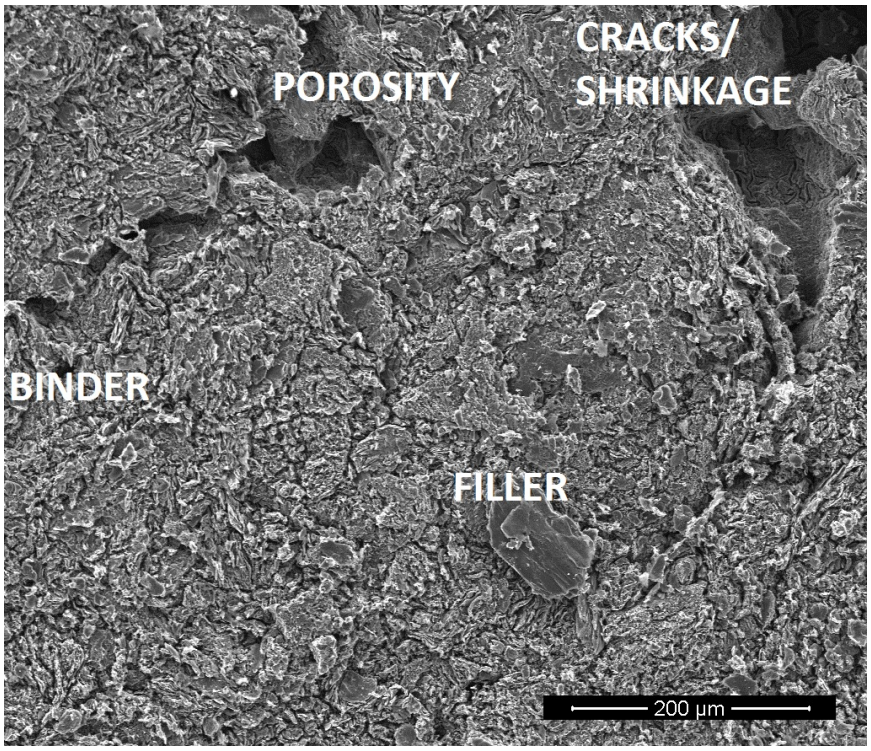

Fig. 11 SEM micrograph of an unmachined portion of pure NBG-18 graphite showing filler, binder, porosity and shrinkage.

The binder material is preferentially oxidized in nuclear graphite given their chaotic structure [30]. SEM micrographs of NBG-18 oxidized in 100% air for 10 hours at 1023 K using TGA are shown in Figs. 12a and 12b.

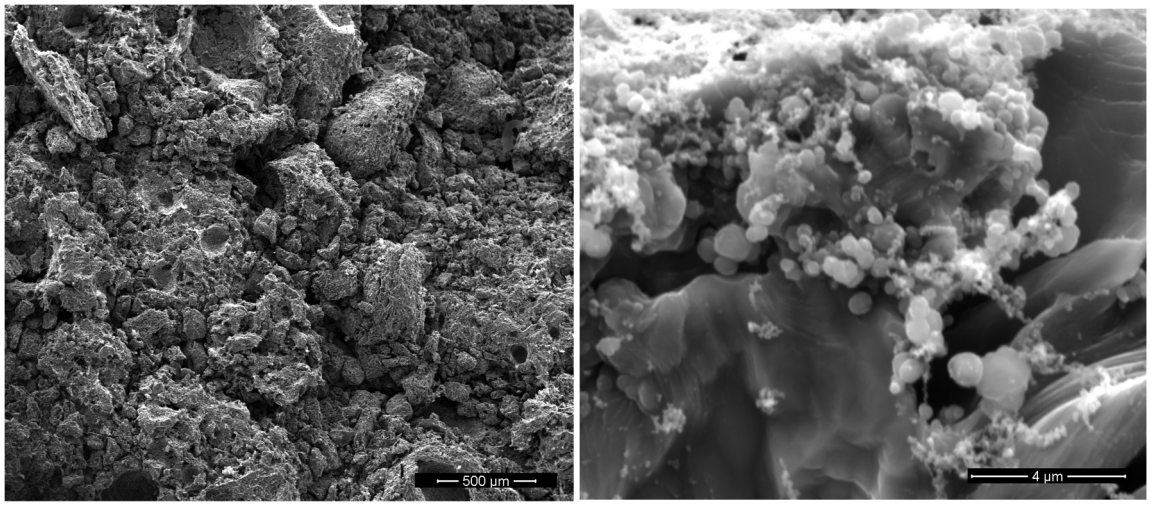

Fig. 12. SEM micrograph of the surface of NBG-18 nuclear-grade graphite after oxidation at 1023 K in 100% air for 10 hours. **a.)** 52X Mag. **b.)** 10000X Mag.

As can be seen from Figs. 12a and 12b, the surface characteristics of NBG-18 changed significantly at this oxidation temperature and the oxidation was not uniform on the surface. Compared to Fig. 10a, the surface of the oxidized sample in Fig. 12a is rough and large voids are visible. Figure 12b is a high magnification micrograph of the filler and surrounding binder material of the same sample. Moorman [20] noted that the activation energy depends on the composition of the graphite and that lower activation energies for oxidation are generally expected for the binder (~123 kJ//mol) compared to the filler material (~152 kJ/mol). In Fig. 12b, most of the carbonaceous layers of the filler are visible while the binder surrounding the filler has been changed by oxidation compared to Fig. 10b.

EDS and XPS methods were used to obtain qualitative information about the elements present on the sample surface and their oxidation state. Figure 13 shows the EDS results of unoxidized and oxidized NBG-18.

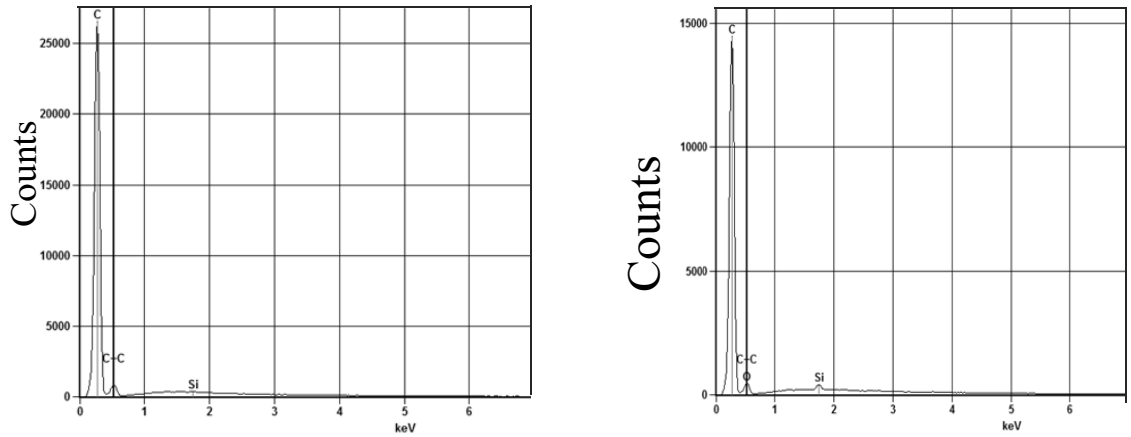

Fig. 13. EDS of pure NBG-18 nuclear-grade graphite (left) and oxidized NBG-18 in 100% air at 1023 K.

EDS results show that oxidized NBG-18 has a smaller carbon signal and larger oxygen signal after oxidation but also silicon was detected in the sample. The silicon was also identified in X-ray photoelectron spectroscopy (XPS) data. However, the source of silicon could not be identified. A larger oxygen signal suggests formation of various oxygen-carbon complexes on the surface.

XPS broad-scan spectrum was used to identify surface elements and also for quantitative analysis. Unoxidized and oxidized samples of nuclear graphite are shown in Fig. 14. The XPS results show that the oxygen content of samples was increased after oxidation. The O_{1s} peak (BE = 532 eV) of oxidized NBG-18 is larger than that of the pure, unoxidized NBG-18. Oxygen-containing groups and complexes have formed on the surface of graphite samples which probably contributed to a higher signal in XPS as well as in EDS. A weak O_{1s} peak for other grades of unoxidized nuclear graphite, such as IG-110, have been observed by Choi et al. [19].

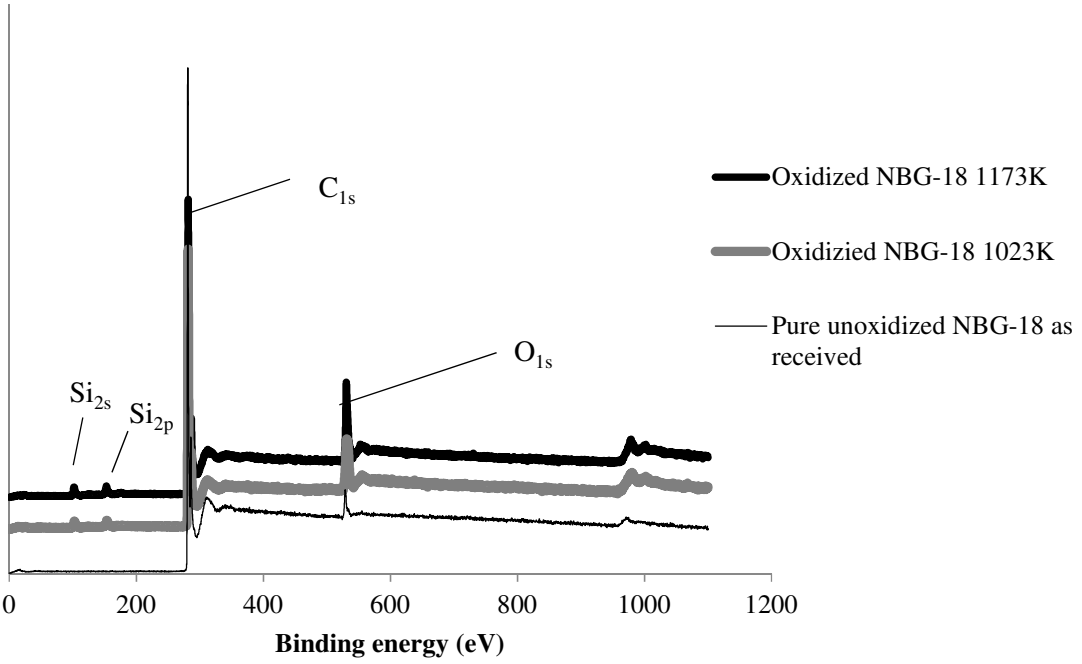

Fig. 14. XPS broad-scan spectra of unoxidized and oxidized NBG-18 at 1023 K and 1173 K.

Figure 15 shows FTIR spectrum for three samples: pure NBG-18 and two NBG-18 samples after oxidation treatment at 1023 K. Two oxidized samples were obtained from the same oxidized cylindrical sample: a.) one sample was the graphite layer machined from the first outer shell of 0.5 mm depth and b) the other sample was from a layer 1.0 mm depth from the oxidation surface. Various oxidation complexes were identified on the surface. The peak around 2400 cm^{-1} is indicative of O=C=O stretch vibration of CO_2 adsorbed in pores. Appearance of several other peaks following oxidation is evident in these spectra and complements the XPS and SEM analyses.

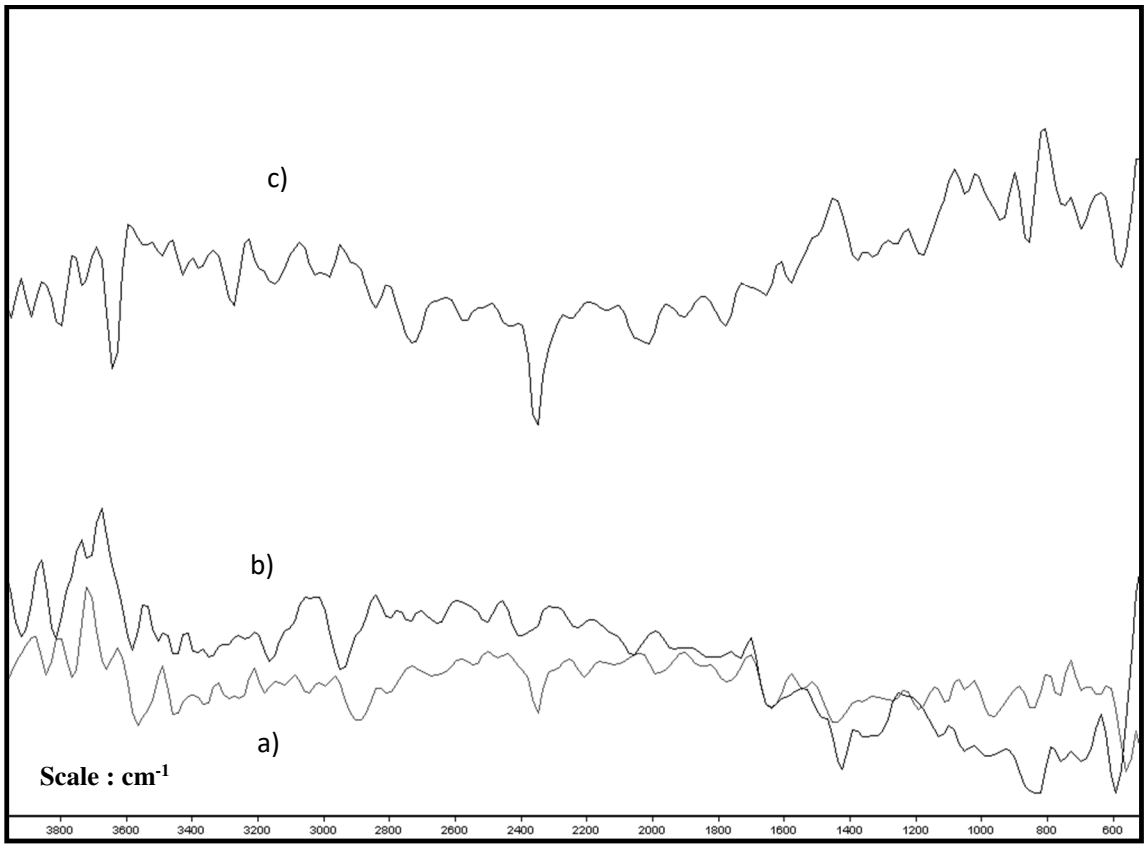

Fig. 15. FTIR spectrum of NBG-18 graphite oxidized in 100% air at 1023 K a.) pure, unoxidized NBG-18, b.) sampled from 0.5 mm from surface, c.) sampled from 1.0 mm from surface.

4.6 Bulk Density Profiling Method for Oxidized Nuclear Graphite

Apart from the kinetic study, graphite cylinders were steadily oxidized in TGA to study the penetration depth of oxygen in NBG-18. There is a strong correlation between the density of nuclear graphite and its physical and mechanical properties [7, 9, 10, 17, 30, 31]. During oxidation, oxygen penetrates the graphite creating more porous structure and in the process degrades structural properties. To investigate the penetration of oxygen into bulk graphite samples and any trend in density, NBG-18 samples were prepared into right cylinders with the following dimension: 19.1 mm x 31.5 mm. Following oxidation of the sample in TGA, bulk density measurements were carried out according to ASTM C559-90 [33]. Machined NBG-18 cylinders were washed in methanol and oven dried in a vented

tube furnace for 2 hours at 423ºK according to ASTM C1179-91 [29]. Then, a single cylindrical sample was freely suspended inside the TGA furnace for oxidation using gas switching to control the flow of initial weight loss of sample during ramping. The graphite rod was positioned inside the reaction tube in a special high temperature wire bucket that was exposed to the flow of air from the base of the cylinder. The oxidation temperature tested was 973 K in 100% dry air flowed at 50 mL/min for 5 hours at a rate of 5 K/min. About 5 hours exposure time in air at 973 K has been correlated to about 10% weight loss of NBG-18.

The oxidized graphite cylinder was then carefully weighed and the diameter and height were recorded. Several measurements of the diameter were taken along the height of the cylinder and were averaged to account for the direction of reaction air flow originating from the base of the sample. The oxidized cylinder was positioned axi-symmetrically on a lathe to remove graphite layer by layer at increments of 0.5 mm each. Radial layers of the oxidized sample were removed sequentially (step machining method) until the sample could not be machined further. For each layer removed, bulk mass measurements were obtained from the remaining cylinder on an analytical balance at room temperature and several diameter and height measurements were carefully made on the remaining sample. Change in density of the removed layers could be obtained from the previous step density measurement.

4.7 Density Profile and Oxygen Penetration

The density profile of NBG-18 oxidized in 100% dry air at 973 K for 5 hours is shown in Fig. 16. Table 6 contains the corresponding densities that were calculated with bulk measurements made after step machining an oxidized NBG-18 cylinder.

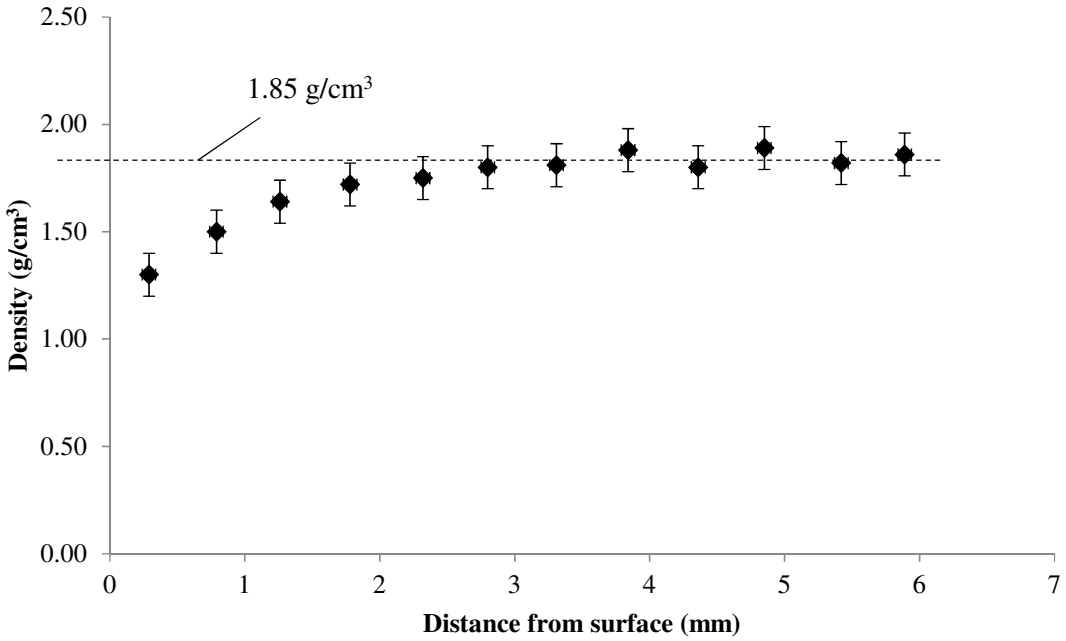

Fig. 16. Density profile of oxidized NBG-18 cylinder in 100% dry air at 973 K

According to the data shown in Fig. 16, the density of NBG-18 changed to a depth of about 3 to 4 mm from the surface. Contescu et al. have noted oxygen penetration depths of about 6 mm for NBG-18 using non-destructive image processing [2] and depths of about 3 to 4 mm for NBG-10 [17].

Table 6
Bulk density measurements from step machining oxidized NBG-18 at 973 K.

Depth from Surface (mm)	**Density of Removed Layer** (g/cm^3)
0.00 ± 0.02	1.68 ± 0.09
0.29	1.30
0.79	1.50
1.26	1.64
1.78	1.72
2.32	1.75
2.80	1.80
3.31	1.81
3.84	1.88
4.36	1.80
4.85	1.89
5.42	1.82
5.89	1.86

5. Conclusions

Nuclear-grade graphite NBG-18 did not oxidize in air up to a temperature of about 873 K. At a temperature higher than 873 K, the oxidation rate was dependent on both temperature and oxygen concentration. The oxidation mechanism depended mainly on the temperature regime. Three regimes were observed; the oxidation rate was chemically controlled between 873 K to 1023 K, both chemically and diffusion-controlled between 1023 K and 1473 K, and mass-transfer dominated at temperatures beyond 1473 K. The activation energy calculated from the mass loss rate was 187kJ/mole for NBG-18 in 100% air and was found to be similar to that reported in the literature for NBG-18. The reaction order for air and NBG-18 graphite was determined to be about 1.25 which is also within an acceptable range of reported values. SEM imaging, XPS, EDS and FTIR spectra

obtained from pure and oxidized NBG-18 samples suggested significant surface damage due to oxidation at 1023 K. Furthermore, the oxygen penetration depth of about 3 to 4 mm at 973 K found in this study is within the same range as those reported in the literature.

ACKNOWLEDGEMENTS: This work was partially supported by the NERI-C-08-043 grant from the Department of Energy. During the course of this work, Jo Jo Lee was a recipient of a Department of Education Graduate Assistance in Areas of National Need (GAANN) Fellowship.

References

[1] IAEA: Thermophysical Properties of Materials for Nuclear Engineering: A Tutorial and Collection of Data, International Atomic Energy Agency, Vienna (2008).

[2] C. I. Contescu, T. Guldan, P. Wang, T. D. Burchell, Carbon 50 (2012) 3354-3366.

[3] J. Kane, C. Karthik, D. P. Butt, W. E. Windes, R. Ubic, J. Nucl. Mater. 415 (2011) 189-197.

[4] B. Castle, INL/EXT-10-19533, November 2010, p. 21.

[5] X. Yu, L. Brissonneau, C. Bourdeloie, S. Yu, Nucl. Eng. Des. 238 (2008) 2230-2238.

[6] S. Sato, K. Hirakawa, A. Kurumada, S. Kimura, E. Yasuda, Nucl. Eng. Des. 118 (1990) 227.

[7] R. E. Smith, Status of Graphite Oxidation Work, INL/EXT-10-18880, May 2010.

[8] M. Eto and F. B. Growcock, Effect of Oxidizing Environment on the Strength and Oxidation Kinetics of HTGR Graphites, Part 1: Reactivity and Strength Loss of H451, PGX and IG-11 Graphites, BNL-NUREG-51493 (1981).

[9] X. Luo, J.-C. Robin, S. Yu, Nucl. Eng. Des. 227 (2004) 273-280.

[10] X. Luo, J.-C. Robin, S. Yu, Nucl. Sci. Eng. 151 (2005) 121-127.

[11] M. S. El-Genk, J.-M. P. Tournier, J. Nucl. Mater. 411 (2011) 193-207.

[12] P. I. Walker, R. I. Taylor, J. M. Ranish, Carbon 29 (1991) 411-421.

[13] S. Ahmed, M. H. Back, Carbon 23 (1985) 513-524.

[14] T. Hurt, B. S. Haynes, Proc Combustion Institute 30 (2005) 2161-2168.

[15] X. Zhou, H. Wang, S. Yu, Nucl. Eng. Des. 241 (2001) 752-754.

[16] S.-H. Chi, G.-C. Kim, J. Nucl. Mater. 381 (2008) 9-14.

[17] S.-H. Chi, C. I. Contescu, T. D. Burchell, J. of Eng. Gas Turb. Pow. 131, September 2009.

[18] E.S. Kim, H. C. No, J. Nucl. Mater. 349 (2006) 182-194.

[19] W.-K. Choi, B.-J. Kim, E.-S. Kim, S.-H. Chi, S.-J. Park, Nucl. Eng. and Des. 241 (2011) 82-87.

[20] H.-K. Hinnsen, K. Kuhn, R. Moormann, B. Schlogl, M. Fechter, M. Mitchell, Nucl. Eng. Des. 238 (2008) 3018-3025.

[21] H.-K. Hinssen, W. Katcher, R. Moormann, Kinetics der Graphite/Sauerstoff Reaction Juel-1875 (1983).

[22] E. L. Fuller and J. M. Okoh, J. Nucl. Mater. 240 (1997) 241-250.

[23] A. Blanchard, Appendix 2, IAEA-TECDOC-1154 (2003) 207-213.

[24] C. I. Contescu, S. Azad, D. Miller, M. J. Lance, F. S. Baker, T. D. Burchell, J. Nucl. Mater. 381 (2008) 15-24.

[25] J. M. Smith, Chemical Engineering Kinetics, McGraw-Hill (2d ed, 1956) 71.

[26] P. L. Walker, Jr., M. Shelef, R. A. Anderson, Chem. and Phys. of Carbon 4 (1968) 287-383.

[27] ASTM D7219-05. Standard specification for isotropic and near-isotropic nuclear graphites. ASTM, Int, 2005.

[28] ASTM D7542-09. Standard test method for air oxidation of carbon and graphite in the kinetic regime.

[29] ASTM C1179-91 (Reapproved 2010), "Standard Test Method for Oxidation Mass Loss of Manufactured Carbon and Graphite Materials in Air."

[30] R. P. Wichner, T. D. Burchell, C. I. Contescu, J. Nucl. Mater. 393 (2009) 518-521.

[31] E. S. Kim, C. H. Oh, H. C. No, B. J. Kim, Nucl. Eng. Des. 238 (2008) 837-847.

[32] J. L. Su and D. D. Perlmuter, AIChE J. 31, (1985) 157-160.

[33] ASTM C559-90 (Reapproved 2010), "Standard Test Method for Bulk Density by Physical Measurements of Manufactured Carbon and Graphite Articles."

CHAPTER 3

Oxidation rate of nuclear-grade graphite IG-110 in the kinetic regime for VHTR air ingress accident scenarios

Jo Jo Lee, Tushar K. Ghosh, Sudarshan K. Loyalka*

Nuclear Science and Engineering Institute, Particulate Systems Research Center,
University of Missouri, Columbia, Missouri 65211
**Corresponding Author: Phone: +15738823568, Fax: +15738844801, Email: loyalkaS@missouri.edu*

Abstract

The oxidation rates of nuclear-grade graphite IG-110 in the kinetically-controlled temperature regime of graphite oxidation were predicted and compared in Very High Temperature Reactor air ingress accident scenarios. The oxidative mass loss of graphite was measured thermogravimetrically from 873 to 1873 K in 100% air (21 mol%). The activation energy was found to be 222.07 kJ/mol, and the order of reaction with respect to oxygen concentration is 0.76. The surfaces of the samples were characterized by Scanning Electron Microscopy, Energy Dispersive Spectroscopy, Fourier Transform Infrared Spectroscopy and X-ray Photoelectron Spectroscopy before and after oxidation. These results are compared with those available in the literature, and our recently reported results for NBG-18 nuclear-grade graphite using the same technique.

---

1. Introduction

Oxidation damage to core structural material and fuel elements constructed of nuclear-grade graphite during an air ingress accident is expected to be severe. The Very High Temperature Reactor (VHTR) is a Generation IV reactor concept which comprises the

High Temperature Gas-Cooled Reactor (HTGR) but with a potential core outlet temperature of at least 1273 K. In the event that the reactor core suffers a depressurization accident and there is long-term loss of forced convection to the core, an air ingress accident due to a pipe break can cause the reactor core to become immersed in air at temperatures approaching 1873 K. Currently, there is a need to study the extent of oxidation damage to reactor components and fuel constructs made from different nuclear-grade graphite types.

Nuclear-grade graphite types vary greatly in manufacturing process, composition and performance, so there is a need to develop oxidation models that are specific to the type. Nuclear-grade graphite tends to differ significantly from non-nuclear grade graphite in purity standards and density but the microstructure is also vastly different due to the formation of pores from gas evolution and thermal contraction during the manufacturing process [1]. Different types of nuclear graphite have been designated for specific uses in the VHTR system. Candidate nuclear-grade graphite, such as IG-110 and NBG-18, are manufactured from different coke types and filler particles of different sizes. The coke type and grain size dictate the development of a pore system during oxidation. Porosity directly correlates to the availability of reaction surface area which ultimately affects the oxidation rate [2,3]. The purpose of this study is to measure the oxidation rates of IG-110 nuclear-grade graphite during VHTR air ingress accident scenarios and compare the oxidation performance of IG-110 to NBG-18 tested under the same conditions in a previous study [4]. Notably, IG-110 and NBG-18 are vastly different nuclear-grade graphite types but both are intended for use in the high-irradiation dose areas of the VHTR system, so there is an additional motivation to compare their oxidation rates and microstructural

changes after oxidation treatment. We have reported results for NBG-18 recently [4], so our focus here is on the results for IG-110 and comparisons with NBG-18.

2. Past graphite oxidation studies

Generally, the coke type and particle size dictate the formation of a pore system during oxidation that is unique to the type [3,5-7]. Nuclear-grade graphite IG-110 is a super fine-grained, historical reference grade which is currently being used as fuel blocks in the High Temperature Graphite-Moderated Helium-Cooled Test Reactor (HTTR) in Japan and also as fuel and replaceable reactor components in the experimental pebble bed reactor at Tsinghua University (HTR-10) in China. IG-110 is isostatically-molded, petroleum coke filler-based nuclear-grade graphite manufactured by Toyo Tanso® in Japan. The average coke filler grain size is about 20 μm and the particles have acicular shape. IG-110 is less porous than most modern graphite types, such as PGX, PCEA or NBG-18.

In short, the difference between the oxidation rate of nuclear-grade graphite types collapses to the difference between the filler coke source, impurity level and especially the coke particle size [2,3,6,7]. Many researchers have compared and contrasted the properties and performance of candidate nuclear-grade graphite types as noted in Table 1. According to past research, there is no real agreement over the oxidation rate measurements for IG-110. Furthermore, data for very high temperatures are generally not available.

Table 1
Survey of current graphite oxidation research comparing modern nuclear grades.

Research group	Graphite types	Temperature ranges	Study
Chi and Kim [2]	NBG-18, NBG-25, IG-110, IG-430	873 and 1223 K	Oxidation performance Coke type
Contescu et al. [7]	NBG-18, IG-110	873 and 1023K	Grain size Frequency Factor
Choi et al. [6]	NBG-17, NBG-25, IG-110, IG-430	873 K	Porosity BET surface area
Luo, Robin and Yu [8]	PAEB, PCEB, PPEA, IG-11	673, 973 and 1473 K	Anisotropy Impurity content

Chi and Kim oxidized various nuclear-grade graphite types and compared the brands based on their coke types irrespective of manufacturing process [2]. They tested NBG-18, NBG-25, IG-110 and IG-430 at six oxidation temperatures between 873 and 1223 K in air using a 3-zone vertical furnace. They observed a clear effect of the coke type on mass loss during oxidation treatment at about 873 and 973 K. At both temperatures, the coal coke-based graphite (IG-430 and NBG-18) demonstrated higher oxidation resistance than petroleum coke-based graphite (IG-110 and NBG-25). It was concluded that oxidation at these temperatures was greatly affected by the characteristics of the materials and chemical reactions. Overall, NBG-18 was observed to be least oxidized among samples for the six temperatures tested between 873 and 1223 K. This was attributed to the higher density, larger grain size, and lower frequency factor for NBG-18. Differences between coke types disappeared at temperatures between 1023 and 1123 K. Tests beyond 1223 K were not performed. The average activation energy of the graphites tested by Chi and Kim was 161 kJ/mol.

Contescu et al. noted that flake-like NBG-18 graphite had volumes of large pores. NBG-18 oxidized less than IG-110 in direct comparison [7]. The smaller grain size of IG-

110 resulted in a larger amount of high energy exposed edges along basal planes in graphite crystallites. They also found, as Chi and Kim [2], that the frequency factor of IG-110 was higher than NBG-18.

Choi et al. oxidized nuclear graphite grades NBG-17, NBG-25, IG-110 and IG-430 at 873 K in a comparative study between coke types [6]. At this temperature a very slow oxidation reaction was observed between air and graphite. Through Scanning Electron Microscopy (SEM), X-ray Photoelectron Spectroscopy (XPS), Brunauner, Emmett and Teller (BET) surface area measurements, they found that pores on average were increased after this treatment for each type of graphite tested, and surface functional groups were identified on the graphite samples. However, the surface of graphite was seen to behave in a unique manner for each grade tested [6]. Interestingly, the surface area of NBG-17, which is a coal coke-based nuclear-grade graphite similar to NBG-18, increased only slightly but for petroleum coke-based IG-110 the surface area increased significantly. The oxidation behavior based on mass loss data was different between the grades. The mass loss rates of IG-110 and NBG-25, which are also petroleum coke-based graphite, were faster than that of NBG-17 and IG-430 coal-coke based grades. The researchers observed a large increase in BET surface area from 0.09 to 1.47 m^2/g after oxidation of IG-110 in air [6].

Studies on IG-11 provide some basis for predicting the performance of isotropic graphite grades in air. Notably, IG-11 is the originally formulated nuclear-grade graphite that is purified into IG-110, bringing the stock impurity level and ash content of about 400 wppm in IG-11 down to less than 20 wppm in IG-110. Luo, Robin and Yu found that

isotropic nuclear-grade graphite, such as IG-11, showed a higher oxidation rate and formed more pores due to having more impurities than anisotropic PAEB, PCEB, and PPEA graphite [8]. Samples were oxidized in a 100% air environment for 4 h at 673, 973 and 1473 K.

Because of the varying range of results and conclusions from the studies surveyed in Table 1, it is not clear whether a particular grade is better suited to the needs of VHTR operation specifically. An extensive report on the oxidation performance of IG-110 in realistic VHTR air ingress accident conditions and comparisons with NBG-18 are the main purposes of this paper. We have reported previously on the oxidation performance and surface characteristics of a current generation nuclear-grade graphite NBG-18 [4], and we are extending that work to another candidate grade IG-110 under the same air ingress accident conditions.

Table 2 compares the basic elemental impurities found in IG-110 and NBG-18 nuclear-grade graphite "as received" from respective manufacturers. Both IG-110 and NBG-18 have been manufactured according to ASTM standard D7219-05 that sets requirements for the chemical purity of nuclear-grade graphite [9]. Table 3 provides a direct comparison of IG-110 and NBG-18 major properties of interest in oxidation and surface studies [7,10]. Considering that IG-110 is a historical grade, it is puzzling that previous studies on the grade have reported a large range of activation energies, as shown in Table 4.

Table 2
Elemental composition of impurities in pure IG-110 and NBG-18 nuclear-grade graphite.

IG-110 Elemental composition	wppm	**NBG-18** Elemental composition	wppm
B	0.15	B	0.57
Si	<0.1	Si	38
Ca	0.08	Ca	5.9
Fe	0.06	Fe	4.8
Al	0.012	Al	0.24
K	0.04	Ta	<5.0
V	0.018	S	4.8
		Zr	0.22
		Na	0.17

Table 3
Major properties and characteristics of IG-110 and NBG-18 nuclear-grade graphite.

	IG-110	**NBG-18**
Grain size	fine, <20 μm	medium, 1.6 mm
BET surface area (m^2/g)	0.224	0.1
Bulk density (g/cm^3)	1.77	1.85
Pore volume (cm^3/g)	0.066	0.069
Pore fraction	11.6%	12.9%
Coke source	petroleum	coal
Forming process	isostatically-molded	vibration-molded

Table 4
The apparent activation energy of IG-110 as reported by several authors in the last 20 years.

Author	E_a (kJ/mol)
Chi and Kim [2]	159
Fuller and Okoh [11]	188
Contescu et al. [7]	201
Wang et al. [3]	205
Kim, Lee and No [12]	218

3. Measurements

IG-110 has a bulk density of about 1.77 g/cm^3 [13]. The density of IG-110 is less than the theoretical density of non-nuclear-grade graphite which is about 2.26 g/cm^3 [13]. This difference is mostly attributed to formation of pores in nuclear-grade graphite during manufacturing [1]. IG-110 has less than 100 wppm metal content and was manufactured according to ASTM standard D7219-05 [9].

3.1. Specimen and sample preparation

Blocks of IG-110 graphite having dimensions of 304.8 mm x 152.4 mm x 152.4 mm were obtained from the manufacturer, which were then machined into approximately 12.5 mm x 12.5 mm x 12.5 mm pieces without the use of lubricant, diamond or carbide tools according to standards established in ASTM standard D7542-09, Section 6.1 and 6.2 [14]. This was the ideal geometry to fit the sample bucket used in the standard thermogravimetric apparatus [4].

3.2. Graphite oxidation equipment

A Thermax700 thermogravimetric analyzer (TGA) from Thermo Scientific® was used to obtain the mass change versus temperature data in real-time during graphite oxidation in air. Graphite samples were placed in an alumina cylindrical sample bucket with a platinum bail held from an alumina extension wire. The volume of the bucket is 35 mL. The balance has a 100 g capacity and resolution of ± 1.0 µg. Mixtures of dry medical-grade air in ultra-high purity research-grade helium having a total flow rate of 50 mL/min were used in the experiment. Mass flow controllers were used to control the flow rate and helium gas streams were flowed through oxygen scrubbers. The concentration of oxygen

in the TGA inlet and purge was monitored with an oxygen meter. A schematic diagram of the experiment is found in our previous NBG-18 study [4].

3.3. Experimental procedure

Mass loss data was collected isothermally and in real-time using TGA. Graphite samples were heated in ultra-high purity helium at a constant rate of about 5 K/min until the desired oxidation temperature was reached, at which point samples were switched to a 100% dry air environment or a mixture of inlet air and helium, as needed. This gas-switching procedure ensured that the initial surface states of samples were protected from oxidation and burnoff (ratio of oxidized to unoxidized sample) during the ramping period, especially for lower temperature runs where greater penetration depths through the bulk of the graphite specimen is generally expected [4]. First, samples were tested isothermally for 10 h from 873 to 1873 K. Then, graphite samples were exposed for 10 h in four different air leak scenarios. The inlet gas stream contained 5, 10, 15 and 21 mol% O_2 concentrations. The mass loss rates were measured isothermally once the desired temperature was reached in the TGA.

3.4. Bulk density profiling of an oxidized IG-110 rod

Apart from the kinetic study, oxidation experiments were also performed on cylindrical IG-110 rods to study the change in density and penetration of oxidant. There is a strong correlation between the density of nuclear graphite and its physical and mechanical properties [4,15-19]. During oxidation, oxygen penetrates the bulk graphite creating more porous structure and in the process, degrades structural properties. To investigate the penetration of oxygen into bulk graphite samples, IG-110 samples were prepared into right

cylinders with the following dimensions: 19.1 mm x 31.5 mm. Following oxidation of the sample using TGA, bulk density measurements were made according to ASTM standard C559-90 [20]. Machined IG-110 cylinders were washed in methanol and dried in a vented tube furnace for 2 h at 423 K according to ASTM standard C1179-91 [21]. Then, a single rod was freely suspended inside the TGA furnace for oxidation using gas switching to control any initial weight loss of sample during ramping.

The graphite rod was positioned inside the reaction tube in a special high temperature wire bucket that was exposed to the flow of air from the base of the cylinder. The oxidation temperature tested was 973 K in 100% dry air flowed at 50 mL/min for 5 h at a rate of 5 K/min. About 5 h exposure time in air at 973 K has been correlated to about 10% weight loss of IG-110. The oxidized graphite cylinder was then carefully weighed and the diameter and height were recorded. Several measurements of the diameter were taken along the height of the cylinder and were averaged to account for the direction of reaction air flow originating from the base of the sample.

3.5. Scanning Electron Microscopy (SEM)

High resolution images of pure and oxidized samples were obtained using the Hitachi S-4700 which is a cold-field emission SEM. Hitachi S-4700 has multiple scanning modes, an accelerating voltage ranging from 0.5 to 30 kV and a maximum resolution of 1.5 nm. For this study, the scanning mode for the secondary electron maxing out at about 40 frames per second, at a working distance between 7 to 10 mm and 10 kV accelerating voltage were suitable to capture details on the surface of graphite samples. Magnification was around

5000X. Energy dispersive spectroscopy (EDS) which gives quantitative surface elemental data was simultaneously available from Hitachi S-4700.

3.6. Fourier Transform Infrared Spectroscopy (FTIR)

The Tensor-27 from Bruker Optics was used to identify the presence of surface functional groups after oxidation treatment of graphite samples. Tensor-27 generates a mid-range (4000 cm^{-1} to 400 cm^{-1}) infrared spectrum and accommodates a diffuse reflectance cell, EasiDiff®, that is convenient for analyzing powdered samples. Graphite powder obtained from machining an oxidized rod as described in Section 3.4 were prepared into 5 to 10% mixtures in spectraphotometric-grade KBr for spectral analysis. Spectral data was obtained for 128 scans at 4 cm^{-1} resolution.

3.7. X-ray Photoelectron Spectroscopy (XPS)

Broad-scan XPS from 0 to 1100 eV was used to collect more quantitative data on oxidized graphite samples and to examine the composition (e.g. the electronic or chemical state of elements) and confirm the presence of elements on the surface. The Kratos Axis 165 with an 8-channel analyzer was used with a monochromatic Al source (150W). The standard slot or "spot" size analysis area was 700 µm x 300 µm. The Kratos Axis 165 was used with a charge neutralizer in Hybrid Mode, employing both magnetic and electrostatic lenses.

4. Results and discussion

Isothermal oxidation data for IG-110 using TGA was collected and compared to the oxidation data previously obtained for NBG-18 under the same experimental conditions

[4]. Pure and TGA-oxidized samples were then examined and compared using several surface characterization techniques including SEM, EDS, FTIR and XPS.

4.1. The effect of temperature on oxidation rate

IG-110 samples were tested isothermally in 100% dry medical-grade air at 873, 923, 973, 1023, 1173, 1473 and 1873 K using TGA. Table 5 displays mass loss data for IG-110 oxidation and also NBG-18. Oxidation runs were performed twice to confirm the reliability and repeatability of the data. A very good repeatability of the data was observed. Figures 1(a) and (b) show the mass loss rates corresponding to Table 5 for oxidation of IG-110 and NBG-18 in air, respectively.

Table 5
Mass loss rates, area-normalized and weight-normalized oxidation rates for IG-110 and NBG-18, average of two trials.

T	Mass loss rates		OR^a		OR^w	
K	mg h^{-1}		g h^{-1} m^{-2}		g h^{-1} g^{-1}	
	IG-110	**NBG-18**	**IG-110**	**NBG-18**	**IG-110**	**NBG-18**
873	0.6037 ± 0.01	1.261 ± 0.01	12.010 ± 0.20	25.070 ± 0.20	0.002	0.002
923	15.629	1.096	310.929	21.810	0.028	0.003
973	45.126	15.023	897.753	298.416	0.100	0.048
1023	70.800	42.870	1408.521	852.900	0.120	0.134
1173	120.32	114.060	2393.690	2269.150	0.271	0.164
1473	158.52	77.075	3153.655	1597.640	0.247	0.259
1873	153.99	174.280	3063.534	3467.190	0.298	0.383

a-area normalized, w-weight normalized

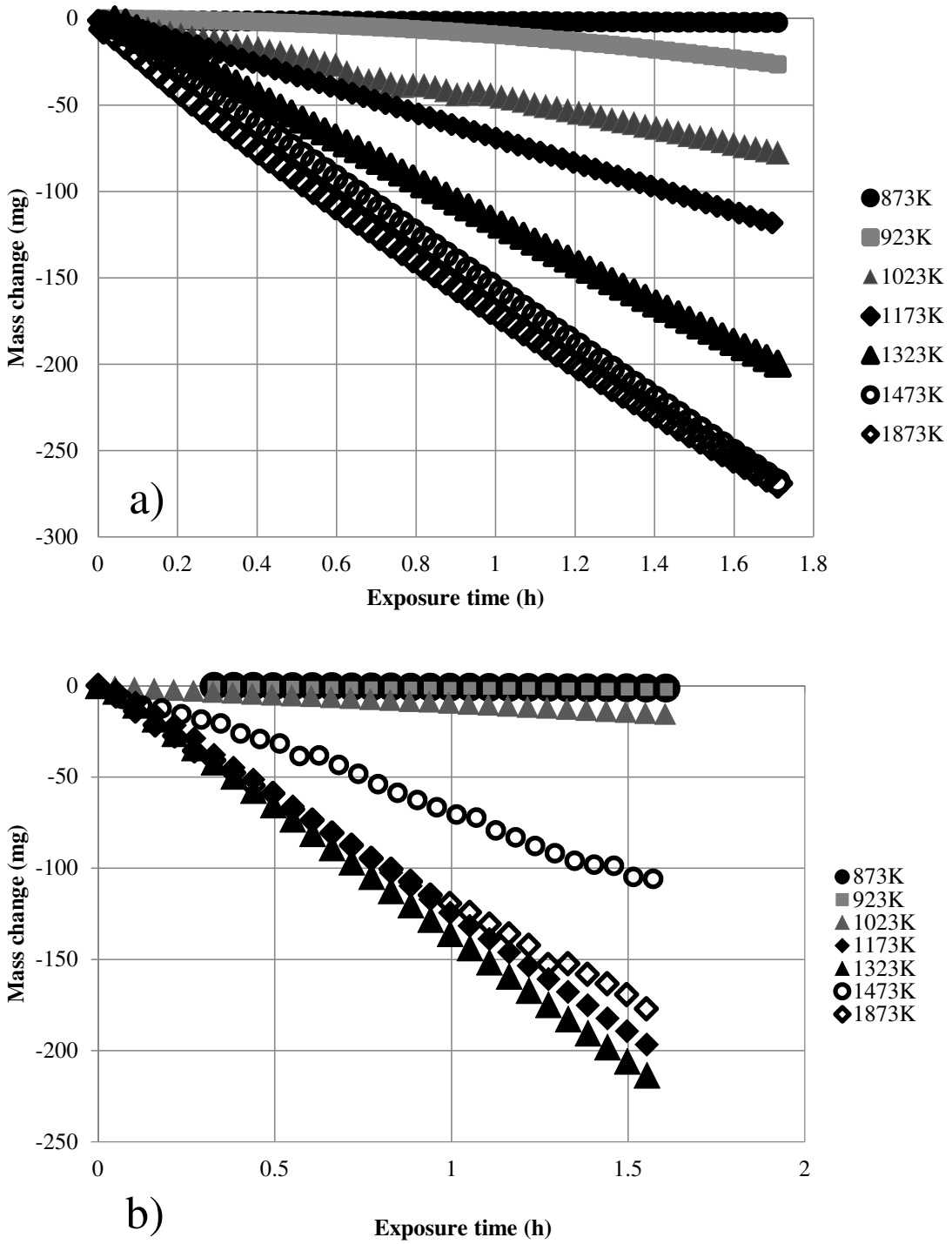

Fig. 1. Mass loss data in 100% dry medical grade air for **(a)** IG-110 and **(b)** NBG-18.

In general, IG-110 sustained more mass loss in the same oxidative environment as NBG-18 for a majority of test temperatures. In Fig. 1(a), the mass loss due to oxidation in IG-110 steadily increases with oxidation temperature up to about 1173 K. At higher

temperatures less penetration of IG-110 was observed. Figure 1(a) shows that the mass loss rate is roughly the same from 1173 to 1873 K for IG-110. Beyond 1173 K, oxidation probably occurs as a surface exterior attack on IG-110 and an oxidized layer is formed. The oxidized layer may be said to protect the bulk from reaching a higher mass loss rate while geometrical changes occur only externally to the sample. In contrast, NBG-18 was prone to a non-uniform attack and shrinkage during bulk oxidation as shown in Fig. 1(b) [4]. For NBG-18 the mass loss rates do not increase linearly with temperature. In fact at 1473 K, the oxidation behavior of NBG-18 can no longer be explained by kinetic theory as the oxidation probably proceeds by mainly diffusive control [4]. Decreased rates beyond this temperature are probably attributed to the accumulation of carbon monoxide from the Bouduard reaction but also from changes in sample geometry [4,22-24].

Figure 2 displays the oxidation rates normalized to the surface area of samples from Table 5 for IG-110 and NBG-18. The oxidation rate of IG-110 was roughly comparable but generally higher than NBG-18 in the same experimental conditions [4]. Moreover, the oxidation rate increased almost linearly at lower temperatures for IG-110 but both grades reach a maximum oxidation rate of around 3000 g/h/m^2 at high temperatures.

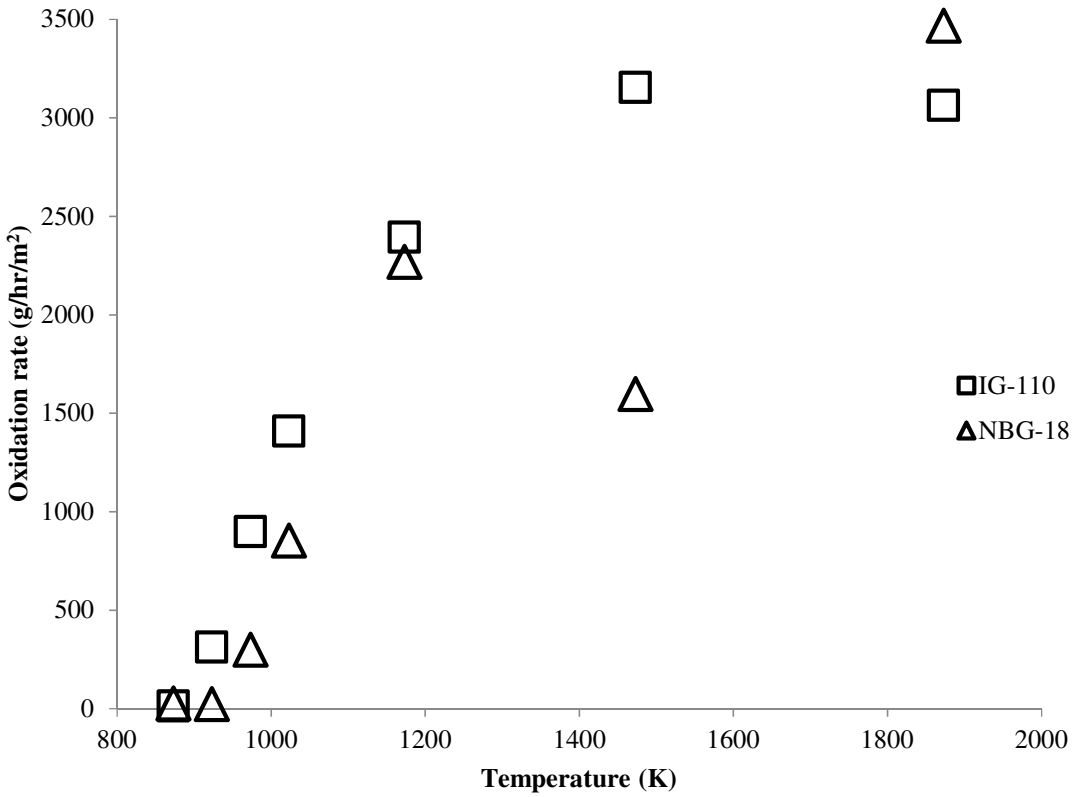

Fig. 2. Comparison of the oxidation rates of IG-110 and NBG-18 in dry medical-grade air.

The oxidation rate of IG-110 in dry medical-grade air was also compared to recently reported oxidation data from Fuller and Okoh [11] and Chi and Kim [2]. Figure 3 shows that the oxidation rates obtained in this study are in very good agreement with the available data for IG-110 for a large range of temperatures. As compared to the previous studies, a larger temperature range for oxidation from 873 to 1873 K was investigated in this study.

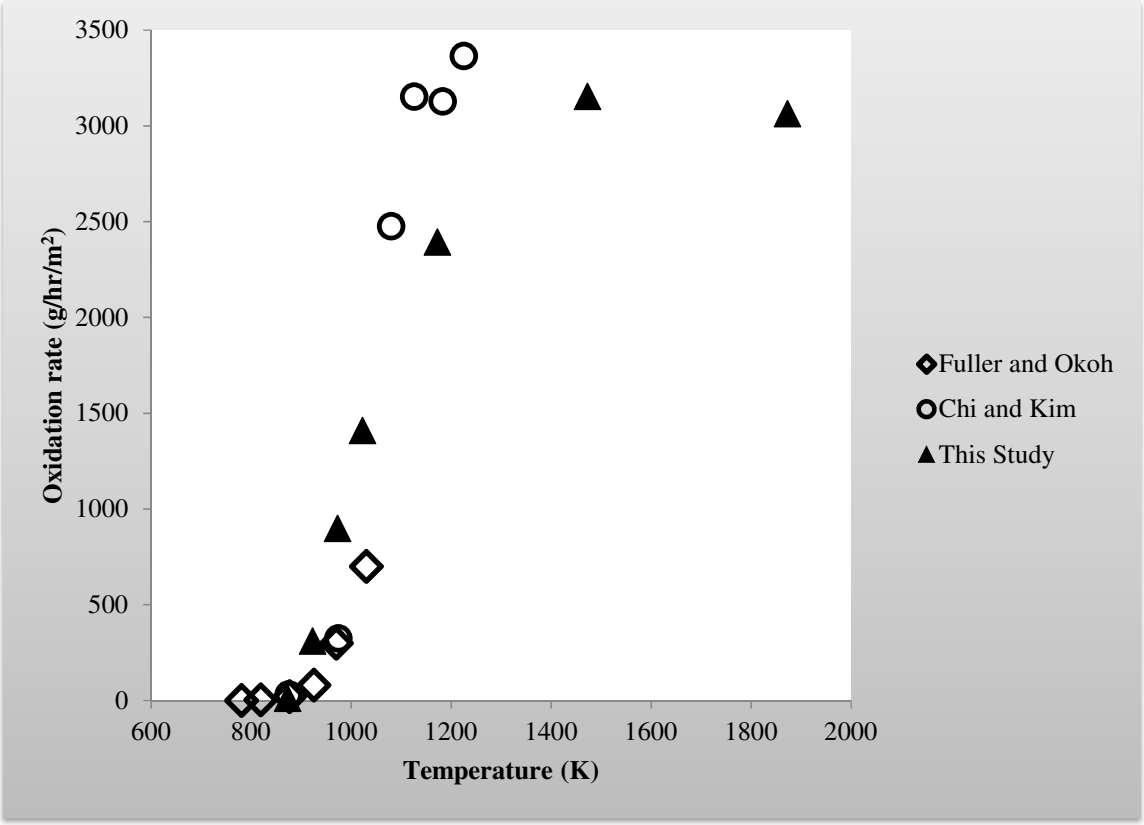

Fig. 3. Comparison of oxidation rate data for IG-110 in 100% dry medical-grade air among recent studies.

The activation energy of IG-110 was determined from the TGA mass loss data collected by following the oxidation experiment outlined in Section 3.3. The mass loss data shown in Figs. 1(a) and (b) along with the procedure outlined in ASTM 7542-09 was used to calculate the activation energies for three regimes from an Arrhenius plot [4,14]. Figure 4 is the Arrhenius plot for IG-110 which delineates the different oxidation regimes for the mass loss rates normalized to sample surface area. The activation energy of IG-110 was determined to be 222.07 kJ/mol in the kinetic regime, Regime I from 873 to 1023 K; 35.28 kJ/mol in the intermediate regime, Regime II from 1023 to 1173 K; and 6.66 kJ/mol in the in-pore diffusion regime, Regime III from 1173 to 1873 K.

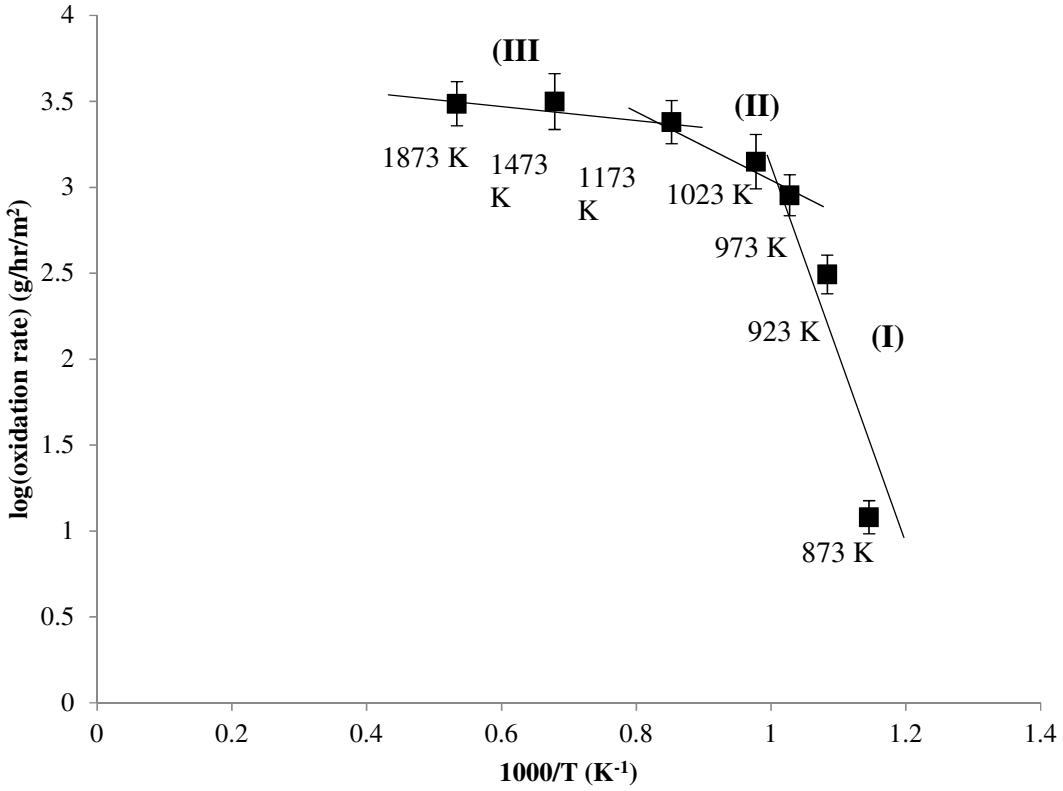

Fig. 4. Arrhenius plot of IG-110 oxidation in 100% air.

4.2. The effect of concentration on oxidation rate

The effect of oxygen concentration on the mass loss rates of IG-110 at 1023 K were studied in order to obtain the reaction order for IG-110. IG-110 samples were oxidized in 5, 10, 15 and 21 mol% air in helium mixtures, as described in Section 3.3.

The experimental mass loss data for four concentrations of oxygen at 1023 K were used to determine the order of the reaction with respect to oxygen partial pressure from a linear fit of the data. Figure 5 is a plot of ln k vs. ln P_{O_2} used to determine the reaction order of IG-110. The reaction order of 0.76 ± 0.15 was found. In this case, the results indicate that the reaction order is approximately first-order of the partial pressure of oxygen on the

surface of graphite. The reaction order obtained in this study is well within experimentally accepted values between 0.54 and 1.3 for dense and nuclear-grade graphites [2,15,22,24].

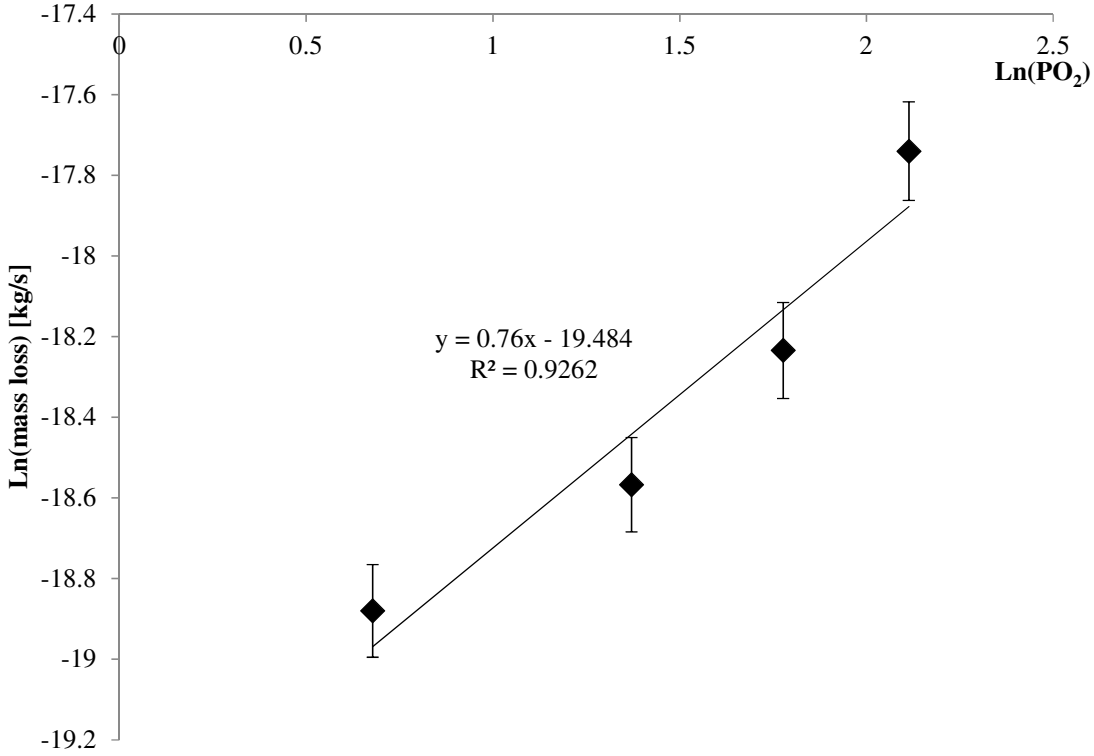

Fig. 5. Order of reaction with respect to the oxygen partial pressure for the elementary reaction between graphite and air.

4.3. The rate equation for the kinetic regime of IG-110 oxidation

The semi-empirical Arrhenius equation can be used to describe most thermally-induced processes, such as oxidation. In practice, it has also demonstrated strong experimental accuracy [4,14,22-27]. An overall kinetic rate equation for the oxidation of IG-110 can be written as in our previous study on NBG-18 [4]. In Regime I between 873 and 1023 K, the slope and intercept from Fig. 4 were $-\frac{E_a}{2.303 \cdot R} = -11.598$ where R = 8.314 J/mol K and $\log_{10} A = 14.734$, respectively. The activation energy E_a of IG-110 oxidation in the

kinetic regime in 100% air was determined to be 222.07 kJ/mol and the frequency factor A was 5.414 x 10^{14} g/h/m^2, which is about two orders of magnitude higher than what was previously reported for NBG-18 [2,4]. Chi and Kim as well as Contescu et al. have also found the frequency factor of IG-110 was higher than NBG-18 [2,7]. According to Table 4, the activation energy found in this study is well within recently reported values. Using the semi-empirical Arrhenius equation as in our previous NBG-18 study [4], the reaction rate velocity for IG-110 in Regime I applicable from 873 to 1023 K becomes

$$k_I\left(\frac{g}{h\cdot m^2}\right) = 5.414 \text{ x } 10^{14}\cdot e^{-\left(\frac{222.07\frac{kJ}{mol}}{T(K)}\right)} \quad (1)$$

Using the semi-empirical Arrhenius equation [4] and the reaction order determined in Section 4.2, the specific reaction rate of reaction with respect to partial pressure of oxygen on the surface is given by Eq. (2) below.

$$r_I\left(\frac{g}{h\cdot m^2}\right) = 5.414 \text{ x } 10^{14}\cdot e^{-\left(\frac{222.07\frac{kJ}{mol}}{T(K)}\right)} P_{O_2}^{0.76} \quad (2)$$

4.4. Surface characterization of pure and oxidized IG-110

The surface of IG-110 samples was explored via SEM and EDS and compared to NBG-18 [4]. Figures 6(a) and (b) display the SEM images and reveal the visible differences between NBG-18 and IG-110 pure, unmachined surfaces before oxidation treatment.

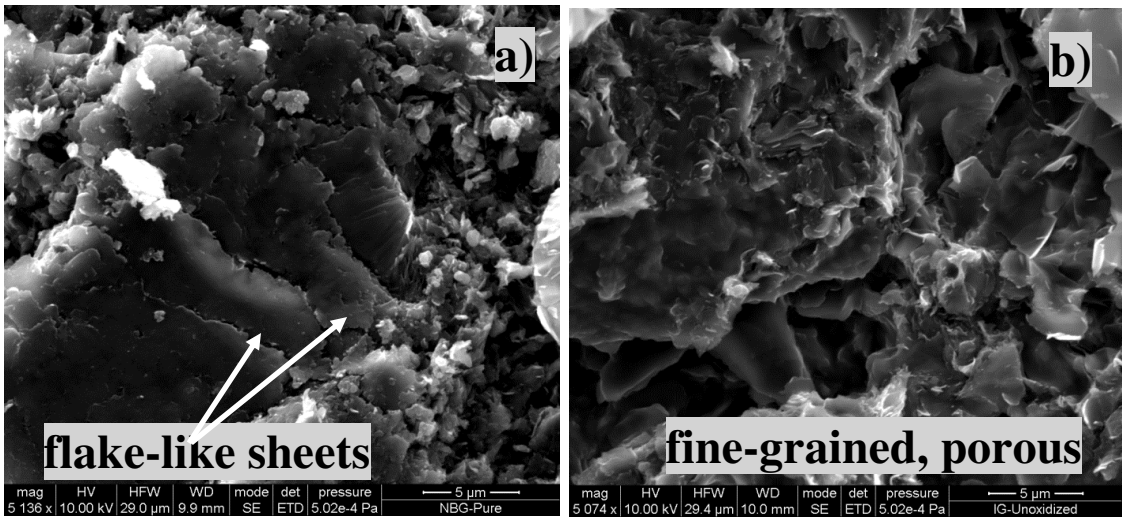

Fig. 6. SEM imaging of unfractured and pure graphite surfaces **a)** NBG-18 and **b)** IG-110 at 5000X Mag.

Figures 7(a) and (b) display the SEM images of the surface of NBG-18 and IG-110 after oxidation in 100% air at 1023 K using TGA. The surface states of the samples were dramatically changed after oxidation treatment but in different ways. Both NBG-18 and IG-110 samples experienced a unique surface attack. However, IG-110 graphite developed large pores and pits on the surface while NBG-18 suffers from formation of "blisters" on its flake-like sheets. The difference could be largely attributed to the filler grain size of each graphite type. In fact, due to its very fine pores, IG-110 has been found to have a larger total surface area and more exposed edges along basal planes in its crystallites than NBG-18 after oxidation treatment [6,7].

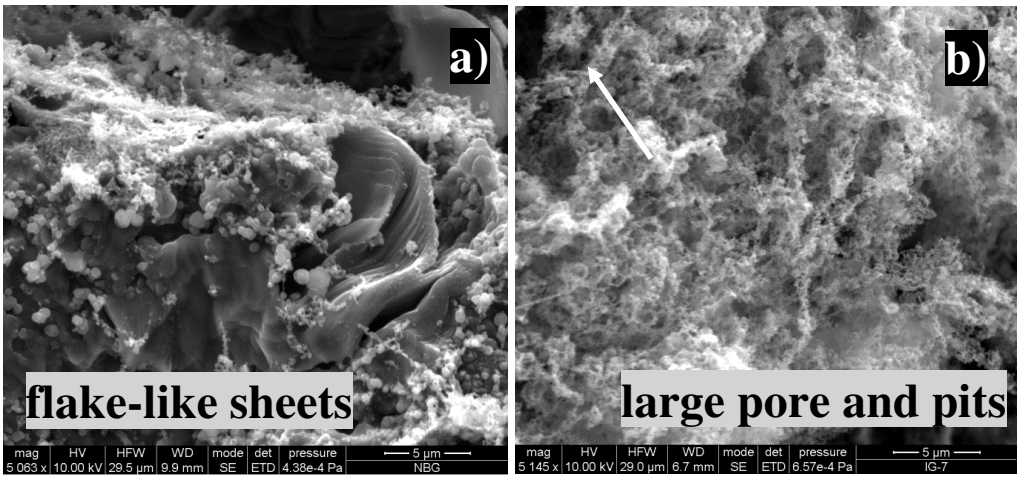

Fig. 7. SEM imaging of the surface of graphite samples oxidized at 1023 K for **a)** NBG-18 and **b)** IG-110 at 5000X Mag.

At higher oxidation temperature, beyond 1473 K, IG-110 has been observed to form even more pits and larger pores on the surface as shown in Fig. 8. At this temperature, there is less penetration of oxidant through the bulk and an exterior attack occurs to IG-110. Certain impurities, such as Fe and Ca, as well as combustion products such as CO and CO_2 may catalyze the reaction between graphite and air [28]. The impurities that could act as catalysts for oxidation also increase the reactivity and the total oxidation rate. The pitting surface may be attributed to the presence of concentrated catalytic centers that aid the rapid removal of carbon atoms from the surface active sites.

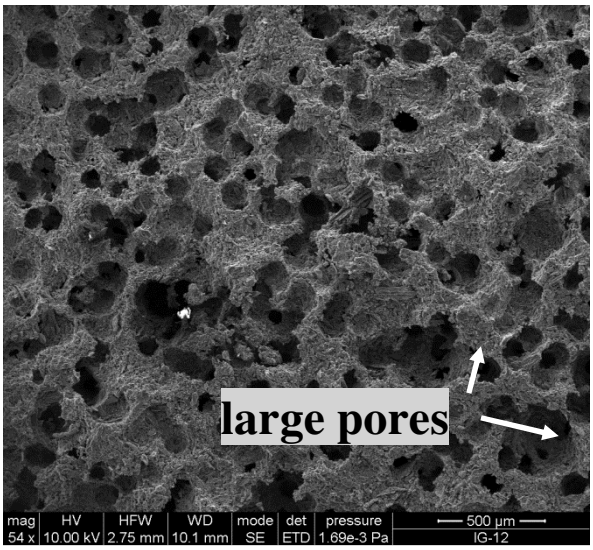

Fig. 8. SEM image of the pitting surface of IG-110 graphite oxidized in 100% air at 1473 K at 50X Mag.

EDS results were obtained on the unoxidized and oxidized samples of IG-110 and NBG-18. Silicon is a persistent impurity in the spectra that probably originates from the sample buckets used with TGA. According to EDS obtained on IG-110 and compared to NBG-18 oxidized in the same environment, IG-110 is initially very pure with a strong carbon-carbon signal. Furthermore, EDS consistently detected a stronger carbon-oxygen signal on the surface of the oxidized sample in IG-110 than in NBG-18. At temperatures beyond 1473 K, oxidized samples of IG-110 suffered a pitting corrosion which was further explored with EDS in Fig. 9 below. Carbon and oxygen were detected as expected but also trace amounts of Ca and V potentially catalytic elements were detected. EDS of the surface around pores, shown in Figs. 9 and 10 show that the surface chemistry is different in oxidized samples depending on the location.

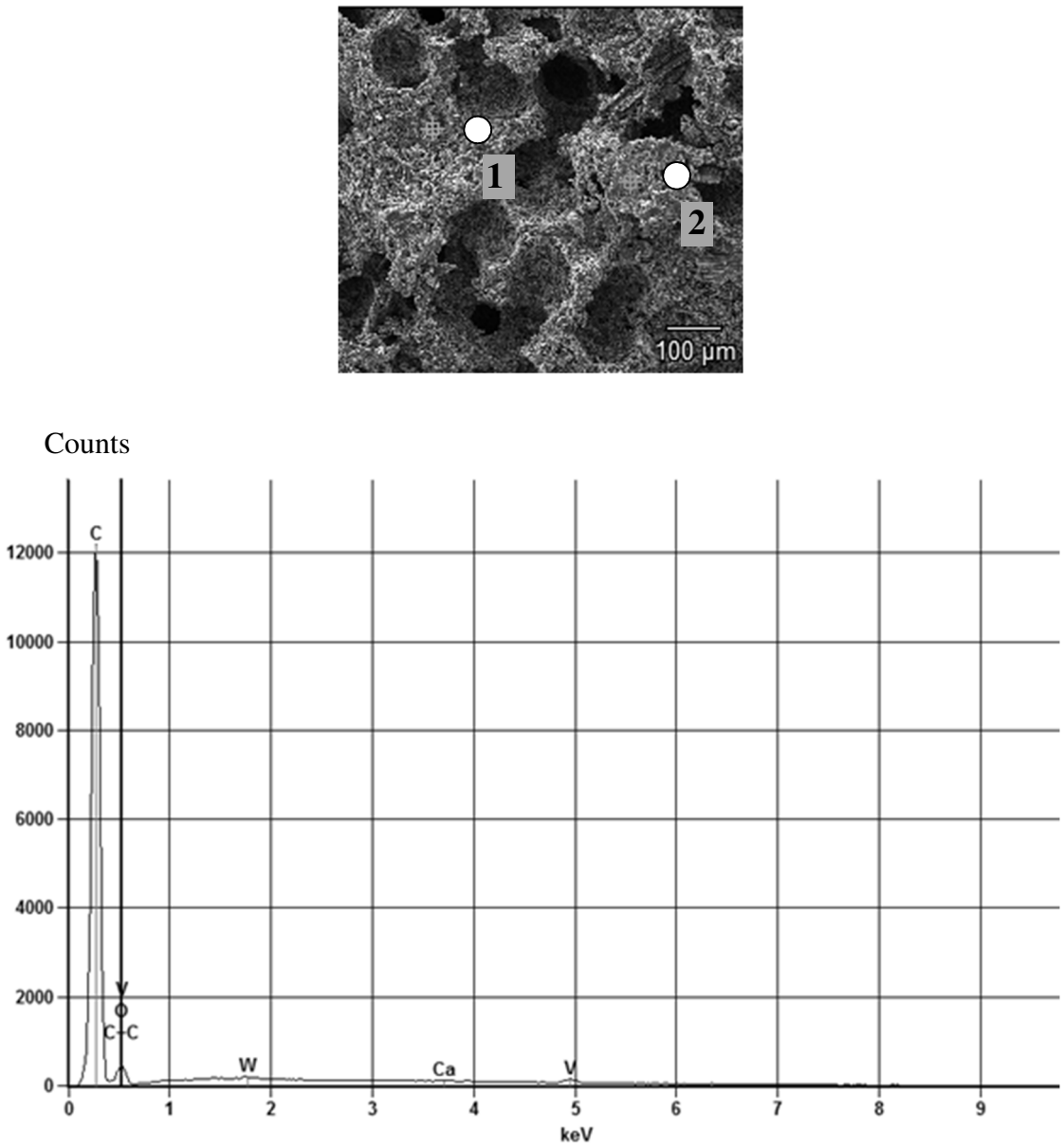

Fig. 9. SEM/EDS of oxidized IG-110 at 1473 K for pore surface chemistry

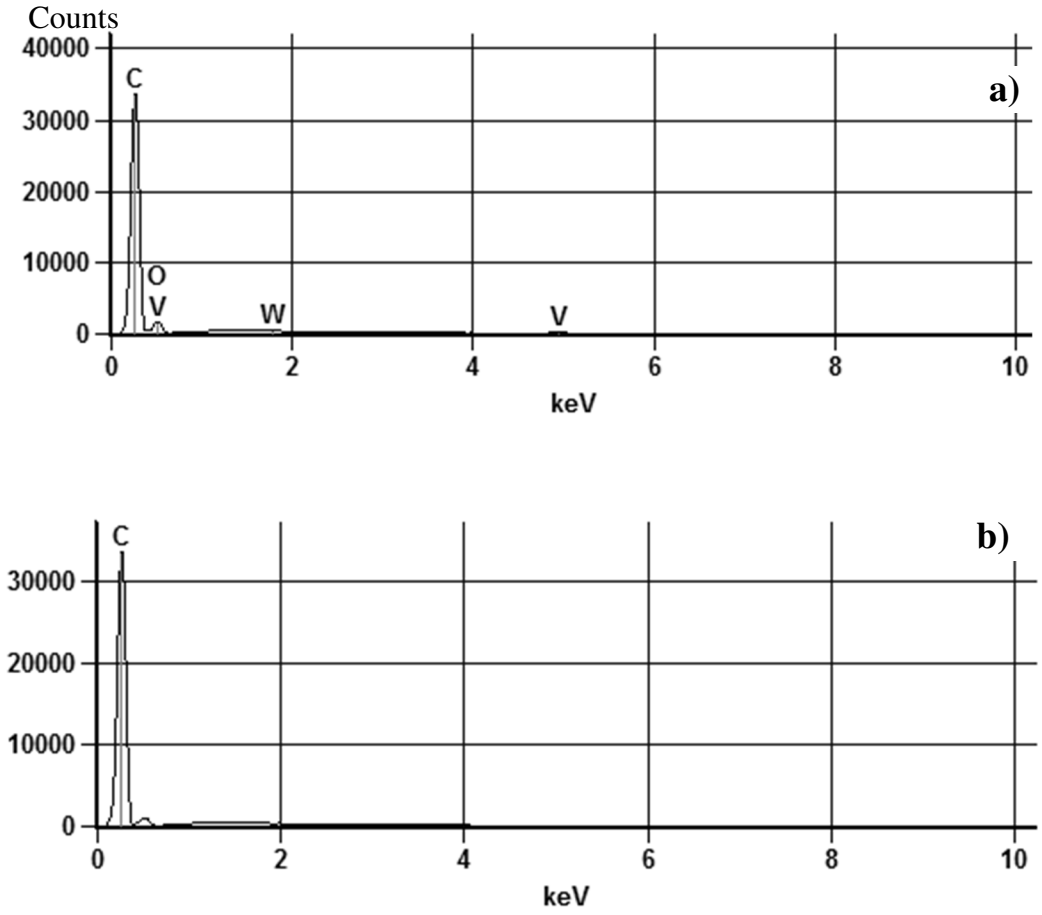

Fig. 10. Location-specific EDS results for a) Location 1 and b) Location 2.

Analysis inside pore cavities of IG-110 after oxidation, such as those shown in Fig. 9, was not feasible due to the lack of a flat touchdown surface for EDS. The locations of the scans are indicated in Fig. 9 as Location 1 and Location 2. Location 1 was directly compared with Location 2 and the quantitative analysis in EDS was different as shown in Fig. 10. After oxidation of IG-110 at 1473 K, samples exhibited surface pits ranging from about 100 μm to several hundred microns in size. Porosity development during oxidation could also be due to rapid oxidation around catalytic centers resulting in carbon removal from the surface.

Oxidized samples of IG-110 were also studied using XPS. Figure 11(a) shows the broad-scan XPS spectra for the surface of IG-110 samples oxidized in medical-grade air at 873, 923 and 1023 K oxidation temperatures. With increasing oxidation temperature, the O_{1s} peak increases and the C_{1s} peak decreased significantly. Like EDS, XPS provided some quantitative data about the surface elemental composition of oxidized graphite samples. For IG-110 oxidized in 100% air, the fraction of carbon atoms on the surface was roughly 89% at 873 K, 86% at 973 K and 85% at 1023 K. Correspondingly, the fraction of oxygen atoms detected was roughly 11% at 873 K, 14 % at 973 K and 15% at 1023 K. A high-resolution scan of the C_{1s} peak revealed a strong C-C peak around 282 eV which decreases with increasing oxidation temperature and a weak C-O peak around 288 eV that increases with oxidation temperature.

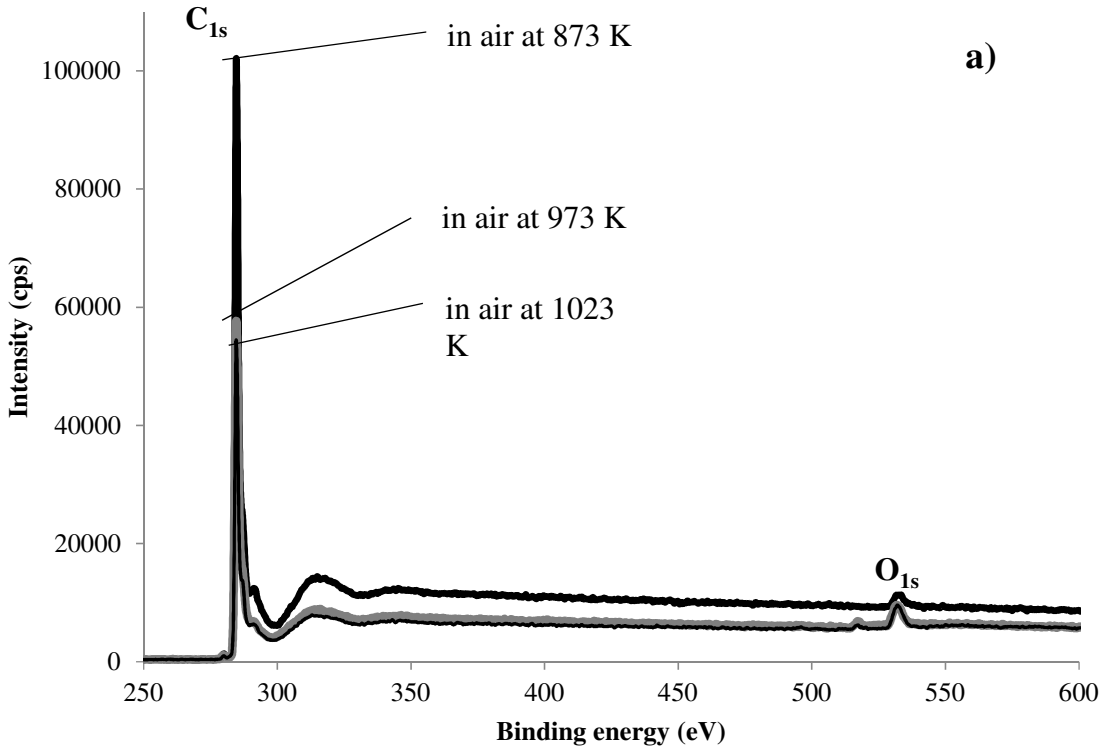

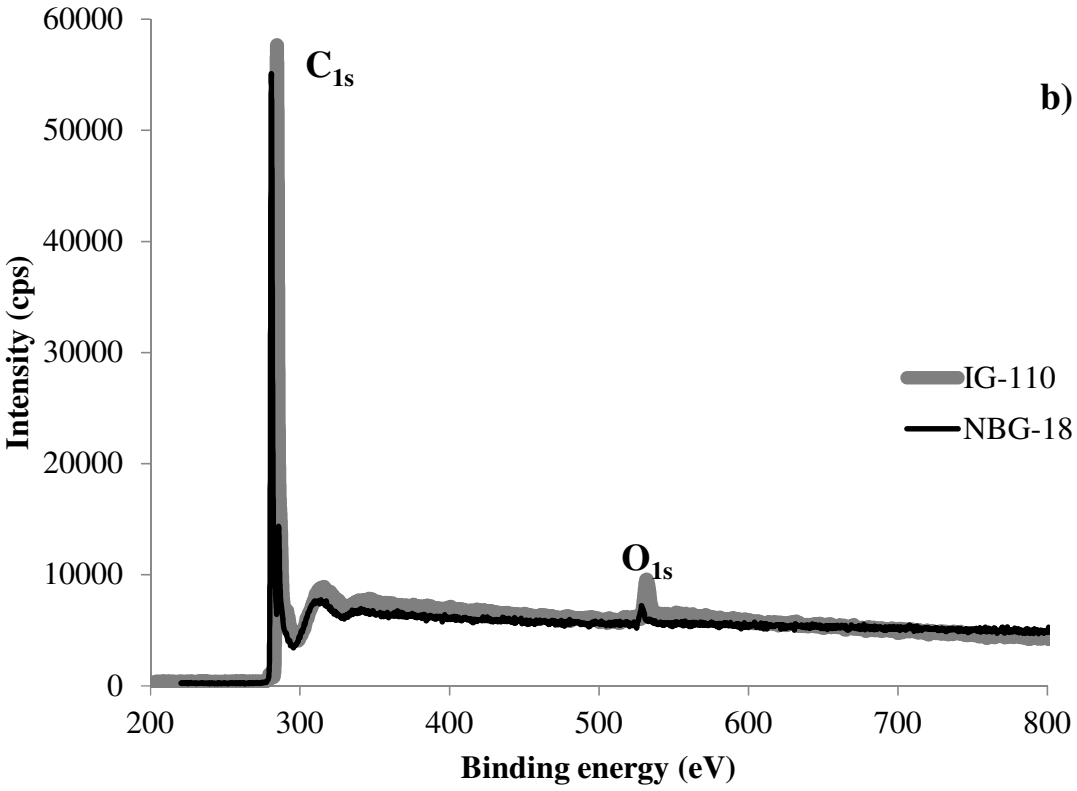

Fig. 11. XPS broad-scan of oxidized **a)** IG-110 in 100% air at 873, 973 and 1023 K and for **b)** oxidized IG-110 versus NBG-18 in 100% air at 1023 K.

Figure 11(b) compares the XPS spectra for IG-110 and NBG-18 oxidized in dry medical-grade air at 1023 K. The oxygen signal in XPS is stronger for IG-110 oxidized in the same conditions as NBG-18. At 1023 K, the fraction of carbon atoms on the surface of IG-110 was 85% and for NBG-18 was 89%. The fraction of oxygen atoms was about 15% for IG-110 and 11% for NBG-18. High-resolution XPS scans of the O_{1s} peak of both IG-110 and NBG-18 were obtained and are shown in Figs. 12(a) and (b), respectively. For IG-110 in Fig. 12(a), the high-resolution XPS scan revealed an O^{2-} peak around 530.6 eV and a strong O-C peak around 532.8 eV. For NBG-18 in Fig. 12(b), the high-resolution XPS scan showed a weak O^{2-} peak around 530.4 eV and an O-C peak around 532.2 eV.

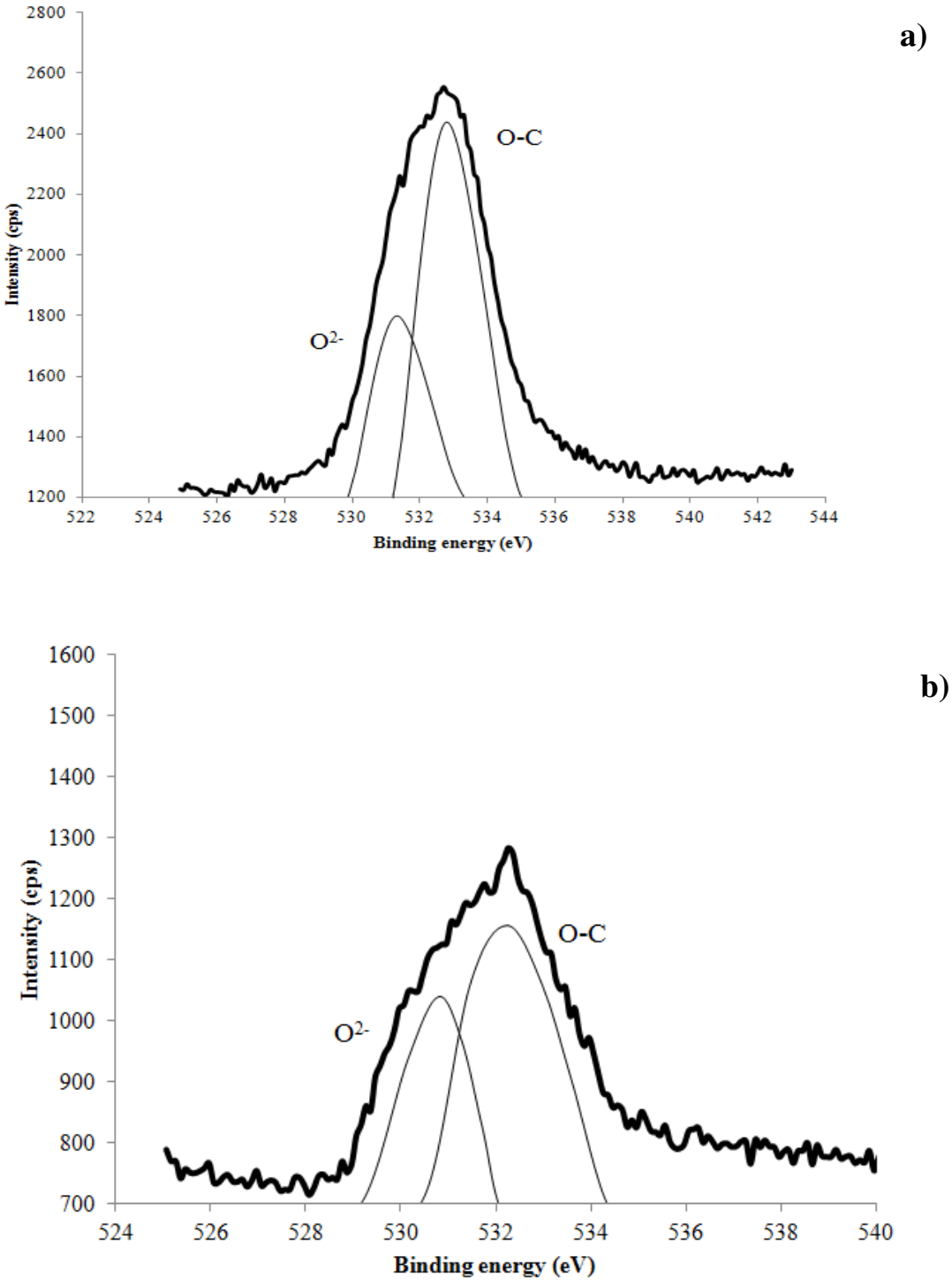

Fig. 12. XPS high-resolution spectrum of oxide peak at 1023 K for **a)** IG-110 and **b)** NBG-18.

The density profile of IG-110 oxidized in 100% dry air at 973 K for 5 h is shown in Fig. 13. Bulk density measurements were calculated through an oxidized rod as described in Section 3.4. Upon experimental observation and compared to oxidized NBG-18 rods [4], loose dust covered the surface of IG-110 after oxidation treatment and also dust would fall from the sample during transport or movement which further add to the uncertainty in the physical measurements.

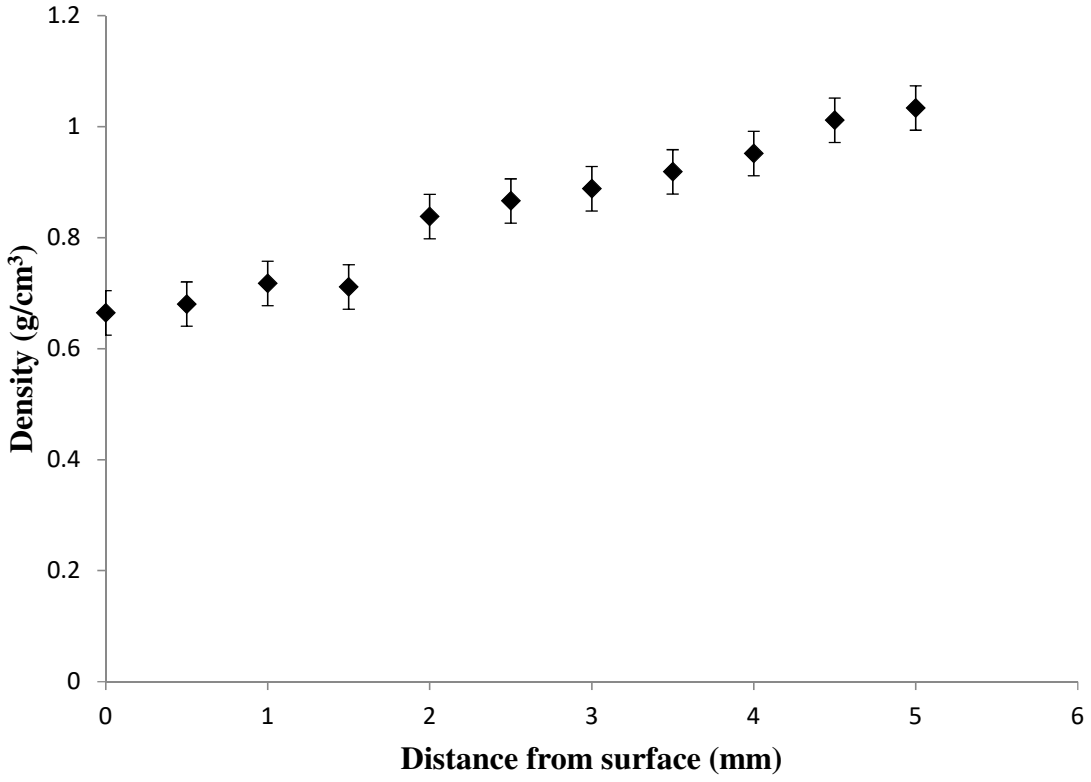

Fig. 13. Density profile of oxidized IG-110 cylinder in 100% dry air at 973 K.

According to the data shown in Fig. 13, the density of IG-110 changed to a depth of at least 5 mm from the surface. Given the theoretical bulk density of 1.77 g/cm^3 for IG-110, at a depth of 5 mm the sample density is only about 1.03 g/cm^3 which would suggest that the density was dramatically reduced throughout the entire depth of the tested rod and beyond the depth measureable in this experiment. The measured bulk density for the first two outer

layers of the oxidized rod was very low, around 0.7 g/cm^3. At 5 mm, the sample was no longer intact to machine or collect further information. Other investigators have noted oxygen penetration depths of about 12 mm for IG-110 at temperatures between 773 and 973 K [3,7,10]. Compared to the penetration depth of about 3 to 4 mm measured in our previous study on NBG-18 graphite [4], in the same conditions, an IG-110 rod sustained a much greater reduction in density and penetration of oxidant beyond 5 mm for the same oxidation test. The density profile for IG-110 suggests that the oxidation mechanism at 973 K is a penetrating bulk attack and occurring through the entire sample. This suggests that the exterior layers of IG-110 are less resistant to oxidation than NBG-18 in the same conditions. For IG-110 the penetration of oxidant is not uniform through the first few millimeters of the rod's surface, as every machined layer had a different density that was much lower than that of pure IG-110 but increasing as the rod was further machined towards the centerline. In contrast, NBG-18 oxidation was occurring strongly on the exterior surface layers of the rod in the same test conditions and the density profile became uniform at about 3 mm from the surface [4].

FTIR was used to confirm the presence of surface active functional groups and combustion products on the surface of the oxidized rods. Figure 14(a) shows the FTIR transmission spectra of oxidized IG-110 in air at 973 K. For IG-110 in Fig. 14(b), the asymmetrical stretching vibration of CO_2 was detected around 2400 to 2300 cm^{-1} and the degenerate scissoring vibrations of CO_2 were detected around 666 cm^{-1}. The intensity of the CO_2 vibration is increased on the surface of oxidized graphite but also internally. The presence of CO_2 in the surface layers also confirms that internal combustion of graphite occurred. Carbonyl functional group C=O broad bands were detected around 1760 to 1690

cm^{-1}. Water was a persistent impurity in the background as O-H stretching vibrations were detected around 3400 cm^{-1}.

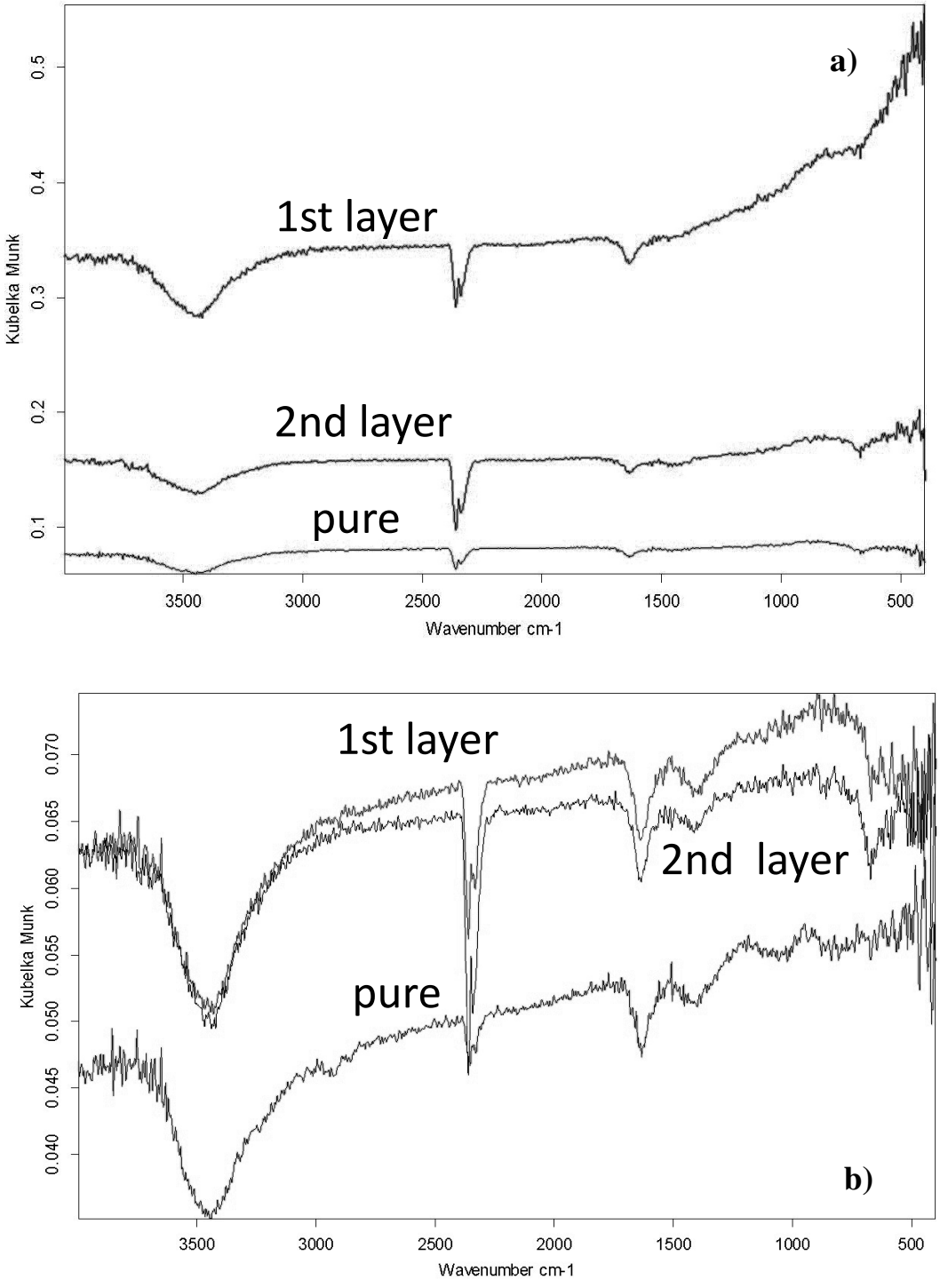

Fig. 14. FTIR spectra of oxidized graphite in 100% air at 973 K sampled at 0.5 mm from surface ("1st layer") and sampled at 1.0 mm from surface ("2nd layer") for **a)** IG-110 and for **b)** NBG-18.

In Fig. 14(b), FTIR spectra for NBG-18 in the same experimental conditions are shown. The asymmetrical stretching vibration of CO_2 was detected around 2400 to 2300 cm^{-1} and the intensity increased with oxidation treatment. Broad band stretching vibrations from carbonyl functional groups were also identified around 1800 to 1600 cm^{-1}. The intensity of the carbonyl functional groups do not change with oxidation treatment as notably as the stretching vibration of CO_2. Two outer layers of an oxidized NBG-18 rod were sampled about 0.5 mm and 1.0 mm from the surface but the results were comparable. The density profile and FTIR results strongly suggest that IG-110 suffers more inner combustion through the rod than NBG-18 due to the greater penetration depth of oxidant.

5. Conclusions

The oxidation rate of IG-110 was modeled in 100% air for the kinetic regime of graphite oxidation in the temperature range of 873 to 1023 K. The activation energy calculated from the Arrhenius equation was 222.07 kJ/mol for IG-110 in 100% air and was found to be similar to the values reported in the literature. The order of reaction for air and IG-110 graphite was determined to be about 0.76 ± 0.15 which is also within an acceptable range of reported values for nuclear-grade graphite. Compared to the oxidation rate and behavior of NBG-18, IG-110 oxidized more rapidly in the same experimental conditions and the oxidation was more uniform; this was attributed to super-fine filler coke microstructure of IG-110 compared to flake-like NBG-18 that has a range of small and mostly medium-sized filler particles. Also, a higher frequency factor was calculated for IG-110. IG-110 is more porous and experiences larger increases in surface area in the kinetic regime for oxidation reaction in comparison to NBG-18. The oxidation rate of IG-110 increases linearly with

temperature in the kinetic regime and the penetration depth of oxygen into IG-110 was shown to be much greater than that of NBG-18 in the same conditions. Compared to NBG-18, the oxidation rate of IG-110 reached a maximum at a higher temperature around 1473 K. The oxidation behavior of IG-110 has been shown to change gradually from a penetrating bulk attack to a pitting surface corrosion that forms an oxidized layer. Combustion products, functional groups and potentially catalytic elements were identified on the surface and internal layers of oxidized graphite samples via XPS, FTIR and EDS, respectively. Beyond 973 K, IG-110 formed visible pits and loose graphite powder, and the penetrating bulk oxidation mechanism changed abruptly to a surface attack.

Acknowledgements

This work was partially supported by the NERI-C-08-043 Grant from the Department of Energy. During the course of this work, Jo Jo Lee was a recipient of a Department of Education Graduate Assistance in Areas of National Need (GAANN) Fellowship.

References

[1] W. E. Windes, T. D. Burchell, R. Bratton, Project #23747, Graphite technology development plan, INL/PLN-2497 (2007).

[2] S.-H. Chi, G.-C. Kim, Comparison of the oxidation rate and degree of graphitization of selected IG and NBG nuclear graphite grades, J. Nucl. Mater. 381 (2008) 9-14.

[3] P. Wang, C. I. Contescu, S. Yu, T. D. Burchell, Pore structure development in oxidized IG-110 nuclear graphite, J. Nucl. Mater. 430 (2012) 229-238.

[4] J. Lee, T. K. Ghosh, S. K. Loyalka, Oxidation rate of nuclear-grade graphite NBG-18 in the kinetic regime for VHTR air ingress accident scenarios, J. Nucl. Mater. 438 (2013) 77-87.

[5] G. Q. Zheng, P. Xu, K. Sridharan, T. R. Allen, Pore structure analysis of nuclear graphites IG-110 and NBG-18, Ceramic Transactions 227 (2011) 251-260.

[6] W.-K. Choi, B.-J. Kim, E.-S. Kim, S.-H. Chi, S.-J. Park, Oxidation behavior of IG and NBG nuclear graphites, Nucl. Eng. and Des. 241 (2011) 82-87.

[7] C. I. Contescu, T. Guldan, P. Wang, T. D. Burchell, The effect of microstructure on air oxidation resistance of nuclear graphite, Carbon 50 (2012) 3354-3366.

[8] X. Luo, J.-C. Robin, S. Yu, Comparison of oxidation behaviors of different grades of nuclear graphite, Nucl. Sci. and Eng. 151 (2005) 121-127.

[9] ASTM D7219-05. "Standard specification for isotropic and near-isotropic nuclear graphites." ASTM, Int, 2005.

[10] J. Kane, C. Karthik, D. P. Butt, W. E. Windes, R. Ubic, Microstructural characterization and pore structure analysis of nuclear graphite, J. Nucl. Mater. 415 (2011) 189-197.

[11] E. L. Fuller and J. M. Okoh, Kinetics and mechanisms of the reaction of air with nuclear grade graphites: IG-110, J. Nucl. Mater. 240 (1997) 241-250.

[12] E. S. Kim, K. W. Lee, H. C. No, Analysis of geometrical effects on graphite oxidation through measurement of internal surface area, J. Nucl. Mater. 348 (2006) 174-180.

[13] IAEA: Thermophysical Properties of Materials for Nuclear Engineering: A Tutorial and Collection of Data, International Atomic Energy Agency, Vienna (2008).

[14] ASTM D7542-09. "Standard test method for air oxidation of carbon and graphite in the kinetic regime."

[15] R. E. Smith, Status of graphite oxidation work, INL/EXT-10-18880 (May 2010).

[16] X. Luo, J.-C. Robin, S. Yu, Effect of temperature on graphite oxidation behavior, Nucl. Eng. Des. 227 (2004) 273-280.

[17] S.-H. Chi, C. I. Contescu, T. D. Burchell, Density change of an oxidized nuclear graphite with acoustic microscopy and image processing, J. Eng. Gas Turb. Pow. 131, September 2009.

[18] R. P. Wichner, T. D. Burchell, C. I. Contescu, Penetration depth and transient oxidation of graphite by oxygen and water vapor, J. Nucl. Mater. 393 (2009) 518-521.

[19] E. S. Kim, H. C. No, B. J. Kim, C. H. Oh, Estimation of graphite density and mechanical strength variation of VHTR during air-ingress accident, Nucl. Eng. Des. 238 (2008) 837-847.

[20] ASTM C559-90 (Reapproved 2010), "Standard test method for bulk density by physical measurements of manufactured carbon and graphite articles."

[21] ASTM C1179-91 (Reapproved 2010), "Standard test method for oxidation mass loss of manufactured carbon and graphite materials in air."

[22] E. S. Kim, H. C. No, Experimental study on the oxidation of nuclear graphite and development of an oxidation model, J. Nucl. Mater. 349 (2006) 182-194.

[23] M. S. El-Genk, J.-M. P. Tournier, Development and validation of a model for the chemical kinetics of graphite oxidation, J. Nucl. Mater. 411 (2011) 193-207.

[24] H.-K. Hinssen, K. Kuhn, R. Moormann, B. Schlogl, M. Fechter, M. Mitchell, Oxidation experiments and theoretical examinations on graphite material relevant for the PMBR, Nucl. Eng. Des. 238 (2008) 3018-3025.

[25] J. P. Redfern, Differential Thermal Analysis, edited by R. C. Mackenzie, vol. I., Academic Press (1970) 123.

[26] J. M. Smith, Chemical Engineering Kinetics, McGraw-Hill (2d ed, 1956) 71.

[27] K. J. Laidler, Chemical Kinetics, Benjamin Cummings (3d ed, 1997).

[28] M. El-Genk, Graphite oxidation simulation in HTR accident conditions, Project No. 09-830 (October 2012).

CHAPTER 4

Oxidation rate of graphitic matrix material in the kinetic regime for VHTR air ingress accident scenarios

Jo Jo Lee, Tushar K. Ghosh, Sudarshan K. Loyalka*

Nuclear Science and Engineering Institute, Particulate Systems Research Center, University of Missouri, Columbia, Missouri 65211
**Corresponding Author: Phone: +15738823568, Fax: +15738844801, Email: loyalkaS@missouri.edu*

Abstract

Data on oxidation rates of matrix-grade graphite in the kinetically-controlled temperature regime of graphite oxidation are needed for safety analysis of High Temperature Gas Cooled Reactors and Very High Temperature Reactors. In this work, the oxidation rate of graphitic matrix material GKrS was measured thermogravimetrically for various oxygen concentrations and with temperatures from 873 to 1873 K. A semi-empirical Arrhenius rate equation was also developed for this temperature range. The activation energy of the graphitic material is found to be about 111.5 kJ/mol. The order of reaction was found to be about 0.89. The surface of oxidized GKrS was characterized by Scanning Electron Microscopy, Electron Dispersive Spectroscopy, Fourier Transform Infrared Spectroscopy and X-ray Photoelectron Spectroscopy.

---

1. Introduction

The Very High Temperature Reactor (VHTR) is a Generation IV reactor concept with two potential core designs, prismatic (block) or pebble bed. The VHTR is powered by spherical tristructural-isotropic (TRISO) fuel particles as shown in Figure 1. A uranium

dioxide (UO_2) containing fuel kernel is coated with a pyrolytic carbon (PyC) binder and then with an inner pyrolytic carbon layer that is covered with a silicon carbide (SiC) ceramic coating and an exterior pyrolytic carbon layer.

In a prismatic reactor the TRISO fuel particles are formed into cylindrical fuel rods with matrix-grade graphite. Then, these fuel compacts are inserted and stacked into hexagonal graphitic blocks that are composed of highly-graphitized nuclear-grade graphite. In contrast, the pebble bed core could consist of over 400,000 or so stacked fuel pebbles wherein each fuel pebble contains over 10,000 TRISO microspheres distributed in a spherical fuel compact composed of matrix-grade graphite [1]. Unlike nuclear-grade graphite, matrix-grade graphite consists of partially-graphitized material. This is due to the temperature of fuel compact fabrication which occurs below 2273 K—if temperatures greater than 2273 K were used, uranium diffusion out of the TRISO fuel kernel becomes a concern [2-4]. Highly-graphitized nuclear-grade graphites are fabricated at temperatures exceeding 2773 K, since graphitization typically occurs between 2773 and 3073 K [5].

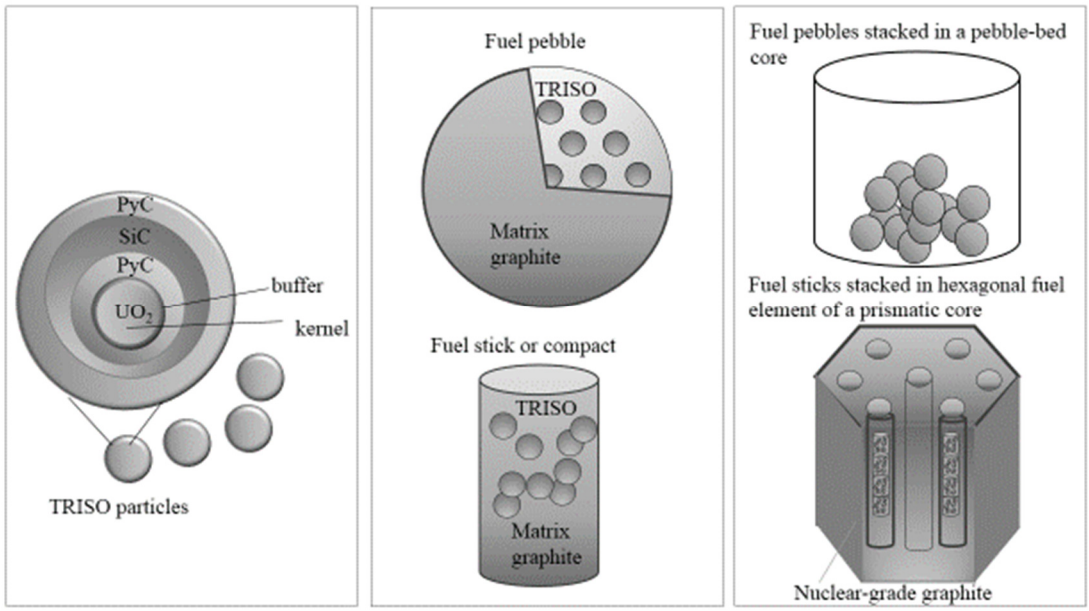

Fig. 1. Basic comparison of fuel pebbles and fuel sticks for pebble bed and prismatic graphite cores, respectively.

Whereas a prismatic reactor core contains small amounts of matrix-grade graphite, a pebble bed core consists predominantly of the partially-graphitized matrix-grade graphite [3]. One could foresee that, in the event of an air ingress accident, a pebble bed core could be more susceptible to oxidation damage versus a prismatic core design. We have previously reported on the oxidation performance of nuclear-grade graphite NBG-18 [6] and IG-110 [7], and we are extending that work to matrix-grade graphite. The purpose of this study is to report the oxidation performance of candidate matrix-grade graphite GKrS under similar VHTR air ingress accident conditions.

2. Background and history of the A3 matrix recipe

Matrix-grade graphite is not nuclear-grade graphite by definition. While both nuclear- and matrix-grade graphite are used as fuel element materials in High Temperature Gas Reactors (HTGRs) and VHTRs, the matrix-grade material was mainly developed for use in manufacturing fuel sticks or pebbles. Historically, the “admix” process was developed

in the UK's DRAGON reactor program. The admix process was basically a method for overcoating fuel particles to produce fuel compacts. In the admix process, about 88 wt% graphitized petroleum coke filler was mixed with about 12 wt% resin binder in a denatured alcohol. The mixture was subsequently dried and then re-ground to produce a resin-coated graphite powder. Coated fuel particles were then "overcoated" with the resinated graphite powder and then warm pressed in a mold. Then, the mix was ejected from the mold, carbonized (baked), and then heat treated to form the fuel compact [8].

In Germany in the 1970s, fuel pebbles were made by incorporating the DRAGON overcoating process. Spherical fuel elements were being developed for use in the prototype pebble bed reactor called AVR (German: Arbeitsgemeinschaft Versuchsreaktor) and the Thorium High Temperature Reactor (THTR). However, instead of the coke filler, a mixture of natural and synthetic graphite was used along with a higher percentage of thermosetting resin binder. The Germans used the proportions of 64 wt% natural graphite with 16 wt% synthetic graphite and 20 wt% thermosetting resin binder; it was called the "A3 matrix" recipe. The A3 matrix was manufactured in a single-mixing step, dried and reground. The matrix powder was used to overcoat fuel particles that were wetted with solvent for better adhesion. The overcoated particles were then mixed again with additional A3 matrix and isostatically pressed into spherical fuel pebbles [8,9].

In the US, General Atomics developed and produced fuel compacts or fuel rods for the Fort Saint Vrain reactor, which had a prismatic core. Fuel compacts were made by using fuel particles that were randomly packed in a mold. Then, molten pitch of matrix material was injected via "slug injection" method. However, impurities from the pitch were later

correlated with problematic fuel performance. Since the early 2000s, Oak Ridge National Laboratory (ORNL) began recommending their novel approach to use the A3 matrix recipe to overcoat fuel particles and then hot press them into a cylindrical shape. ORNL developed a matrix production method wherein the A3 matrix formulation by the Germans was adopted but with modern graphites. The process allows flexibility in fuel particle loading fraction and fuel compact shape [9,10].

The novel process by ORNL consists of matrix graphite production and fuel compacting method. In brief, the ORNL matrix graphite production process uses natural graphite for compressibility, synthetic graphite for toughness and thermosetting resin for better adhesion to TRISO particles but also to help harden and fuse the compact into a solid piece during carbonization. Resinated graphite powder is reground into a very fine powder that is used for overcoating fuel particles. Overcoated fuel particles are then compacted with a hot press. The carbonization step occurs at around 350 K/h in helium and then held at 1223 K for one hour. In a final carbonization step the compact is heat treated for 20 K/min in vacuum furnace and held between 1923 and 2123 K for one hour [8]. The graphitic matrix material produced from ORNL's process was called "GKrS;" numerals that follow the name indicate the date of manufacturing of a particular batch. The graphitic matrix material GKrS that was received from ORNL is the subject of the oxidation experiments and kinetic parameters reported here.

In past studies, oxidation experiments and basic kinetic data for matrix-grade graphite in air are sparse. The historic grades of A3-3 or A3-27 are no longer commercially available and modern candidate grades are still being developed and are hard to obtain.

Generally, from past studies the activation energy of historic matrix-grade graphitic materials is lower than most modern nuclear-grade graphites [3,11,12]. Table 1 displays the activation energies of matrix-grade graphite and VHTR nuclear-grade graphites from past studies.

Table 1
Activation energies of matrix- and nuclear-grade graphite oxidation.

Research group	Graphite type	Activation energy (kJ/mol)
Contescu et al. [12]	ORNL in-house matrix material	160*
Hinssen et al. [11]	V483T5	165
	A3-27 Filler	166
	A3-27 Binder	123
Chi and Kim [13]	NBG-25	163**
	IG-430	167**
Lee et al. [6,7]	NBG-18	187**
	IG-110	222**

*batch unspecified, **VHTR candidate materials.

Moorman et al. noted that the activation energy of fine-grained nuclear-grade graphite V483T was similar to matrix-grade graphite A3-27, and the activation energies of filler and binder for A3-27 were reported separately [3]. A number of researchers have observed preferential binder oxidation in their studies [11-14]. It is theorized that the activation energy of the binder is lower than that of the filler material in matrix-grade graphite due to the binder having smaller number of accessible reactive sites, but also the filler microstructure tends to be more ordered with smaller crystallite sizes [12]. Porosity often develops first in the binder. Preferential binder oxidation is often correlated with degradation of mechanical properties of graphite in the kinetic regime of graphite oxidation.

3. Measurements

GKrS was received from ORNL in August 2011. ORNL produced GKrS from GrafTech International® Natural Flake Milled graphite "GTI-NFM" (6.52 μm), SGL Carbon® KRB2000 synthetic graphite "SGL-KRB2000" (29.20 μm) and Borden Durite® SC1008 thermosetting resin [8]. The mixing ratio was 64: 16: 20 by weight, respectively. The final GKrS graphite particles are super-fine and have an average particle size of about 11.30 μm; the averages could include aggregate particle sizes so actual particle sizes could be smaller. The final materials to produce GKrS were chosen by ORNL due to their low anisotropy, superior overcoating performance, low impurity content but also commercial availability [8]. Table 2 displays the average impurity concentrations obtained with Glow Discharge Mass Spectrometry (GDMS) by ORNL for natural graphite, synthetic graphite and resin raw materials for their graphitic matrix materials [8,10].

Table 2
Typical elemental composition of matrix materials obtained by ORNL by using GDMS.

ELEMENT	GTI-NFM	SGL-KRB2000	DURITE SC1008
AL	1.6	0.35	50
CA	3.1	0.70	1.0
TI	43	0.06	0.35
V	5.1	0.02	0.02
CR	0.61	<0.5	<0.5
MN	<0.05	<0.5	0.1
FE	13	1.4	2.5
CO	<0.05	0.25	0.25
NI	0.45	1.2	0.25
NA	1.5	0.45	25
BA	<0.1	<0.1	<0.1
SI	25	3.1	60

3.1. Specimen and sample preparation

GKrS cylinders approximately 12 mm x 12 mm were obtained from ORNL. However, the batch was far limited in number compared to the experiments that were ideally planned. The manufacturing date of the batch is also unknown. Given the uncertainty of the stock of future test cylinders, the cylinders here were crushed with mortar and pestle to be used in the standard thermogravimetric apparatus. The average sample mass was around 1.0 g.

3.2. Graphite oxidation equipment

A Thermax700 thermogravimetric analyzer (TGA) from Thermo Scientific® was used to obtain the mass change versus temperature data in real-time during graphite oxidation in air. Graphite samples were placed in an alumina cylindrical sample bucket with a platinum bail held from an alumina extension wire. The volume of the bucket is 35 mL. The balance has a 100 g capacity and resolution of ±1.0 µg. Mixtures of dry medical-grade air in ultra-high purity research-grade helium having a total flow rate of 50 mL/min were used in the experiment. Mass flow controllers were used to control the flow rate and helium gas streams were flowed through oxygen scrubbers. The concentration of oxygen in the TGA inlet and purge was monitored with an oxygen meter. A schematic diagram of the experiment is found in our previous graphite study [6].

3.3. Experimental procedure

Mass loss data was collected isothermally and in real-time using TGA. Graphite samples were heated in ultra-high purity helium at a constant rate of about 5 K/min until the desired oxidation temperature was reached, at which point samples were switched to a

100% dry air environment or a mixture of inlet air and helium, as needed. This gas-switching procedure ensured that the initial surface states of samples were protected from oxidation and burnoff (ratio of oxidized to unoxidized sample) during the ramping period, especially for lower temperature runs where greater penetration depths through the bulk of the graphite specimen is generally expected [6,7]. First, samples were tested isothermally for several temperatures between 873 to 1873 K. Then, graphite samples were exposed for 10 h in four different air leak scenarios. The inlet gas stream contained 5, 10, 15 and 21 mol% O_2 concentrations. The mass loss rates were measured isothermally once the desired temperature was reached in the TGA.

3.4. Scanning Electron Microscopy (SEM)

High resolution images of pure and oxidized samples were obtained using the Hitachi S-4700 which is a cold-field emission SEM. Hitachi S-4700 has multiple scanning modes, an accelerating voltage ranging from 0.5 to 30 kV and a maximum resolution of 1.5 nm. For this study, the scanning mode for the secondary electron maxing out at about 40 frames per second, at a working distance between 7 to 10 mm and 10 kV accelerating voltage were suitable to capture details on the surface of graphite samples. Magnification was around 5000X. Energy dispersive spectroscopy (EDS) which gives quantitative surface elemental data was simultaneously available from Hitachi S-4700.

3.5. Fourier Transform Infrared Spectroscopy (FTIR)

The Tensor-27 from Bruker Optics was used to identify the presence of surface functional groups after oxidation treatment of graphite samples. Tensor-27 generates a mid-range (4000 cm^{-1} to 400 cm^{-1}) infrared spectrum and accommodates a diffuse

reflectance cell, EasiDiff® that is convenient for analyzing powdered samples. Graphite powder samples were prepared into 5 to 10% mixtures in spectraphotometric-grade KBr for spectral analysis. Spectral data was obtained for 128 scans at 4 cm^{-1} resolution.

3.6. X-ray Photoelectron Spectroscopy (XPS)

Broad-scan XPS from 0 to 1100 eV was used to collect more quantitative data on oxidized graphite samples and to examine the composition (e.g. the electronic or chemical state of elements) and confirm the presence of elements on the surface. The Kratos Axis 165 with an 8-channel analyzer was used with a monochromatic Al source (150W). The standard slot or "spot" size analysis area was 700 µm x 300 µm. The Kratos Axis 165 was used with a charge neutralizer in Hybrid Mode, employing both magnetic and electrostatic lenses.

4. Results and discussion

Isothermal oxidation data for GKrS using TGA was collected under similar experimental conditions as our previous studies on nuclear-grade graphite [6,7]. Pure and TGA-oxidized samples were then examined and compared using several surface characterization techniques including SEM, EDS, FTIR and XPS.

4.1. The effect of temperature on oxidation rate

GKrS samples were tested isothermally in 100% dry medical-grade air at 873, 923, 973, 1023, 1173, 1473 and 1873 K using TGA. Table 3 displays mass loss data for GKrS oxidation in air and also the weight-normalized oxidation rates. Oxidation runs were

performed twice to confirm the reliability and repeatability of the data. A very good repeatability of the data was observed.

Table 3
Mass loss rates and weight-normalized oxidation rates for GKrS, average of two trials.

T	**Mass loss rates**	**OR^w**
K	mg hr^{-1}	g hr^{-1} g^{-1}
873	3.60	0.043
923	16.20	0.191
973	30.60	0.213
1023	83.88	0.499
1173	54.00	0.240
1473	66.60	0.331
1873	131.40	0.378

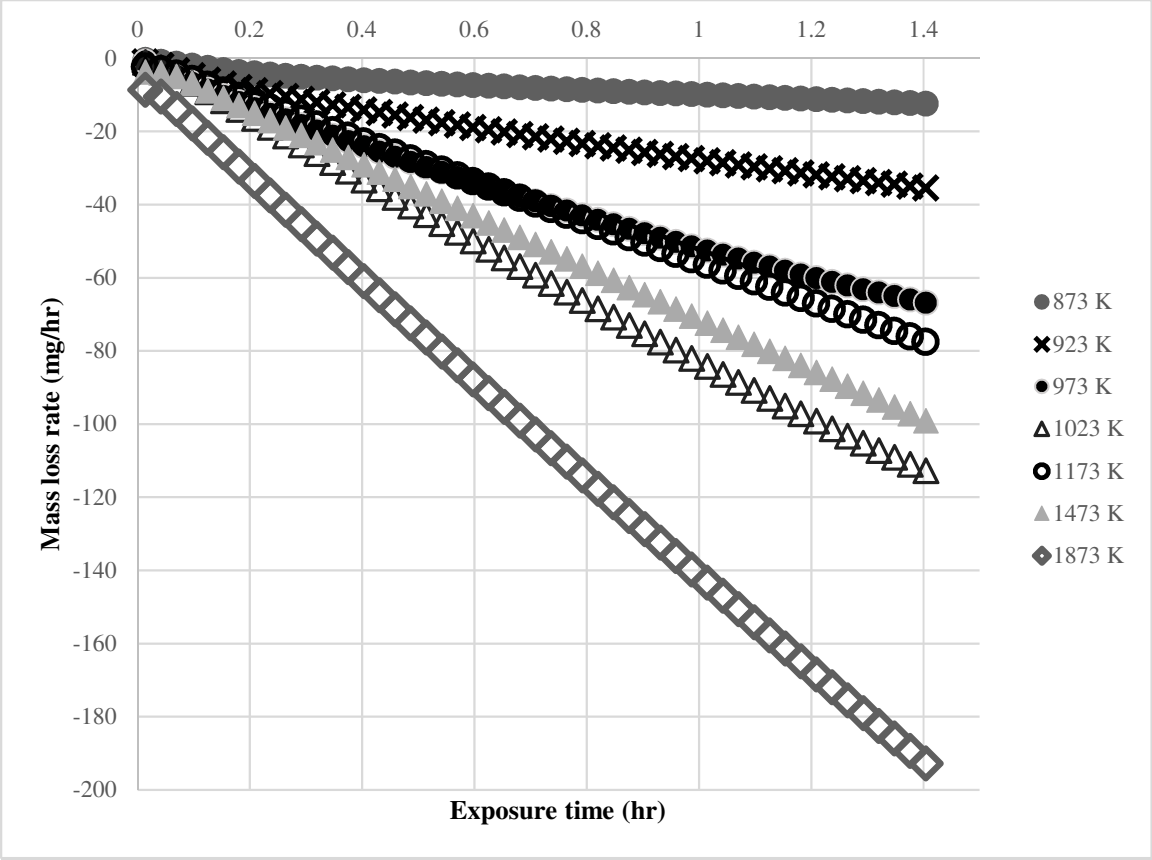

Fig. 2. Isothermal mass loss data in 100% dry medical grade air for GKrS.

Figure 2 displays the GKrS data from TGA for isothermal oxidation in 100% air between 873 and 1873. In general, the mass loss rates of GKrS increase steadily with the isothermal oxidation temperatures tested up to 1873 K as shown in Table 3 and Fig. 2. Figure 3 displays the weight-normalized oxidation rates for GKrS alongside the data for nuclear-grade graphite IG-110 and NBG-18 from our previous studies [6,7]. From Fig. 3 the difference in oxidation rates between nuclear- and matrix-grade is more apparent in the kinetic regime, between 873 to 1023 K, wherein GKrS tends to oxidize a bit faster than nuclear grades IG-110 and NBG-18.

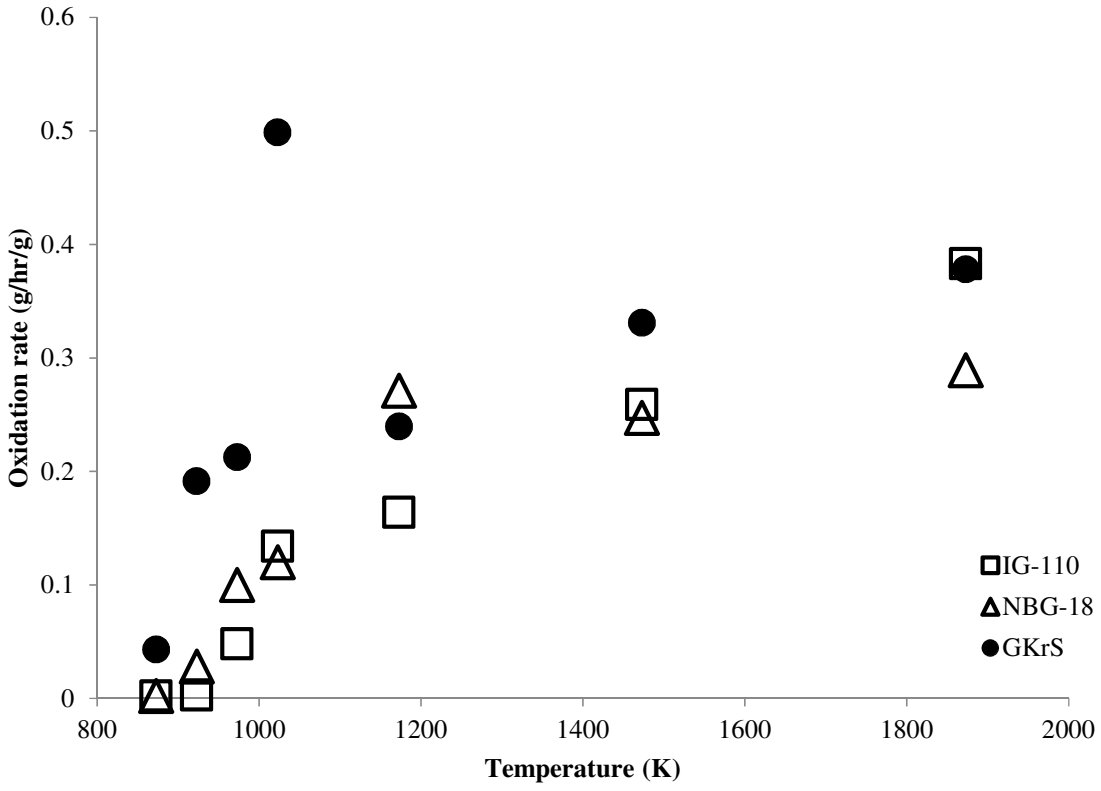

Fig. 3. Comparison of the isothermal oxidation rates of GKrS with nuclear-grade graphite IG-110 and NBG-18.

The activation energy of GKrS was determined from the TGA mass loss data collected by following the oxidation experiment outlined in Section 3.3. The mass loss data from Table 3 along with the procedure outlined in ASTM 7542-09 was used to calculate the activation energies from an Arrhenius plot [6,15]. Figure 4 is the Arrhenius plot for GKrS along with nuclear-grade graphite IG-110 and NBG-18 data in the same experimental conditions [6,7,12]. The activation energy for GKrS was determined to be 111.5 kJ/mol in the kinetic regime, from 873 to 1023 K. The activation energy determined in this study is within the range of values from past studies as shown in Table 1. The lower activation energy of matrix graphite could be attributed to the preferential oxidation of the binder phase in the kinetic regime.

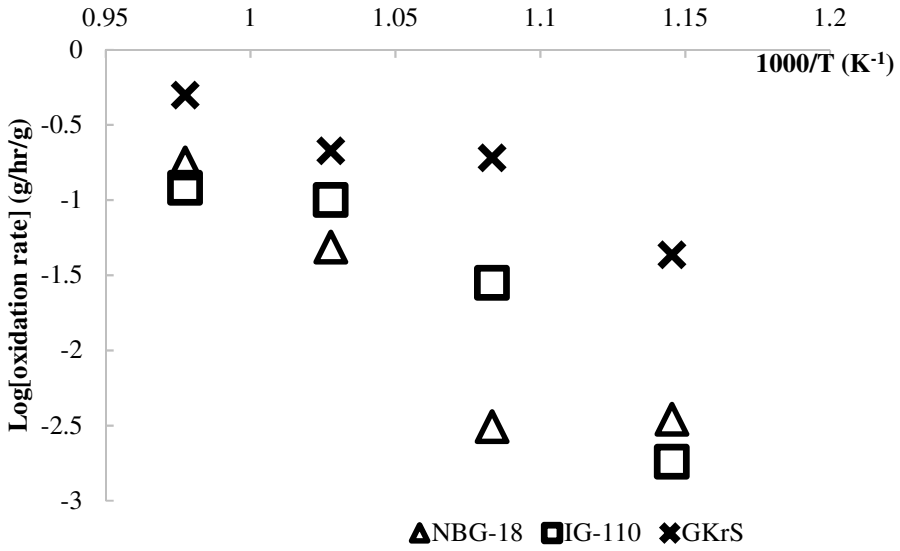

Fig. 4. Comparison of Arrhenius data for oxidation of GKrS with nuclear-grade graphite IG-110 and NBG-18 in 100% air.

4.2. The effect of concentration on oxidation rate

The effect of oxygen concentration on the mass loss rates of GKrS at 1023 K were studied in order to obtain the reaction order. GKrS samples were oxidized in 5, 10, 15 and 21 mol% air in helium mixtures, as described in Section 3.3.

The experimental mass loss data for four concentrations of oxygen at 1023 K were used to determine the order of the reaction with respect to oxygen partial pressure from a linear fit of the data. Figure 5 is a plot of ln k vs. ln P_{O_2} used to determine the reaction order of GKrS. The reaction order of 0.89 ± 0.09 was found. In this case, the results indicate that the reaction order is approximately first-order of the partial pressure of oxygen on the surface of graphite.

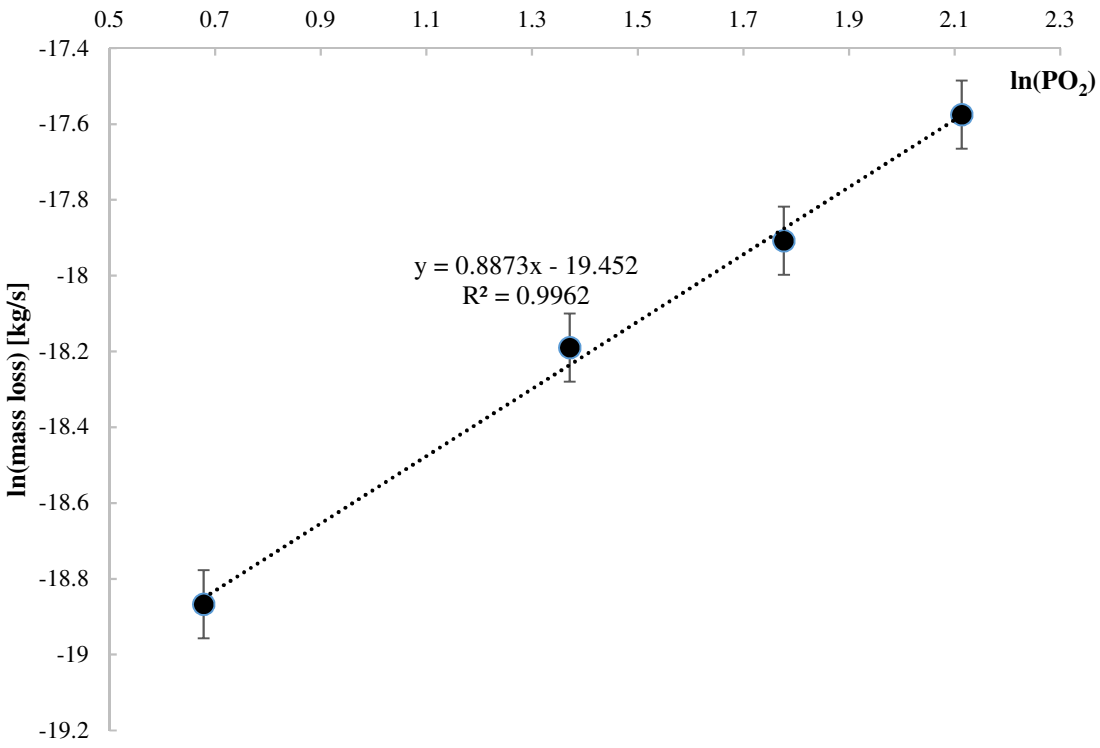

Fig. 5. Order of reaction with respect to the oxygen partial pressure for the elementary reaction between GKrS graphite and air.

4.3. The rate equation for the kinetic regime of GKrS oxidation

The semi-empirical Arrhenius equation can be used to describe most thermally-induced processes, such as oxidation. In practice, it has also demonstrated strong experimental accuracy [6,15-20]. An overall kinetic rate equation for the oxidation of GKrS can be written as in our previous study on nuclear-grade graphite [6,7]. In Fig. 4 between 873 and 1023 K, the slope was $-\frac{E_a}{2.303 \cdot R} = -5.8262$ where R = 8.314 J/mol K and the intercept was $\log_{10} A = 5.4025$. The activation energy E_a of GKrS in the kinetic regime in 100% air was 111.5 kJ/mol and the frequency factor A was 2.526 x 10^5, which is lower than that of nuclear-grade graphites previously studied [6,7]. According to Table 1, the activation energy found in this study is similar for other matrix-grade materials, although the

comparison is really limited. According to Table 1 and this study, the activation energy of nuclear-grade graphites range from 170 to 220 kJ/mol while matrix materials range from about 110 to 160 kJ/mol.

Using the semi-empirical Arrhenius equation as in our previous study [6], the reaction rate velocity for GKrS in the kinetic regime applicable from 873 to 1023 K becomes

$$k_I\left(\frac{g}{h\cdot g}\right) = 2.526 \text{ x } 10^5 \cdot e^{-\left(\frac{111.5\frac{kJ}{mol}}{T(K)}\right)} \quad (1)$$

Using the semi-empirical Arrhenius equation and the reaction order determined in Section 4.2, the specific rate of reaction with respect to partial pressure of oxygen on the surface is given by Eq. (2) below.

$$r_I\left(\frac{g}{h\cdot g}\right) = 2.526 \text{ x } 10^5 \cdot e^{-\left(\frac{111.5\frac{kJ}{mol}}{T(K)}\right)} \cdot P_{O_2}^{0.89} \quad (2)$$

4.4. Surface characterization of pure and oxidized GKrS

The surface of matrix material GKrS was explored via SEM/EDS. Figures 6(a) and (b) display the SEM images of the pure, unoxidized GKrS surface. The surface appears fine-grained with flake-like sheets.

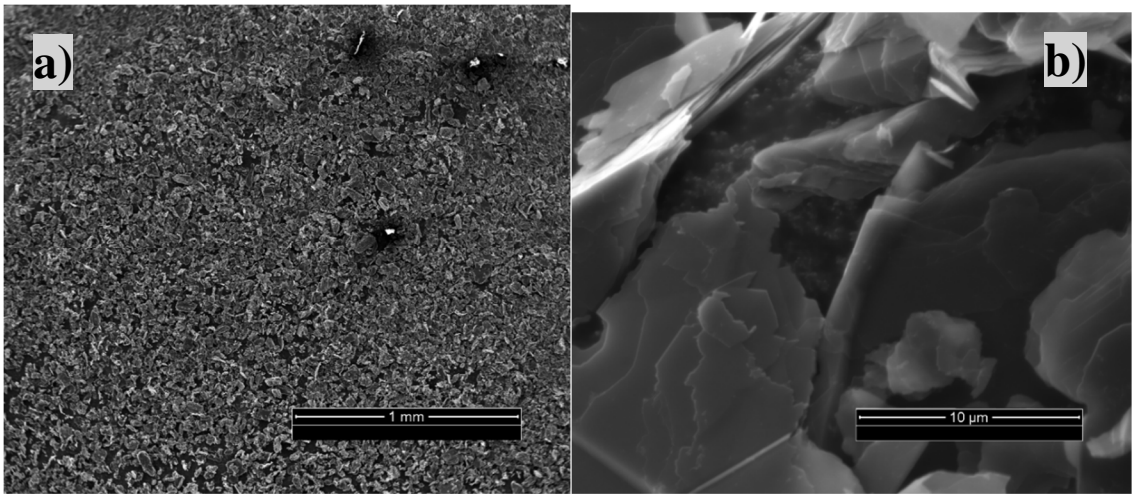

Fig. 6. SEM imaging of pure GKrS surface **a)** at 50X and **b)** 5000X Mag.

Figures 7(a) and (b) display the SEM images of the surface of GKrS after oxidation in 100% air at 1023 K using TGA. The surface is dramatically changed after oxidation treatment. In Figure 7(a) the binder material is shrinking around the filler grains. Oxidation on the surface of samples did not appear uniform.

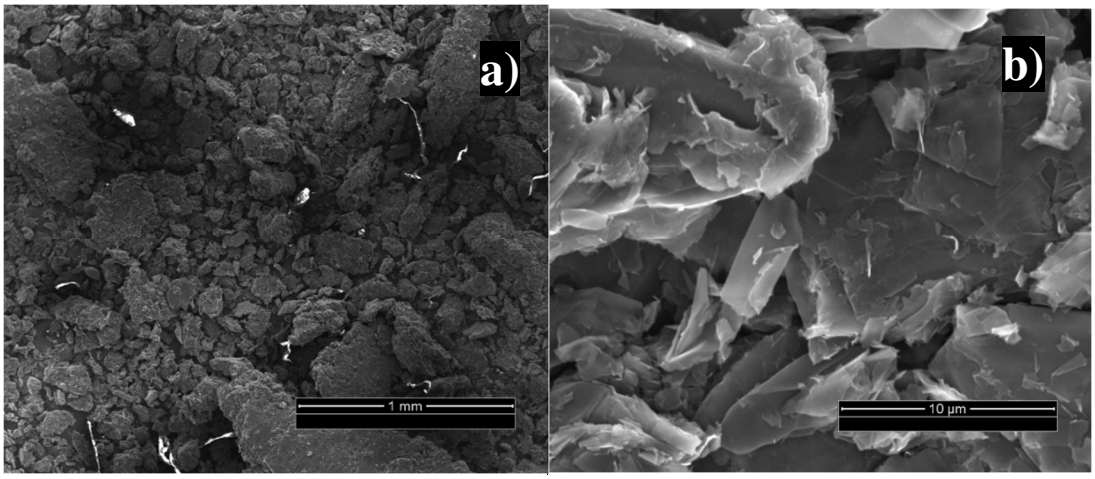

Fig. 7. SEM imaging of the surface of GKrS samples oxidized at 1023 K at **a)** 50X and **b)** at 5000X Mag.

EDS results were obtained on pure and oxidized samples of GKrS. According to EDS obtained on oxidized samples in Figs. 8(a) and (b), GKrS is initially pure with a strong

carbon signal which reduces with oxidation treatment at just 1023 K. Depending on where the EDS was taken, the samples exhibited trace amounts of silicon and potassium but other elements were not detected with EDS.

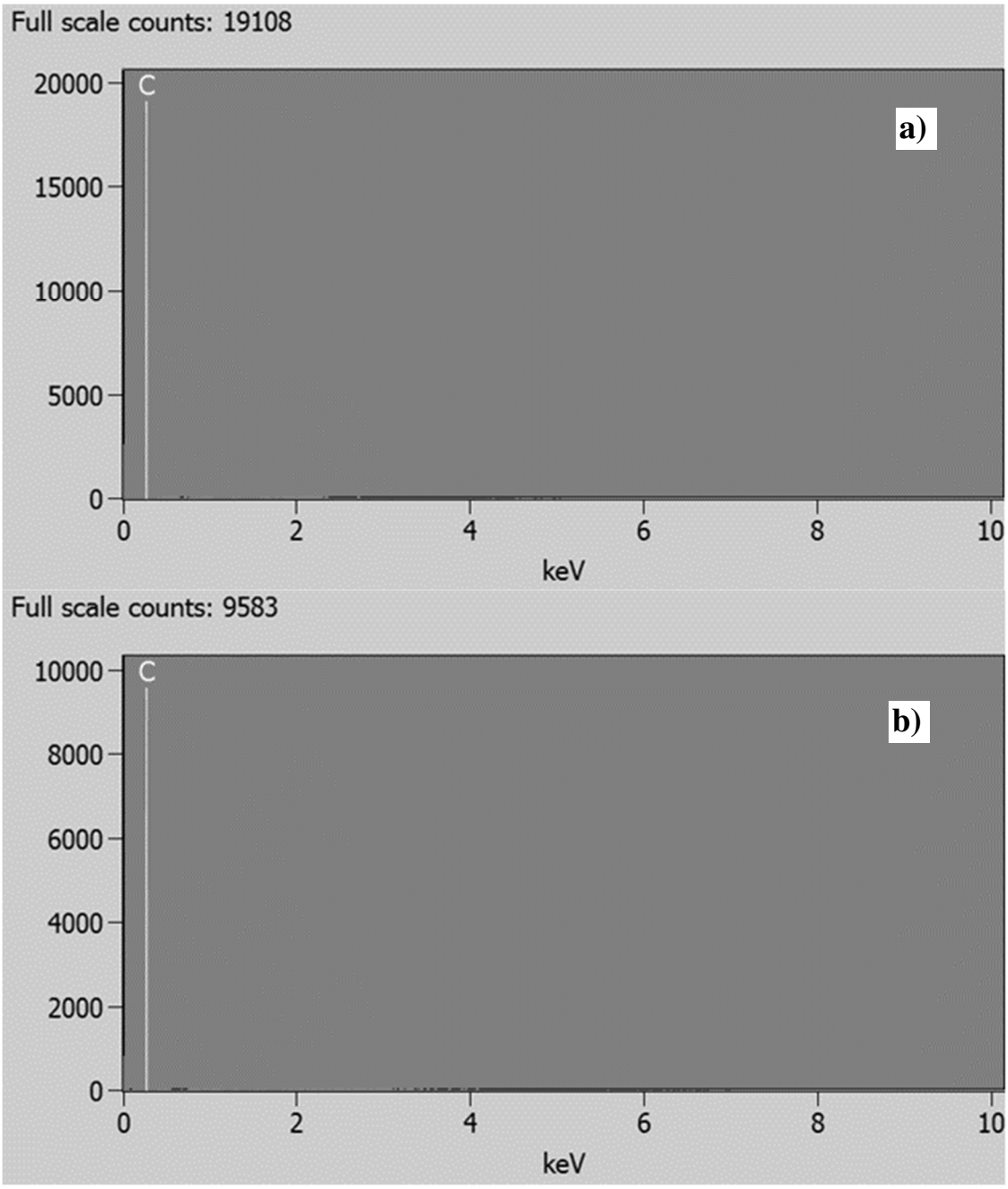

Fig. 8. SEM/EDS of **a)** pure and **b)** oxidized GKrS at 1023 K.

Oxidized graphite samples were also studied using XPS which detected more trace elements on the surface of GKrS. Figure 9 shows the broad-scan XPS spectra for the surface of GKrS samples oxidized in 100% air at 1023 K versus a pure sample. With oxidation, the O_{1s} peak increases and the C_{1s} peak decreased significantly. There is a slight signal for the O_{2s} peak. Ba_{3d} and Ba_{4d} signals also appeared in the oxidized samples although barium is an impurity that is only expected in trace amounts according to Table 2.

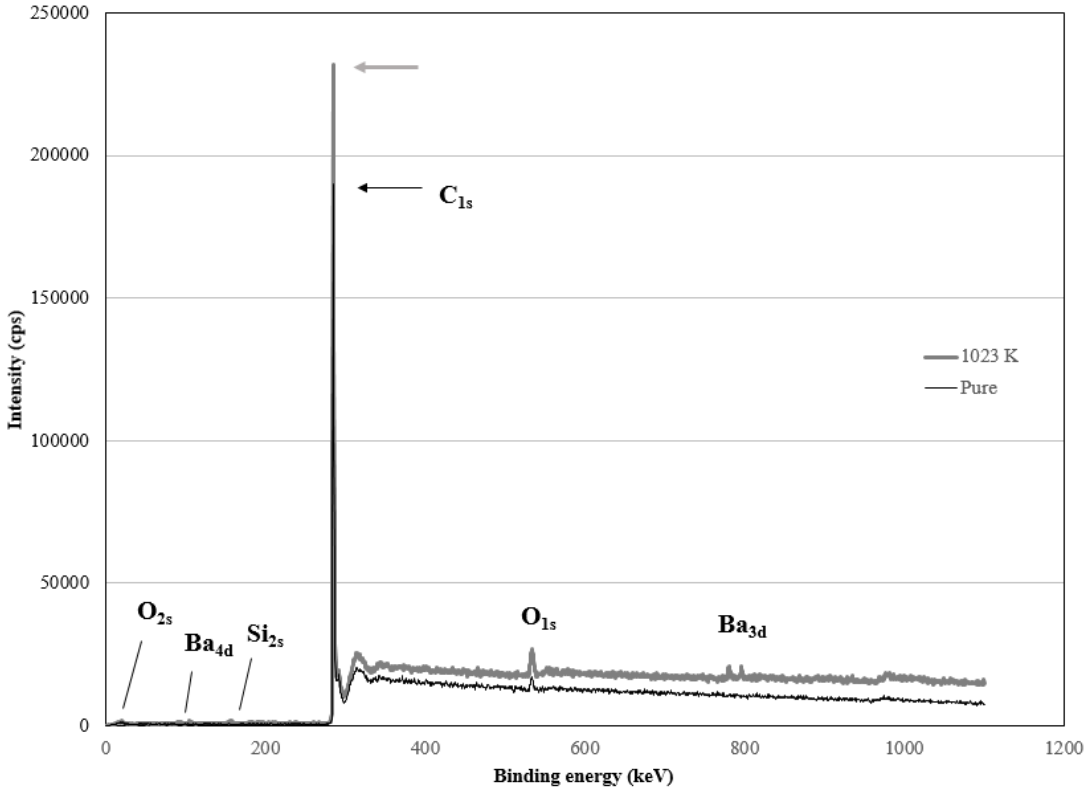

Fig. 9. XPS broad-scan of GKrS pure and oxidized in air at 1023 K.

FTIR was used to confirm the presence of surface active functional groups and combustion products on the surface of the oxidized matrix material. Figure 10 shows the FTIR transmission spectra of oxidized GKrS in air between 873 and 1023 K. In Fig. 10,

the asymmetrical stretching vibration of -CO_2 was detected around 2400 to 2300 cm^{-1} and the degenerate scissoring vibrations of -CO_2 were detected around 666 cm^{-1}. The intensity of the -CO_2 vibration increased with oxidation temperature. Broad band stretching vibration from carbonyl functional group -C=O were detected between 1800-1600 cm^{-1}. Around 1600 cm^{-1}, the stretching vibration from -C=C- in an aromatic ring were detected. The structure of phenolic resin contains benzene rings. Three peaks associated with a methylene bridge from the resin were detected at about 2925, 2850 and 1470 cm^{-1}. Alkane -C-H bonds were detected between 2950-2850 cm^{-1}. Water was a persistent impurity in the background as -O-H stretching vibrations were detected around 3400 cm^{-1}.

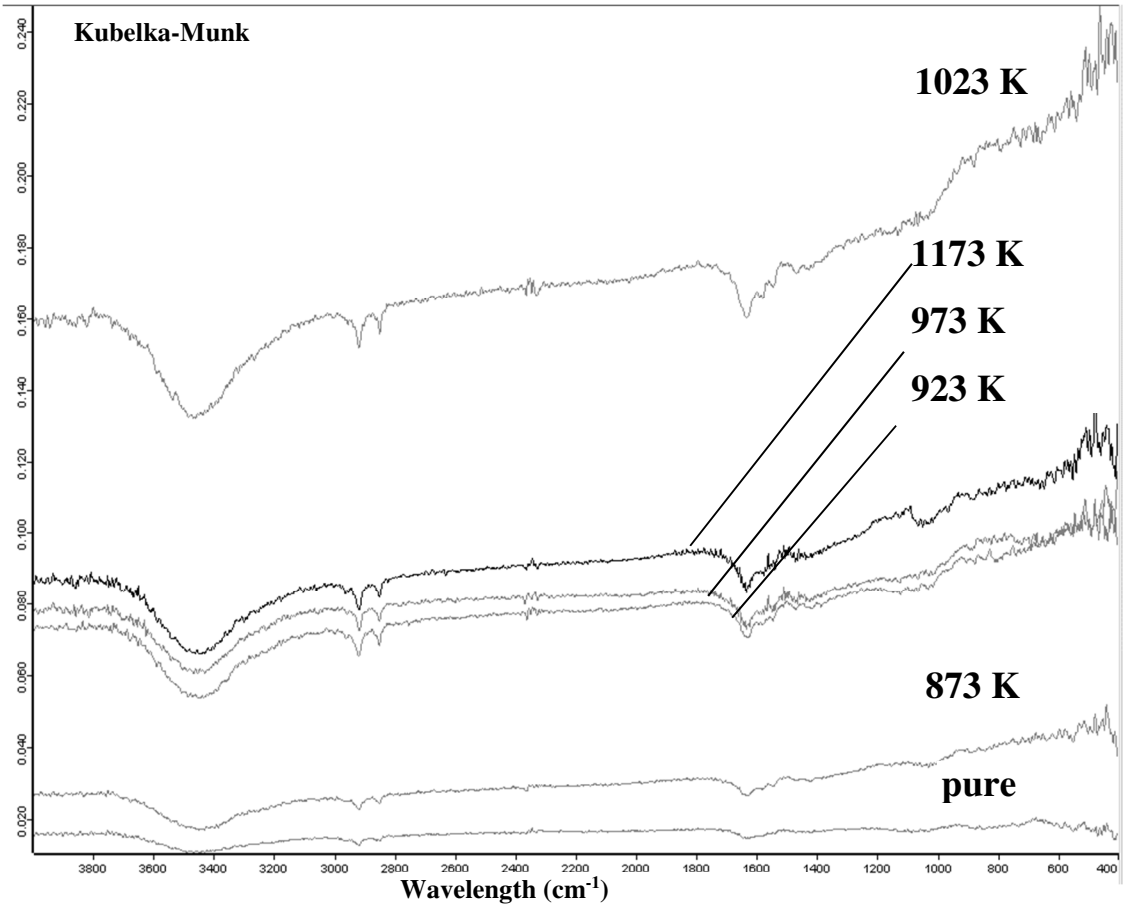

Fig. 10. FTIR spectra of pure and oxidized GKrS in 100% air between 873 and 1173 K.

5. Conclusions

The oxidation rate of GKrS was modeled in 100% air for the kinetic regime of graphite oxidation in the temperature range of 873 to 1023 K and various oxygen concentrations. The activation energy calculated from the Arrhenius equation was 111.5 kJ/mol for GKrS which is within other limited reported values. Given the lower activation energy compared to nuclear-grade graphites that were tested in similar conditions, GKrS oxidizes at a high rate in the kinetic regime similar to the oxidation rates of nuclear-grade graphite. Most of the resin binder in the graphitic material is probably oxidized in this regime. However, at higher temperatures, GKrS is less oxidized than nuclear-grade graphite overall. The order of reaction for GKrS in air was determined to be about 0.89 ± 0.09. The surface of oxidized samples was active with combustion products, functional groups, binder resin compounds and potentially catalytic elements that were identified using XPS, FTIR and EDS, respectively.

Acknowledgements

This work was partially supported by the NERI-C-08-043 Grant from the Department of Energy. During the course of this work, Jo Jo Lee was a recipient of a Department of Education Graduate Assistance in Areas of National Need (GAANN) Fellowship. We also thank ORNL for providing us with matrix graphite samples.

References

[1] X. Yu, S. Yu, Analysis of fuel element matrix graphite corrosion in HTR-PM for normal operating conditions, Nucl. Eng. and Des. 240 (2010) 738-743.

[2] E. Hoinkis, E. Robens, Surface area and porosity of unmodified graphitic matrices A3-27 and A3-3 (1050) and oxidized matrix A3-3 (1950), Carbon 27 (1989) 157-168.

[3] R. Moormann, H.-K. Hinssen, K. Kuhn, Oxidation behaviour of an HTR fuel element matrix graphite in oxygen compared to a standard nuclear graphite, Nucl. Eng. and Des. 227 (2004) 281-284.

[4] Response of fuel, fuel elements and gas cooled reactor cores under accidental air or water ingress conditions, IAEA-TECDOC-784, October 1993.

[5] W.E. Windes, T.D. Burchell, R. Bratton, Project #23747, Graphite technology development plan, INL/PLN-2497 (2007).

[6] J. Lee, T.K. Ghosh, S.K. Loyalka, Oxidation rate of nuclear-grade graphite NBG-18 in the kinetic regime for VHTR air ingress accident scenarios, J. Nucl. Mater. 438 (2013) 77-87.

[7] J. Lee, T.K. Ghosh, S.K. Loyalka, Oxidation rate of nuclear-grade graphite IG-110 in the kinetic regime for VHTR air ingress accident scenarios, J. Nucl. Mater. 446 (2014) 38-48.

[8] P.J. Pappano, T.D. Burchell, J.D. Hunn, M.P. Trammell, A novel approach to fabricating fuel compacts for the next generation nuclear plant (NGNP), J. Nucl. Mater. 318 (2008) 25-38.

[9] E. Hoinkis, Transport of Fission Products in Matrix and Graphite, Proceedings of a Colloquium held at Hahn –Meitner-Institut Berlin, November 1981.

[10] M.P. Trammell, P.J. Pappano, Analysis of natural graphite, synthetic graphite, and thermosetting resin candidates for use in fuel compact matrix, ORNL/TM-2011/315.

[11] H.-K. Hinssen, K. Kuhn, R. Moormann, B. Schlogl, M. Fechter, M. Mitchell, Oxidation experiments and theoretical examinations on graphite material relevant for the PBMR, Nucl. Eng. Des. 238 (2008) 3018-3025.

[12] C.I. Contescu, S. Azad, D. Miller, M.J. Lance, F.S. Baker, T.D. Burchell, Practical aspects for characterizing air oxidation of graphite, J. Nucl. Mater. 381 (2008) 15-24.

[13] S.-H. Chi, G.-C. Kim, Comparison of the oxidation rate and degree of graphitization of selected IG and NBG nuclear graphite grades, J. Nucl. Mater. 381 (2008) 9-14.

[14] R.P. Wichner, T.D. Burchell, C.I. Contescu, Penetration depth and transient oxidation of graphite by oxygen and water vapor, J. Nucl. Mater. 393 (2009) 518-521.

[15] ASTM D7542-09. "Standard test method for air oxidation of carbon and graphite in the kinetic regime."

[16] E.S. Kim, H.C. No, Experimental study on the oxidation of nuclear graphite and development of an oxidation model, J. Nucl. Mater. 349 (2006) 182-194.

[17] M.S. El-Genk, J.-M. P. Tournier, Development and validation of a model for the chemical kinetics of graphite oxidation, J. Nucl. Mater. 411 (2011) 193-207.

[18] J.P. Redfern, Differential Thermal Analysis, edited by R. C. Mackenzie, vol. I., Academic Press (1970) 123.

[19] J.M. Smith, Chemical Engineering Kinetics, McGraw-Hill (2d ed, 1956) 71.

[20] K.J. Laidler, Chemical Kinetics, Benjamin Cummings (3d ed, 1997).

CHAPTER 5

5.1 Discussion and conclusions

An overall comparison of the oxidation behavior among the three graphite grades in air revealed that NBG-18 was the most oxidation-resistant grade in the kinetic regime, between 873 and 1023 K, and also in the higher temperature regimes, between 1023 K and 1873 K. Specifically, it was observed that for all three grades the oxidation rates reach a maximum rate between 0.29 and 0.38 g/h g. However, NBG-18 is still the least oxidized grade. Table 5.1 shows the comparison of the oxidation rates and mass loss rates of the three grades. Figure 5.1 corresponds to the oxidation rates in Table 5.1.

Table 5.1. Mass loss rates and weight-normalized oxidation rates for NBG-18, IG-110 and GKrS.

T	**Mass loss rates**			**Oxidation rates**		
K	(mg h^{-1})			(g h^{-1} g^{-1})		
	+/- 0.01			+/- 0.001		
	NBG-18	**IG-110**	**GKrS**	**NBG-18**	**IG-110**	**GKrS**
873	1.26	0.60	3.60	0.002	0.002	0.043
923	1.10	15.63	16.20	0.003	0.028	0.191
973	15.02	45.13	30.60	0.048	0.100	0.213
1023	42.87	70.80	83.88	0.134	0.120	0.499
1173	114.06	120.32	54.00	0.164	0.271	0.240
1473	77.08	158.52	66.60	0.259	0.247	0.331
1873	174.28	153.99	131.40	0.383	0.298	0.378

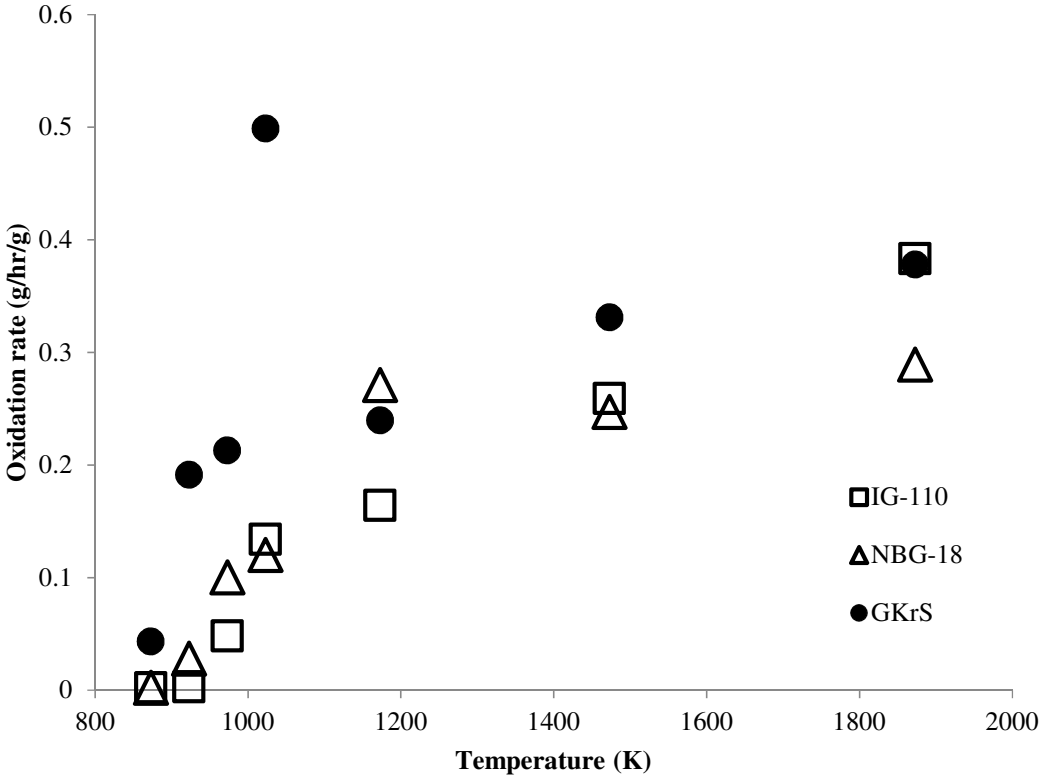

Fig. 1. Comparison of the isothermal oxidation rates of GKrS with nuclear-grade IG-110 and NBG-18.

Table 2 displays the activation energies and reaction orders of the three grades. A lower activation energy could mean less accessible reactive sites or a less ordered microstructure. Based on what we know of the microstructures of each grade, the results are in very good agreement with what we expected. The range for the activation energies of nuclear grade graphite found in the literature are between 170 and 220 kJ/mol while the very limited literature on matrix-grade graphite suggests the overall activation energy is between 110 and 160 kJ/mol [3].

Table 2. Comparison of the activation energy and order of reaction for NBG-18, IG-110 and GKrS.

	E_a (kJ/mol)	Reaction order
NBG-18	187	1.25
IG-110	222	0.76
GKrS	112	0.89

After all, we concluded previously in our first publication that NBG-18 was least oxidized due to its higher anisotropy, large coal coke filler grains of varying size and shorter penetration depth [1]. Due to its more chaotic and varying microstructure compared to IG-110, NBG-18 was observed to suffer a surface attack rather than a penetrative bulk oxidation. On the other hand, IG-110 was observed to suffer a more penetrative oxidation attack through its microporous structure even if chemically it is more pure than NBG-18. Loose graphite powder was commonly observed falling out from the samples of IG-110 after oxidation. Based on the SEM images, the surface of IG-110 was dramatically changed as it suffered a pitting corrosion while NBG-18 maintained most of its flake-like grain structure [2]. Further, we learned from our density profiling measurements that the density of IG-110 was dramatically reduced through the entire test rod, most likely due to the formation of more pores compared to NBG-18 after the same oxidation treatment. GKrS was observed to be most oxidized or the least oxidation-resistant in the kinetic regime among the three grades [3]. This result was expected considering the lower activation energy of GKrS and the disorderly microstructure of partially-graphitized graphite that is more susceptible to oxidation. At higher temperatures, GKrS reaches a maximum oxidation rate that is similar to that

of IG-110. Being least oxidized after all temperature trials and oxygen concentrations, this research concludes that the NGNP candidate grade NBG-18 is the superior choice for oxidation resistance for VHTR use among the three grades investigated here.

The main recommendation for continuation of this research would be to focus on the higher temperature regimes of graphite oxidation beyond the kinetic regime and devise a diffusion-based model therein. The other aspect of the experiment that could have been performed differently was the choice of test temperatures. In this study we used intervals of 50 and 100 K but one might use smaller temperature intervals and collect more data for each regime, instead of the minimum data for forming an Arrhenius plot, which is three data points. Particularly in the kinetic regime, one might want to test more temperature increments. While it is easy to determine when the kinetic regime of graphite oxidation begins, it is not easy to discriminate when the diffusively-controlled regime begins or ends. Some researchers feel there are only two regimes while others feel there are at least three. For future work or continuation, it would be prudent to obtain more matrix-grade graphite wherever possible. Another point of improvement for this research could be to the try the experiments with large graphite cylinders with a geometry similar to actual fuel compacts. Currently, the Thermax700 is not calibrated for use with samples over a certain weight and volume capacity but the effect of sample geometry and size on graphite oxidation is not well known and it was not studied here. The oxidation mechanism of graphite cannot be fully understood without a thorough surface study. While we studied the surface here, there is much to be learned about the surface in future work.

REFERENCES

[1] J. Lee, T.K. Ghosh, S.K. Loyalka, Oxidation rate of nuclear-grade graphite NBG-18 in the kinetic regime for VHTR air ingress accident scenarios, J. Nucl. Mater. 438 (2013) 77-87.

[2] J. Lee, T.K. Ghosh, S.K. Loyalka, Oxidation rate of nuclear-grade graphite IG-110 in the kinetic regime for VHTR air ingress accident scenarios, J. Nucl. Mater. 446 (2014) 38-48.

[3] J. Lee, T.K. Ghosh, S.K. Loyalka, Oxidation rate of graphitic matrix material in the kinetic regime for VHTR air ingress accident scenarios, J. Nucl. Mater. 451 (2014) 48-54.

VITA

Yoonjo ("Jo Jo") Lee was born in Akron, Ohio, United States of America in the evening of January 27, 1983. She attended private schools around the north eastern Ohio suburbs. She attended high schools in Akron, Ohio and finished in Columbia, Missouri. Jo Jo attended the University of Minnesota in Minneapolis, Minnesota and received a Bachelor's degree in Chemical Engineering and Minor in Chemistry in 2004. Then, she decided to go to law school and become a lawyer. She graduated from Hamline University School of Law in St. Paul, Minnesota in 2008 and passed the Minnesota bar exam the same year. After working about a year in the patent industry, she decided to pursue an advanced engineering degree and joined the doctoral program in 2010 at the Nuclear Science and Engineering Institute at the University of Missouri in Columbia, Missouri. She finished her doctoral work in Nuclear Engineering in late 2015.